PL-TR-96-2226

STUDIES OF NON-LTE ATMOSPHERIC EMISSIONS: MODELING AND DATA ANALYSIS

Peter P. Wintersteiner
Armand J. Paboojian
Robert A. Joseph

ARCON Corporation
260 Bear Hill Road
Waltham, MA 02154

20 August 1996

19970527 054
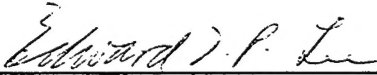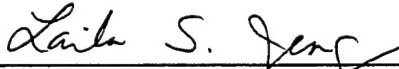
Final Report
March 1, 1990-September 30, 1995

PHILLIPS LABORATORY
Directorate of Geophysics
AIR FORCE MATERIEL COMMAND
HANSCOM AFB, MA 01731-3010

DTIC QUALITY INSPECTED 1

"This technical report has been reviewed and is approved for publication"

Edward T.P. Lee (signature)

EDWARD T.P. LEE
Contract Manager

Laila S. Jeong (signature)

LAILA S. JEONG
Acting Chief

William A.M. Blumberg (signature)

WILLIAM A.M. BLUMBERG
Acting Division Director

REPORT DOCUMENTATION PAGE

Public reporting burden for this collection of information is estimated to average 1 hour per response, including the time for reviewing instructions, searching existing data sources, gathering and maintaining the data needed, and completing and reviewing the collection of information. Send comments regarding this burden estimate or any other aspect of this collection of information, including suggestions for reducing this burden. to Washington Headquarters Services, Directorate for Information Operations and Reports, 1215 Jefferson Davis Highway, Suite 1204, Arlington, VA 22202-4302, and to the Office of Management and Budget, Paperwork Reduction Project (0704-0188), Washington, DC 20503.

1. AGENCY USE ONLY (Leave blank)	2. REPORT DATE	3. REPORT TYPE AND DATES COVERED
	20 August 1996	Final Report March 1, 1990-Sept 30, 1995

4. TITLE AND SUBTITLE
Studies of Non-LTE Atmospheric Emissions: Modeling and Data Analysis

5. FUNDING NUMBERS
PE: 61102F
PR 2310 TA G5 WU AG

Contract F19628-90-C-0060

6. AUTHOR(S)
Peter P. Wintersteiner
Armand J. Paboojian
Robert A. Joseph

7. PERFORMING ORGANIZATION NAME(S) AND ADDRESS(ES)
ARCON Corporation
260 Bear Hill Road
Waltham, MA 02154

8. PERFORMING ORGANIZATION REPORT NUMBER

9. SPONSORING/MONITORING AGENCY NAME(S) AND ADDRESS(ES)
Phillips Laboratory
29 Randolph Road
Hanscom AFB, MA 01731-3010

Contract Manager: Edward Lee/GPOS

10. SPONSORING/MONITORING AGENCY REPORT NUMBER

PL-TR-96-2226

11. SUPPLEMENTARY NOTES

12a. DISTRIBUTION/AVAILABILITY STATEMENT

Approved for public release; distribution unlimited.

12b. DISTRIBUTION CODE

13. ABSTRACT (Maximum 200 words)

This report documents research that has been carried out for the purpose of furthering the understanding of infrared emissions in the non-LTE regions of the Earth's atmosphere. Our effort has consisted of developing and exercising computer models of the quiescent and aurorally-disturbed atmosphere, analyzing data from rocket and satellite experiments to validate and extend the models, and drawing upon our experience to help plan for the MSX mission. Specifically, we have used our models to simulate data from the SISSI and MAP/WINE campaigns and the CIRRIS mission, perform benchmark calculations to validate radiative transfer algorithms, and study the effects of gravity waves on non-LTE populations and atmospheric cooling in the mesopause region. We have performed spectral analysis on CIRRIS data, and used the models to identify processes contributing to the 4.3 um emissions seen in the data. We present a detailed description of how to use Atmospheric Radiance Code (ARC), the non-LTE code that we employ for these purposes. We also summarize our role in MSX experiment planning, and software development for automated analysis of MSX Spectrographic Imager data.

14. SUBJECT TERMS KEYWORDS:
Infrared emission; non-LTE; upper atmosphere; radiative transfer; cooling; CO_2; $O(^1D)$; 15 µm; 4.3 µm; ARC; CIRRIS; SISSI; MAP/WINE; MSX; Spectrographic Imagers; SPIMDRVR

15. NUMBER OF PAGES
124

16. PRICE CODE

17. SECURITY CLASSIFICATION OF REPORT	18. SECURITY CLASSIFICATION OF THIS PAGE	19. SECURITY CLASSIFICATION OF ABSTRACT	20. LIMITATION OF ABSTRACT
Unclassified	Unclassified	Unclassified	SAR

TABLE OF CONTENTS

PREFACE

1. INTRODUCTION

Infrared emissions in the upper atmosphere play an important role in the establishment of the heat balance, structure, and dynamical properties of the atmosphere as a whole. During the period of time covered by this report, we have devoted considerable effort to constructing, testing, and validating models of infrared emission in the non-LTE regions of the atmosphere. More importantly, we have used the models to study particular problems that are important for understanding basic physical processes that contribute to the infrared signature of the atmosphere and to the structure of these emissions. This has been done in many cases using corroborative data sets.

We have also participated in planning and development activities of the Midcourse Space Experiment (MSX) as part of the Earthlimb Backgrounds Team, prior to the launch of the satellite in 1996.

This report describes work accomplished under the provisions of contract F19628-C-90-0060. It has three principal technical sections, 2-4, following this introduction. The first of these deals with the principal modeling activities that we carried out during the performance period. We used the Phillips Laboratory Atmospheric Radiance Code (ARC), which we developed in collaboration with Phillips Lab personnel, for most of these calculations. Section 3 discusses ARC itself. Since the principal algorithms developed for use in ARC have been explicated in the open literature (see references in Section 5.2), we do not review them explicitly but instead give a discussion of how to use the code.

Section 4 deals with our MSX activities. Much of this effort involved experiment planning and instrument specifications for the Earthlimb data collection events (DCEs), but we also provided software for automated data processing. This work was all part of a larger integrated planning process, and evolved in consort with that process. It has been carefully described at numerous formal meetings and design reviews, and presented in the form of tables, summaries, and source code, as appropriate. The MSX discussion attempts to describe, but not reproduce, these products of our work.

The figures and tables are numbered consecutively within each section of this report. Papers that are cited in the three technical sections are listed in the Technical References part of Section 5. Journal articles reporting on work carried out by us during the performance period of this contract are listed separately as Refereed Publications, notwithstanding some overlap with papers listed as References. Many of the principal scientific conclusions that we reached have been described in detail in those publications, so we reference them extensively, and attempt to summarize rather than repeat their content. Last of all, having orally reported on our work at meetings and workshops on many occasions, we provide a list of such reports in the section entitled Presentations. This list includes presentations made by ARCON personnel, and some made by Phillips Laboratory researchers when the presentation was significantly based on work performed by us. This list is arranged in reverse chronological order.

2. MODELING AND DATA ANALYSIS

We have used our state-of-the-art radiative transfer codes, realized as the Phillips Laboratory Atmospheric Radiance Code (ARC) to develop models for infrared radiance for different emitters, to simulate their emissions under a great variety of atmospheric conditions, and to evaluate the physical processes incorporated in them by comparing their results to infrared radiance data sets. This section describes several studies that have been performed with the help of these codes.

2.1 Simulations of High-Latitude 15 μm Emissions

The use of experimental radiance data to validate theoretically-based model calculations is often frustrated by incomplete knowledge of the prevailing atmospheric background conditions. Lacking measurements of kinetic temperature, the major atmospheric constituents, and whatever minor constituents (including the radiator) might be needed for the calculations, one must resort to climatological models and hope that the actual state of the atmosphere is fairly accurately represented by them. When such measurements are available, on the other hand, modeling can be carried out with fewer unconstrained parameters, and the results thus provide better tests of the physics underlying the calculations.

We have used the ARC model to simulate the results of two rocket experiments that obtained infrared radiance data and were, in addition, supported by coincident or nearly coincident measurements of temperature and atomic oxygen. The results corroborate the model calculations quite convincingly in both cases. They also provide an interesting comparison because of the greatly disparate conditions that prevailed during the two flights, neither of which closely mimic climatological mean conditions predicted by empirical models. The work is reported by *Ratkowski et al (1994)*, and summarized in this section.

The measurements in question were taken during the DYANA *(Offermann, 1994)* and MAP/WINE *(von Zahn, 1987)* campaigns, in 1990 and 1984 respectively. The 1990 data come from one of four launches conducted at that time, and are known by the acronym SISSI-F1. Both experiments were conducted at Esrange in Sweden in late winter, at approximately the same local time (dawn), and in both cases spectral data were obtained with a zenith-looking instrument. This geometry enhances the value of supporting measurements, because (in contrast to limb views) the instrument samples a region of small horizontal extent and does not, in effect, average over a great range of atmospheric conditions.

3

Kinetic Temperature
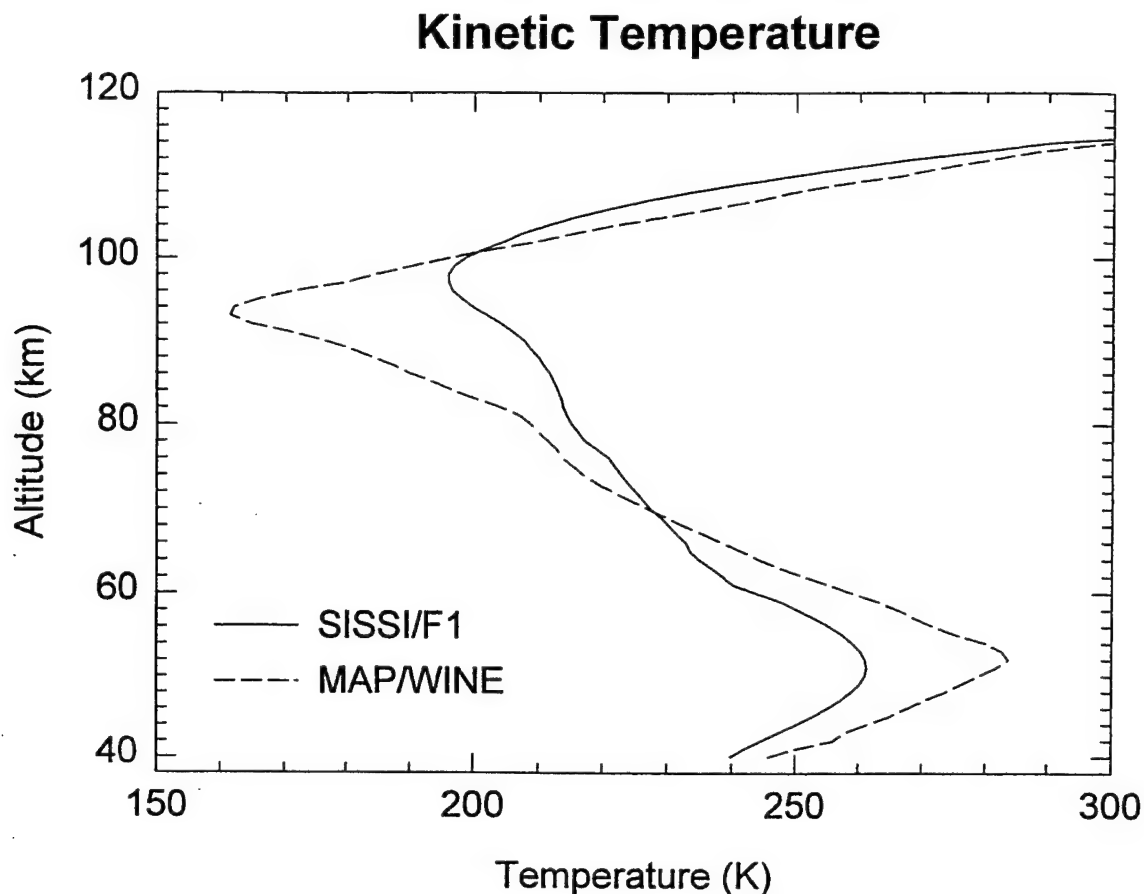
Figure 1. Kinetic temperature profiles used for the SISSI and MAP/WINE simulations.

In both cases, we modeled the CO_2 15 μm data, which are especially sensitive to both atomic oxygen and kinetic temperature as a result of the efficient excitation of the bending modes by the former, and which therefore constitute an excellent test of the significance of this process and the parameters that describe it.

The kinetic temperature profiles that were used for the SISSI and MAP/WINE simulations are plotted in Figure 1. These are composite temperature profiles, determined by running a smooth curve through data points derived from separate temperature measurements (falling spheres; OH rotational temperature) or inferred from results from on-board instruments (atomic oxygen scale height; infrared data). For modeling purposes, the contrast between the profiles is particularly noteworthy in that the mesopause temperatures differ by almost 40 K. The MAP/WINE profile has a cold narrow minimum at about 94 km, while the SISSI mesopause is much broader and warmer and the mesosphere as a whole has quite small temperature gradients. The stratopause regions also are quite dif-

4
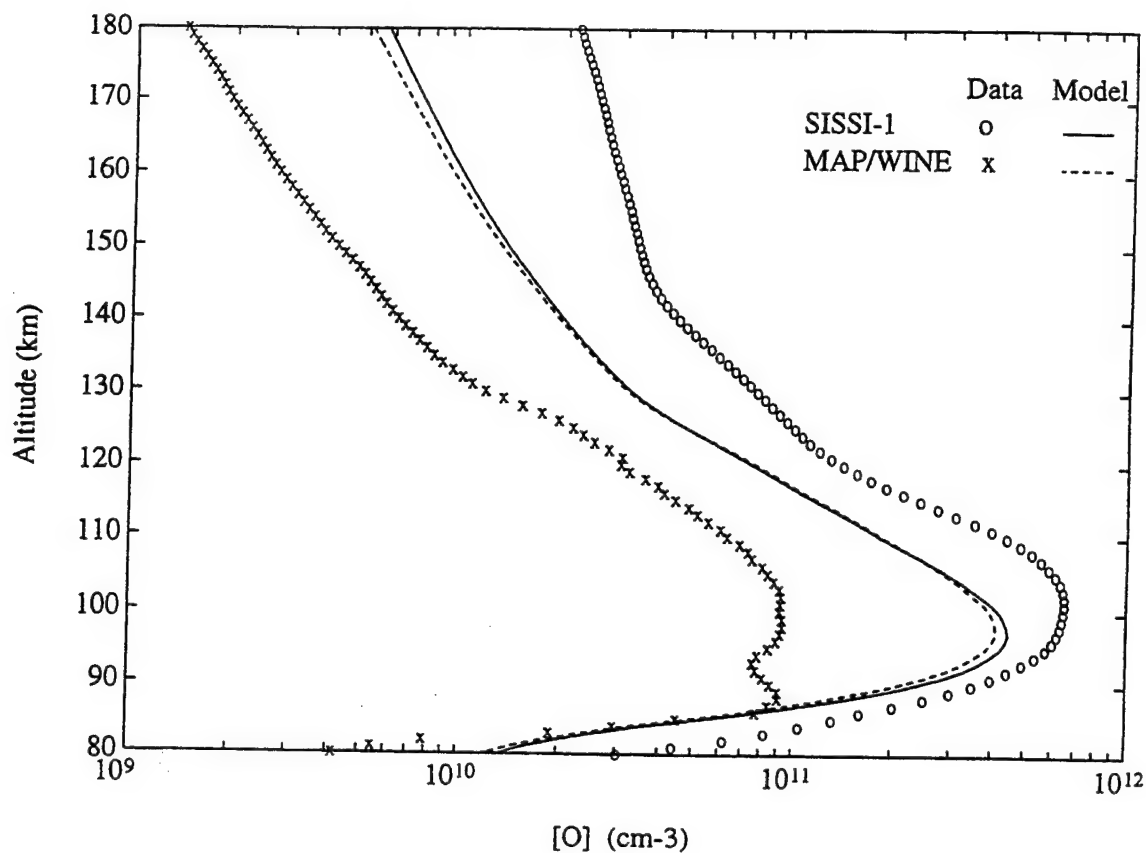
Figure 2. Atomic oxygen profiles used for the SISSI and MAP/WINE simulations, compared with profiles derived from MSIS-86 for the dates of the two experiments.

ferent, but at those altitudes the temperature was considerably lower for SISSI than for MAP/WINE.

The atomic oxygen profiles, plotted in Figure 2, also provide a stark contrast that is significant for the 15 μm emissions. The SISSI atomic oxygen peak is very high, both in number density ($> 6 \times 10^{11}$ cm^{-3}) and altitude. In contrast, the MAP/WINE atomic oxygen has a peak that never exceeds 10^{11} cm^{-3}, to go with the cold temperatures in the mesopause region. Climatologically-based profiles from MSIS for the dates of the two experiments are also shown in Figure 2, to make the point that the measured densities are, in the two cases, between two and three times higher and lower, respectively, than the "expected" or typical densities.

Results for the vibrational temperatures of the 01101 states for the four main isotopes of CO_2 are shown in Figures 3 and 4. In both cases, the major-isotope 626 vibrational temperature tracks the kinetic temperature quite closely right up to the mesopause. For the

Vibrational Temperatures
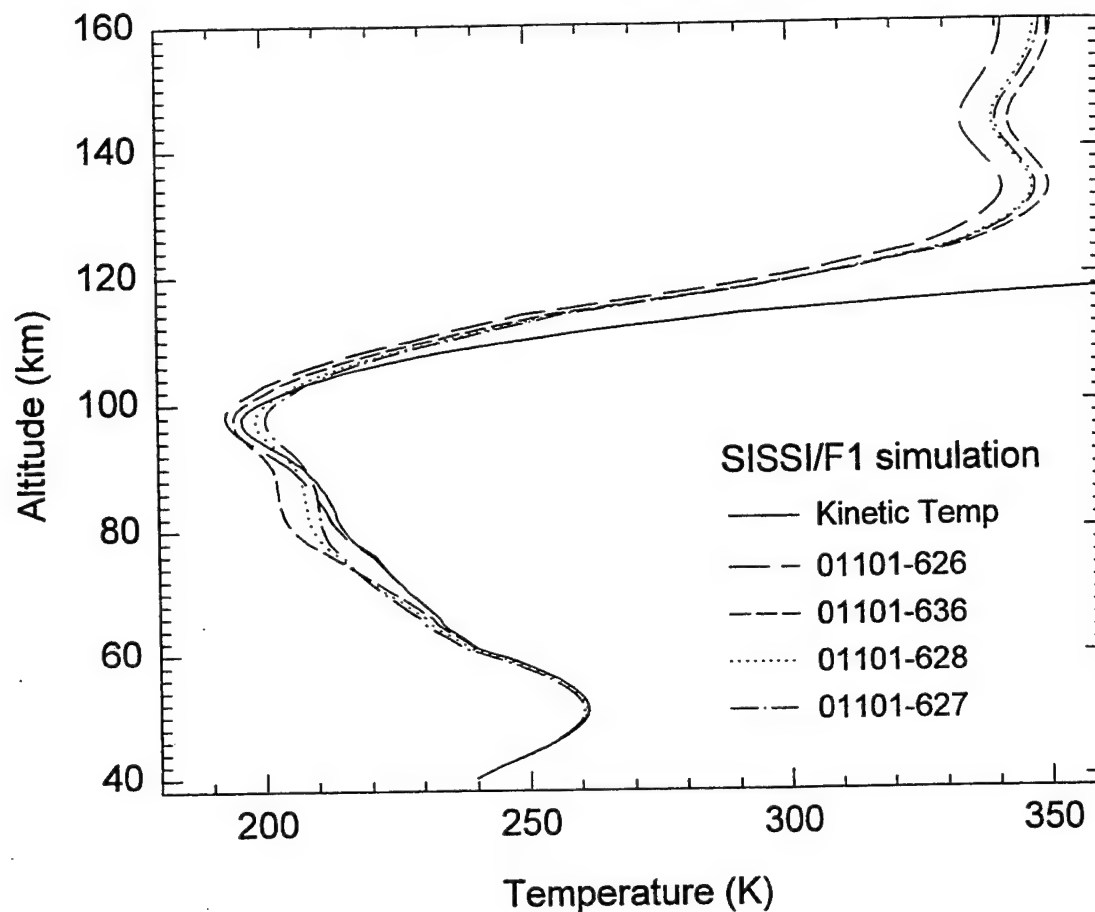
Figure 3. Vibrational temperatures of the CO_2 01101 states for four isotopes, for the SISSI simulation.

SISSI simulation the minor-isotope temperatures also track the kinetic temperature, but for the MAP/WINE case they don't.

In the case of the 626 isotope, the explanation of this similarity is that the infrared bands are sufficiently thick, optically, that radiative excitation is due to photons that are primarily local in origin. The absorption rate thus reflects the local emission rate, which in turn reflects the local temperature regardless of the rapidity of the thermal processes that also populate the states. Generally speaking, the rate of thermal processes depends on the atomic oxygen density in this region. The more atomic oxygen there is, the closer the vibrational temperatures will be to the kinetic temperature because the thermal processes that by definition drive things toward LTE then comprise a larger fraction of the overall production and loss for the CO_2 states. But for 626 it doesn't matter very much what fraction of the production and loss is thermal, because the radiative excitation, being local in origin, produces similar results.

6

Vibrational Temperatures
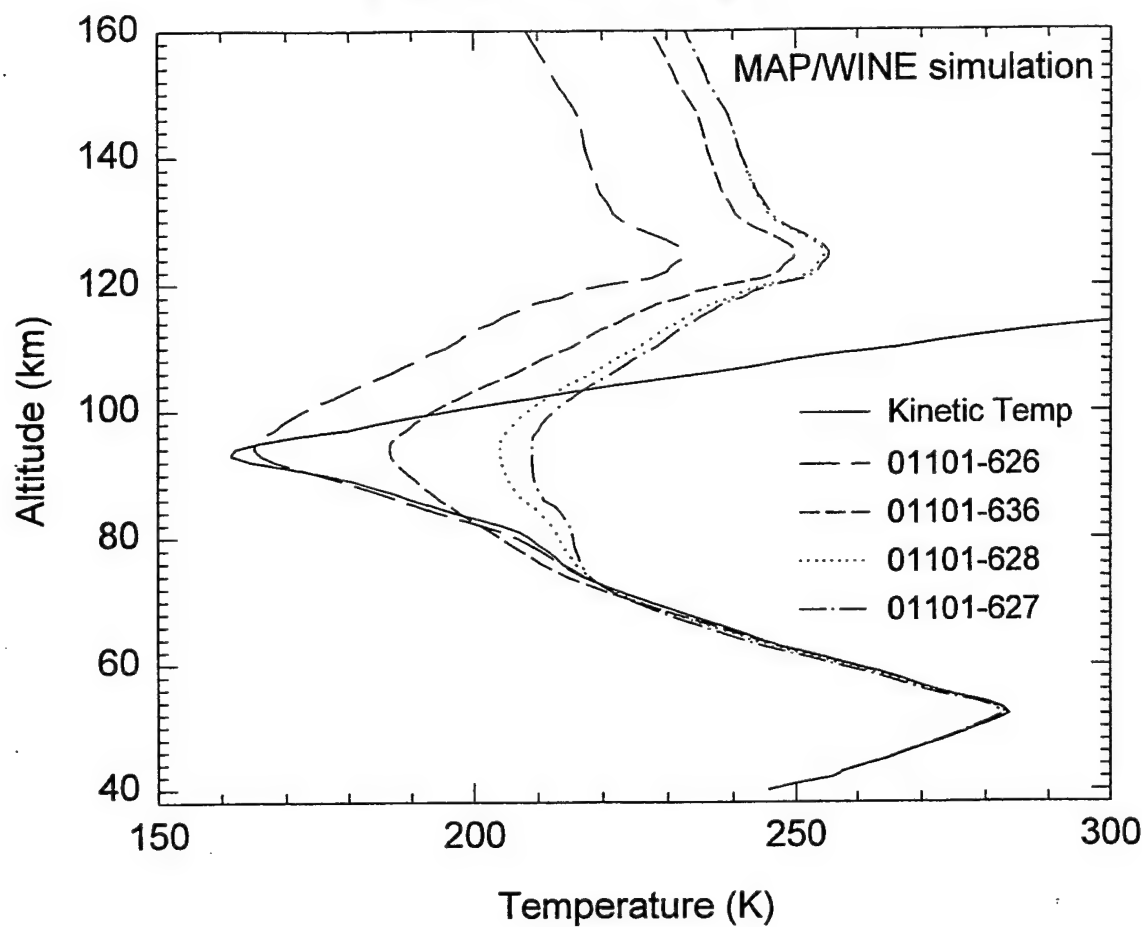
Figure 4. Vibrational temperatures of the CO_2 01101 states for four isotopes, for the MAP/WINE simulation.

For the minor isotopes, however, it matters a great deal what fraction of the excitation is thermal and what fraction is radiative. The radiative absorption in the minor-isotope bands is largely that of photons arriving from the upper mesosphere and even the stratopause, and thus reflects conditions prevailing there rather than in the local region. The vibrational temperatures therefore usually begin to depart from LTE in the upper mesosphere, due to the larger flux from the warmer regions. The departure is greater for the less populous isotopes because the infrared bands are thinner, the MAP/WINE calculation in Figure 4 exemplifying this. It is only when the thermal processes are dominant, making the radiative absorption relatively much less important, that the minor-isotope vibrational temperatures also track the kinetic temperature. This is the case with the SISSI simulation. The differences between the results shown in Figures 3 and 4 come primarily, then, from the differences in the rate of thermal processes in the upper mesosphere due to atomic oxygen. A secondary reason, however, is that the stratopause-mesopause temperature difference is much greater for MAP/WINE than for SISSI. That is, not only is the

Fractional Excitation Rates
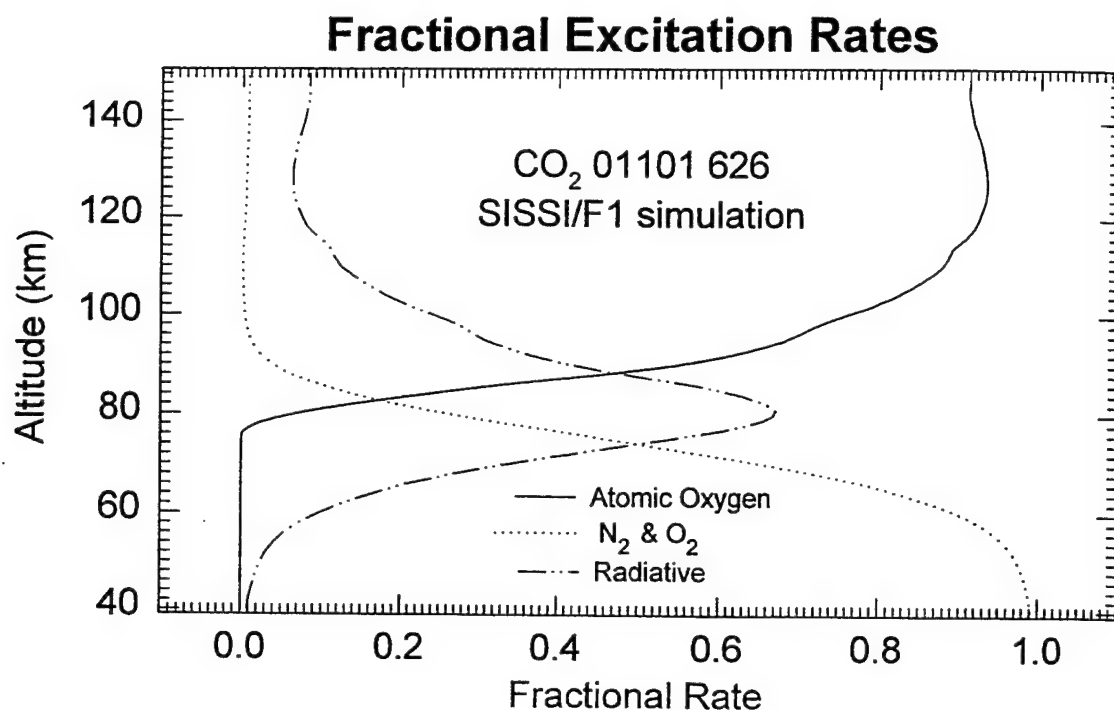
Figure 5. Fractional excitation rates for the CO_2 626 01101 state, for the SISSI simulation.

Fractional Excitation Rates
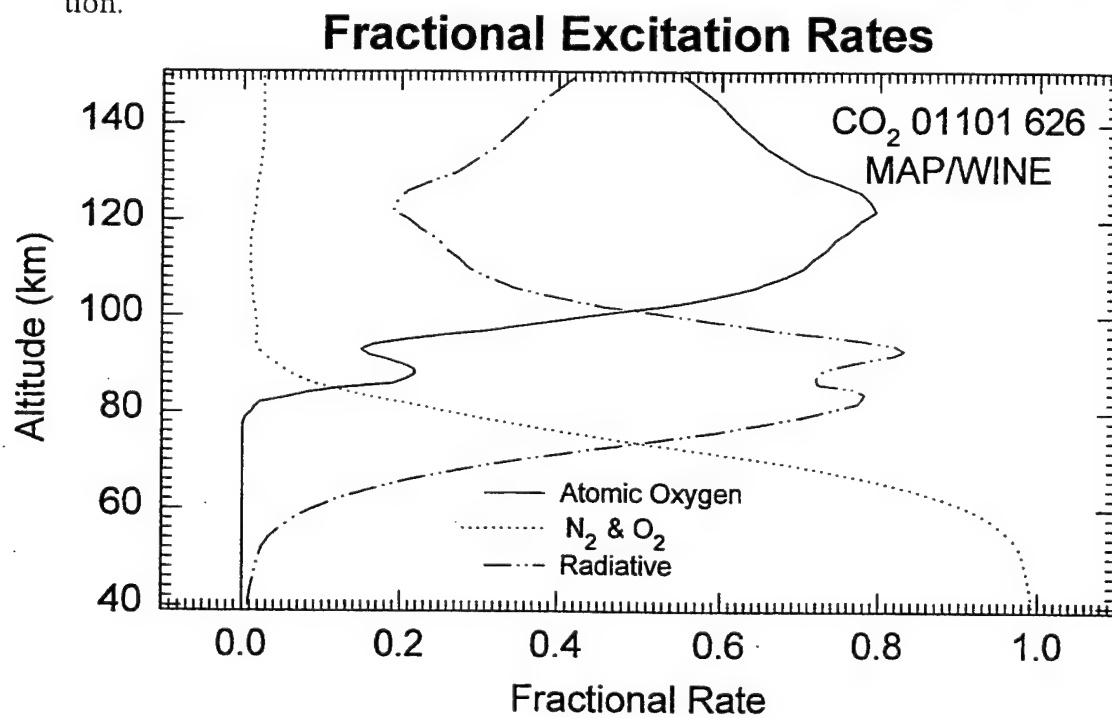
Figure 6. Fractional excitation rates for the CO_2 626 01101 state, for the MAP/WINE simulation.

thermal excitation rate for MAP/WINE much lower, but the upwelling infrared flux in the minor-isotope bands is also higher, causing the departure from LTE conditions to be even greater.

The other major difference between Figures 3 and 4 is the thermospheric vibrational temperatures, which differ by more than 100 K above 120 km. This is a direct reflection of the atomic oxygen densities for these two cases.

The vibrational temperatures of the 02201 states, not shown here, of course depend strongly on the 01101 vibrational temperatures because the excitation processes couple the states directly. For the SISSI case the thermal processes are again dominant and cause the 626 02201 temperature to track the 01101 temperature quite closely despite larger radiative contributions from lower-altitude regions. The 03301 temperature tracks the 02201 temperature in similar fashion. In contrast, for the MAP/WINE case the higher lying states deviate from the ones directly below them by approximately 10 K at the mesopause, which reflects the much larger relative contribution from radiative absorption from lower altitudes. The 10 K difference is much greater than that for SISSI, but it is noteworthy that it is a lot less than the deviations of the MAP/WINE minor-isotope 01101 states (whose infrared bands are similarly opaque) from the kinetic temperature.

Figures 5 and 6 show the fractional excitation rates for the 626 01101 states, to illustrate the extent to which atomic oxygen dominates in the thermosphere (in both cases), and to contrast the role of radiative excitation in the upper mesosphere for these two simulations. Clearly the radiative component is much stronger, and dominant over a much broader altitude range, for MAP/WINE than it is for SISSI.

Figure 7 compares the zenith radiance data with model predictions generated from these vibrational temperatures using NLTE and CONV. The plot shows the spectral radiance at the peak of the emission at 14.96 μm, rather than the band radiance, for both cases. The model successfully reproduces these data throughout the respective acquisition ranges. For SISSI, a full synthetic spectrum from 95 km is shown along with corresponding data in Figure 8. The model does not completely reproduce the radiance at the Q-branch peaks of the first hot bands at 13.9 and 16.2 μm at the lower altitudes.

Figure 9 shows the total infrared cooling rates due to the CO_2 bands that occurs for these two cases. Despite being run for very similar seasons, local times, and locations, these simulations yield completely different cooling rate profiles, and peak cooling rates that differ by a factor of four. One might expect great variability in cooling on a global scale for different locations and seasons, although models generally do not predict disparities as great as this. However, these results emphasize that tremendous variability in
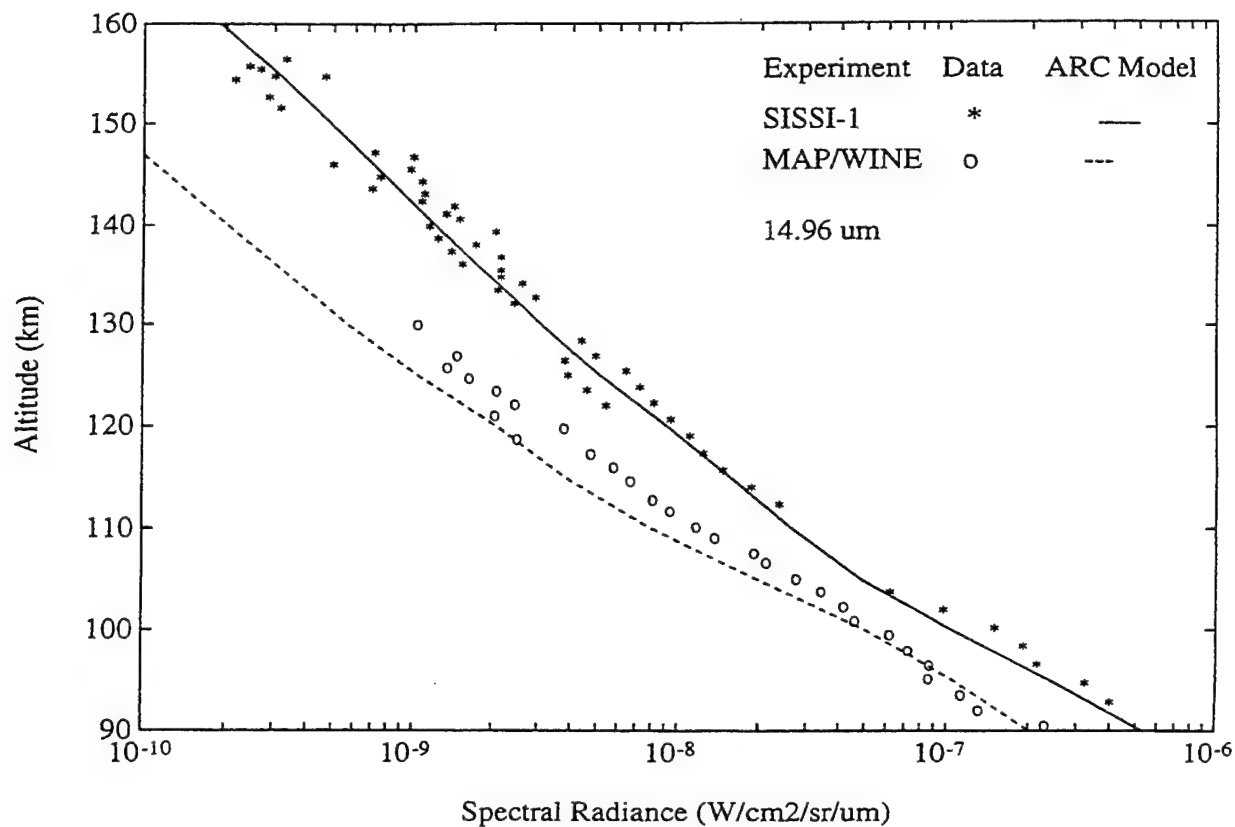
Figure 7. Comparisons of modeled and observed zenith spectral radiance at 14.96 μm, plotted versus tangent height, for the SISSI and MAP/WINE experiments.
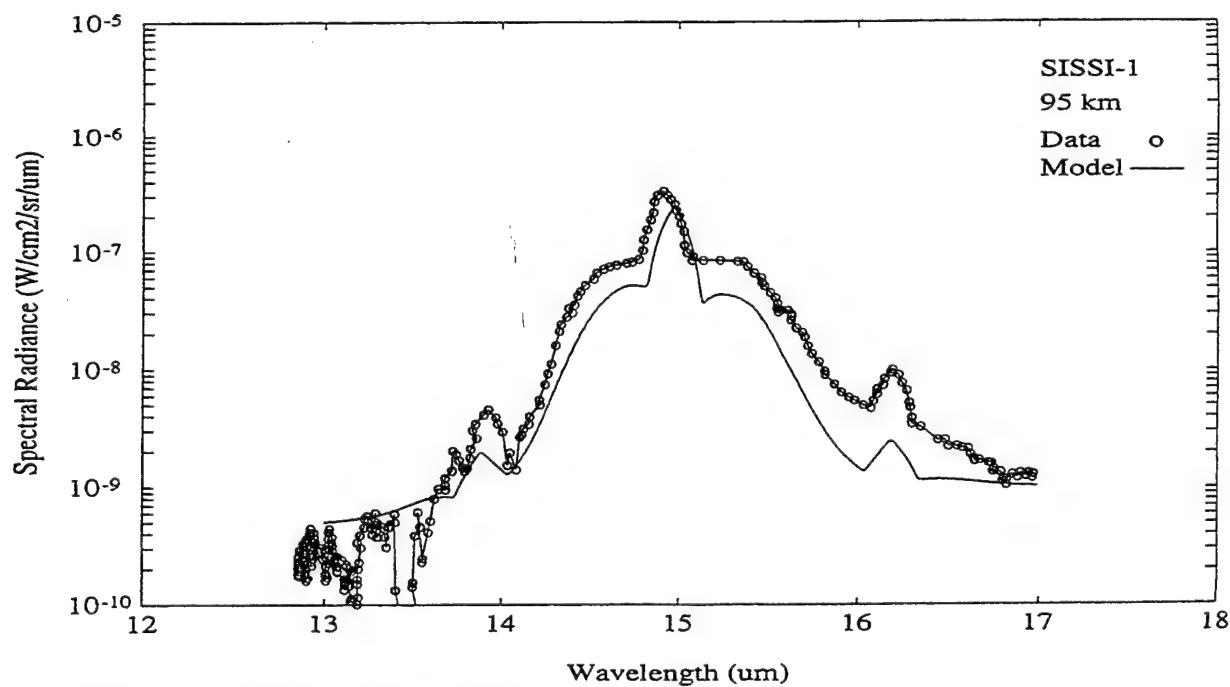
Figure 8. Comparison of a modeled and observed spectrum for a 95-km tangent height, for the SISSI experiment.

the MLT region may also be expected within a rather small "climatological box". By extension, it follows that great variability may also be seen over time and distance scales that are quite small compared to global scale.

In summary, the comparison of the simulations with the infrared radiance data from these two rocket experiments provides a precise test of the non-LTE ARC calculations. The experimental characterization of the temperature and atomic oxygen profiles makes the study even more stringent, and together with the disparate conditions prevailing during the two campaigns it helps to demonstrate that the calculations are robust.

The study also reveals great variability in the cooling rates in the MLT region. Recognition of this variability may ultimately be one of the more important results of this study.
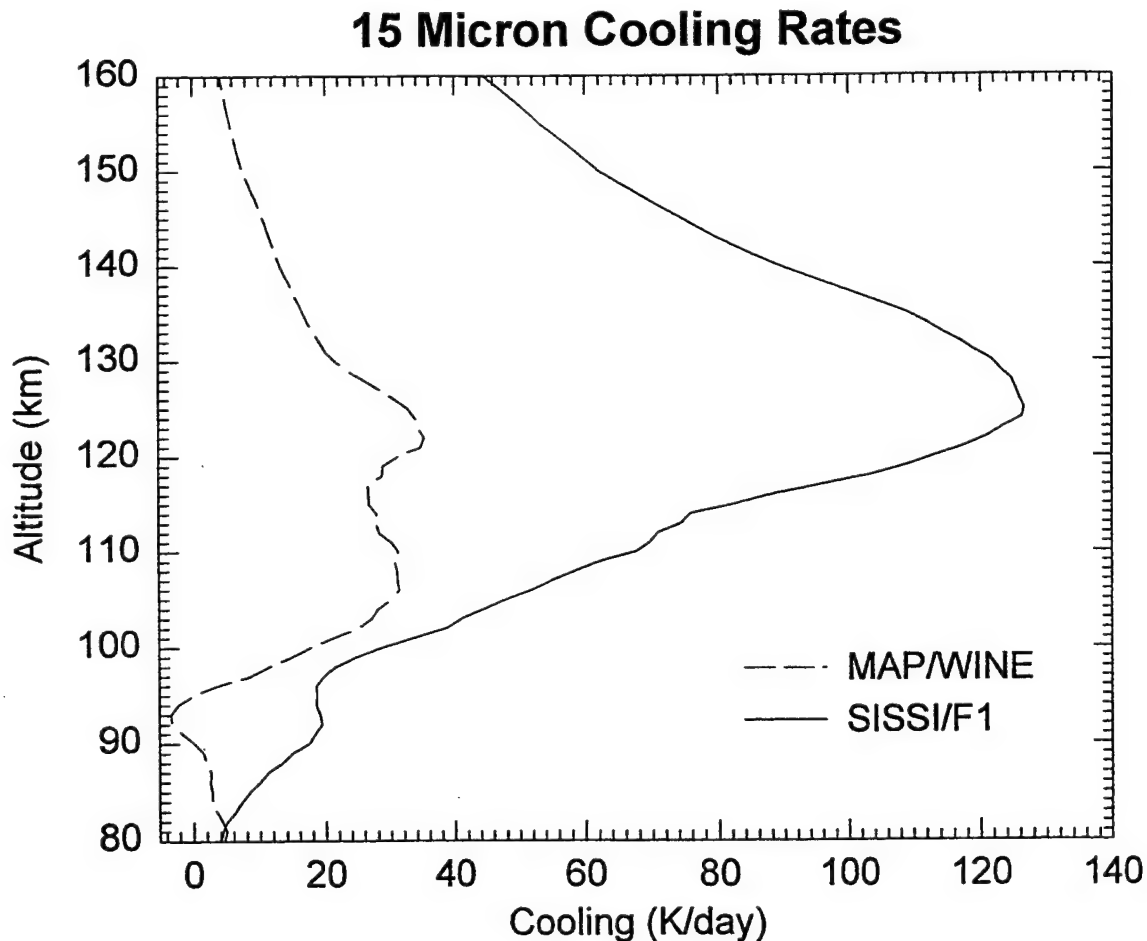
Figure 9. Comparison of the calculated total cooling in the CO_2 bands for the SISSI and MAP/WINE experiments.

2.2 Benchmark Calculations

In the past ten years, important advances have resulted in vastly improved infrared radiative transfer calculations. Such calculations are a critical component of predictive models for non-LTE emissions in the upper atmosphere for many active emitters, notably CO_2 and CO. Among these advances are the modified Curtis matrix (MCM) inversion method of Lopez-Puertas (e.g., *Lopez-Puertas et al, 1992a* and earlier papers referenced therein) and the iterative line-by-line RAD algorithm developed by us and incorporated into some of the ARC codes *(Wintersteiner et al, 1992)*.

In order to validate the results of the new emission models, and in particular the radiative-transfer component of the calculations, we conducted a comparative study of results derived from the MCM and RAD calculations, concentrating upon the CO_2 15 μm bands. This work was published in 1994 *(Lopez-Puertas et al, 1994)* in a paper which contains many of the details of the comparison. In this section we outline the motivation for the work, the procedures we adopted, and the principal conclusions that we drew.

One reason for pursuing the MCM-RAD comparison was to insure that the former approach to radiative transfer, which may be thought of as a narrow-band model because individual lines are treated in groups, is intrinsically accurate. However, during the past few years, it has also been recognized *(Sharma and Wintersteiner, 1990; Rodgers et al, 1992; Lopez-Puertas et al, 1992b)* that the CO_2 ν_2 states lie quite close to local thermodynamic equilibrium (LTE) even at quite high altitudes, which is important because as a result it is possible to use their emissions to retrieve the kinetic temperature at least to the mesopause, perhaps up to 100 km. Another goal, therefore, was to validate the models' complete formulations, for the purpose of eliminating doubts about the retrievals that might arise if potential discrepancies between the model results could not be resolved, and also to eliminate the possibility that significant errors in the actual results could be due to anything but errors in the input profiles.

[The near-LTE behavior comes about because of the low energies of the states, the optical thickness of the infrared bands connecting them, and the significance of collisions with atomic oxygen as an excitation mechanism for the bending modes, and was not fully recognized until the currently-accepted value for the atomic oxygen rate constant was inferred from experimental data *(Sharma and Wintersteiner, 1990)*.]

A third goal was to check the results for atmospheric cooling in the mesosphere and lower thermosphere (MLT), which is much enhanced by the near-LTE conditions and whose significance for the thermal balance of the region is thereby increased.
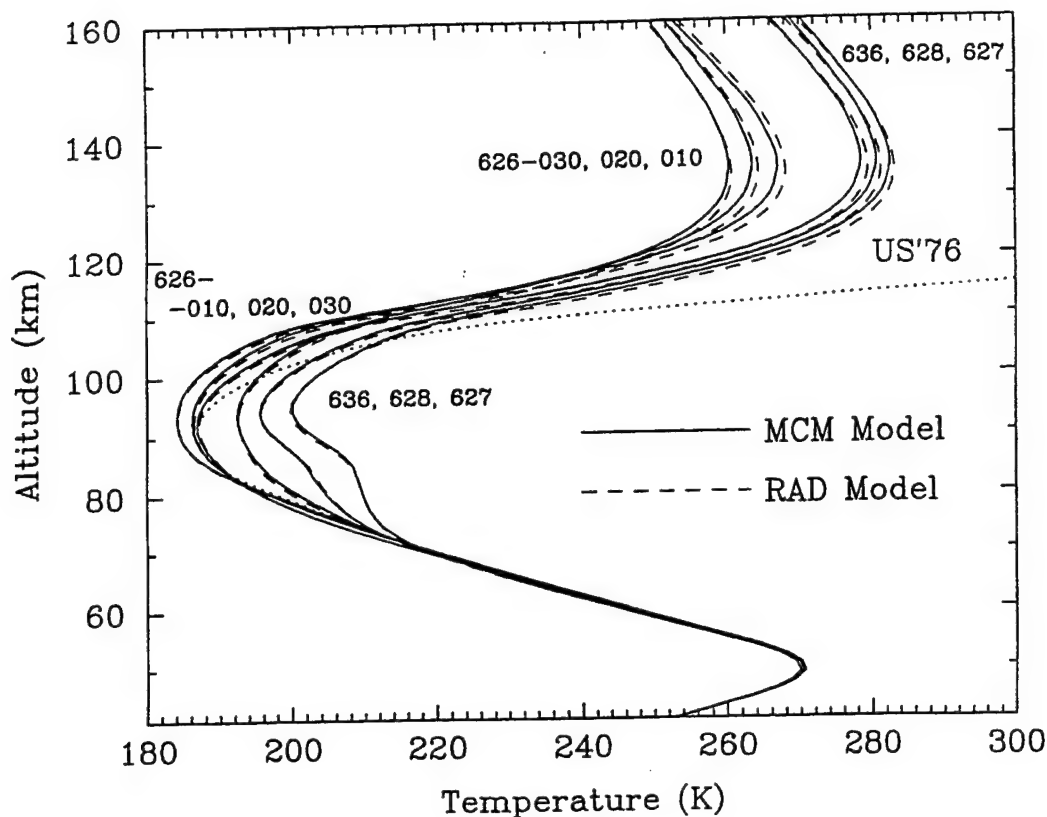
Figure 10. Comparison of MCM and RAD vibrational temperatures for the CO_2 01101 states for four isotopes, plus the 02201 and 03301 states for the major isotope. The calculations were performed with the larger oxygen-atom rate constant (the "fast" case; see text) using the smoothed U.S. Standard Atmosphere temperature profile

The approach that was adopted was to do parallel calculations with the two non-LTE models and compare the results for vibrational temperatures and cooling rates. We used the same input profiles for temperature, density, and pressure, the same layering (1.5 km layers between 40 and 160 km), the same line parameters and isotopic abundances from the HITRAN database, and the same collision mechanisms and rate constants. We regarded the Fermi-degenerate 10002 and 10001 states as being in mutual equilibrium with the 02201 state, as discussed in Section 3.3.4, with a similar treatment for the 11102, 03301, and 11101 states. We chose three model atmospheres to cover a fairly extreme range of climatological conditions, namely the CIRA 80^0 north and 80^0 south models for December (which have mesopause temperatures differing by almost 70 K, and stratopause temperatures different by 30 K in the opposite sense) and a mid-latitude model derived from the U.S. Standard Atmosphere (1976) that has the temperature profile smoothed to avoid discontinuities in the temperature gradient.

We also chose to test two values of the oxygen-atom rate constant, namely 2×10^{-13} cm^3/s used by *Dickinson (1984)* and others in the past, and the one of *Sharma and Win-*
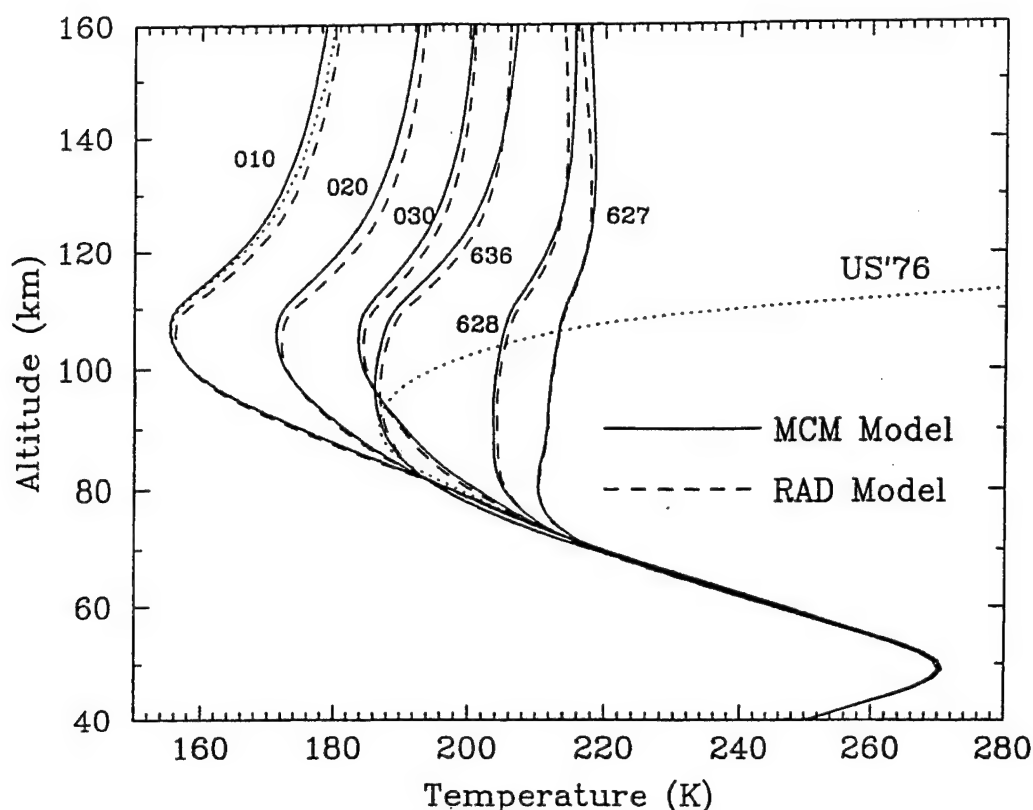
Figure 11. As Figure 10, but for the slow case.

tersteiner (1990), which is approximately thirty times larger. These are referred to as "slow" and fast" cases, respectively. The reason for testing the smaller rate constant was that, by minimizing the thermal excitation, we exaggerated the importance of radiative absorption as an excitation mechanism and thus enhanced the effects of the differences in the radiative transfer algorithms that we wished to evaluate. Therefore, with the three model atmospheres, there were six sets of calculations to be compared. For each case, the vibrational temperatures of nine states were calculated, as well as the cooling associated with them. The RAD calculations were performed as described in Section 3.3.4.

Typical results, which are discussed in detail by *Lopez-Puertas et al (1994)*, are presented in Figures 10-17. The vibrational temperature profiles calculated by the two models were quite similar in all cases, as shown for some states in Figures 10 and 11, so the results were plotted as differences in vibrational temperature, as in Figures 12-17, or as percent differences, as in the abovementioned paper.

For the fast cases and two of the three model atmospheres, discrepancies between the models' results for all states were less than 1 K throughout the entire region below 100

VIBRATIONAL TEMPERATURE DIFFERENCES
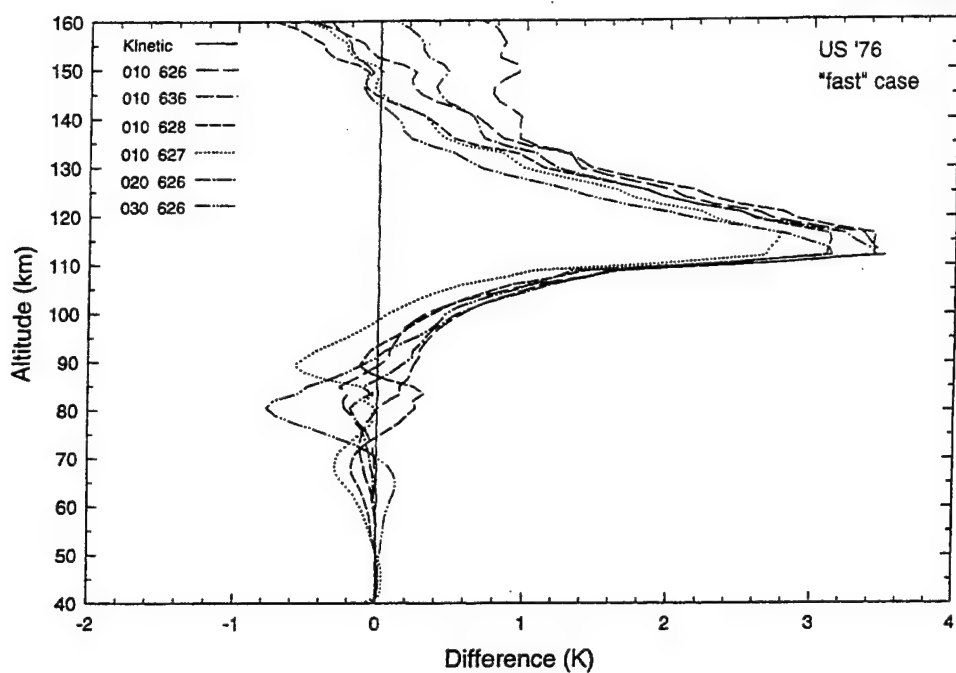
Figure 12. RAD-MCM vibrational temperature differences for fast case using the mid-latitude model. A positive difference indicates that RAD calculates a higher vibrational temperature.

VIBRATIONAL TEMPERATURE DIFFERENCES
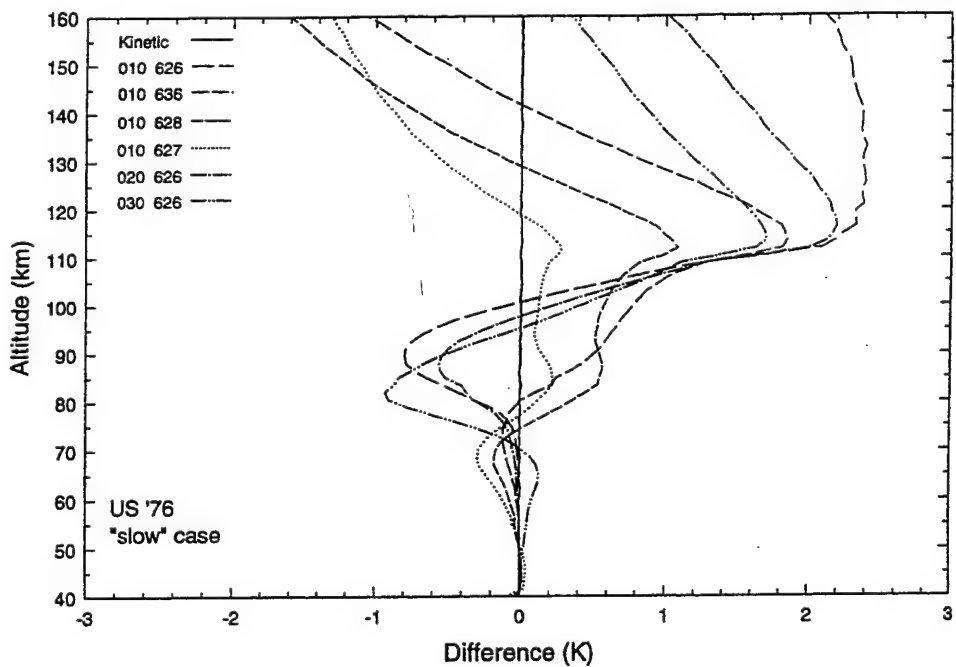
Figure 13. As Figure 12, but for the slow case.

VIBRATIONAL TEMPERATURE DIFFERENCES

RAD - MCM
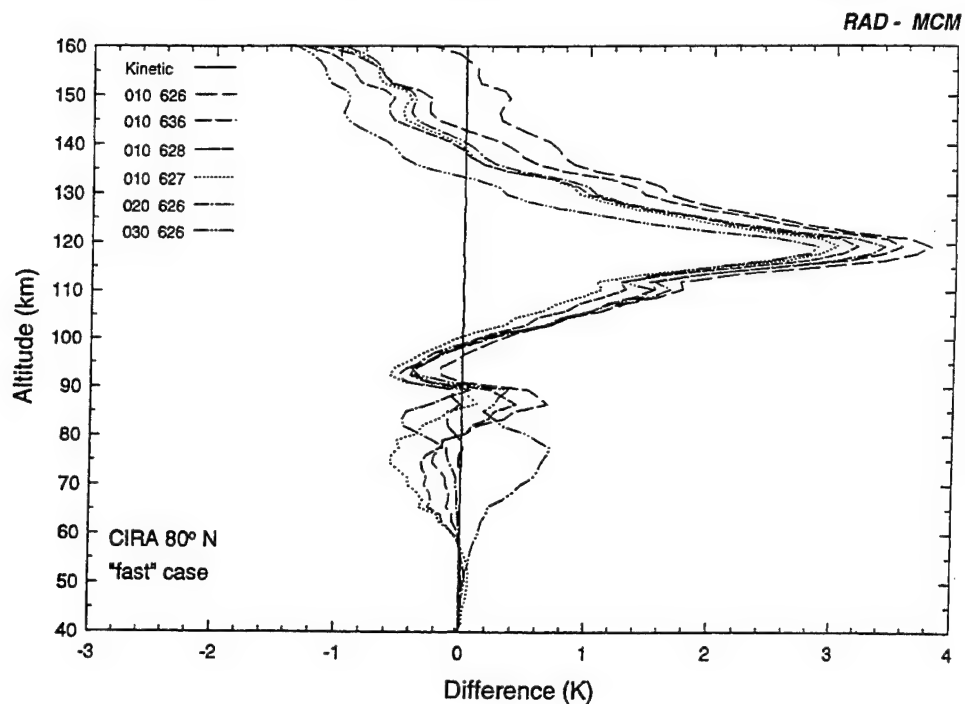
Figure 14. As Figure 12, but for the CIRA 80⁰ N model atmosphere

VIBRATIONAL TEMPERATURE DIFFERENCES

RAD - MCM
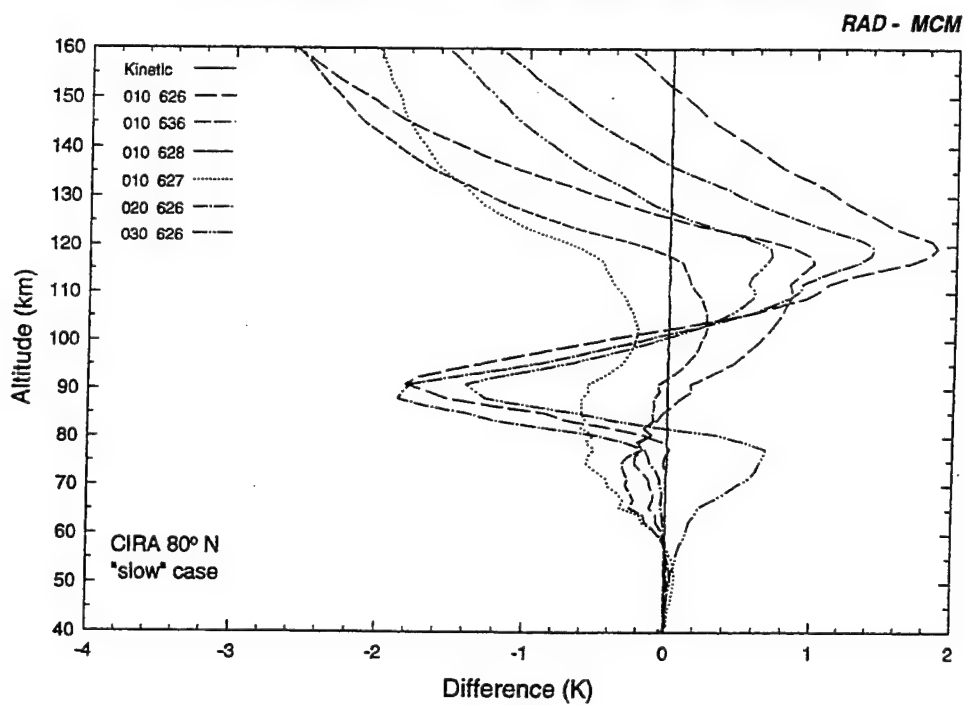
Figure 15. As Figure 14, but for the slow case.

16

VIBRATIONAL TEMPERATURE DIFFERENCES

RAD - MCM
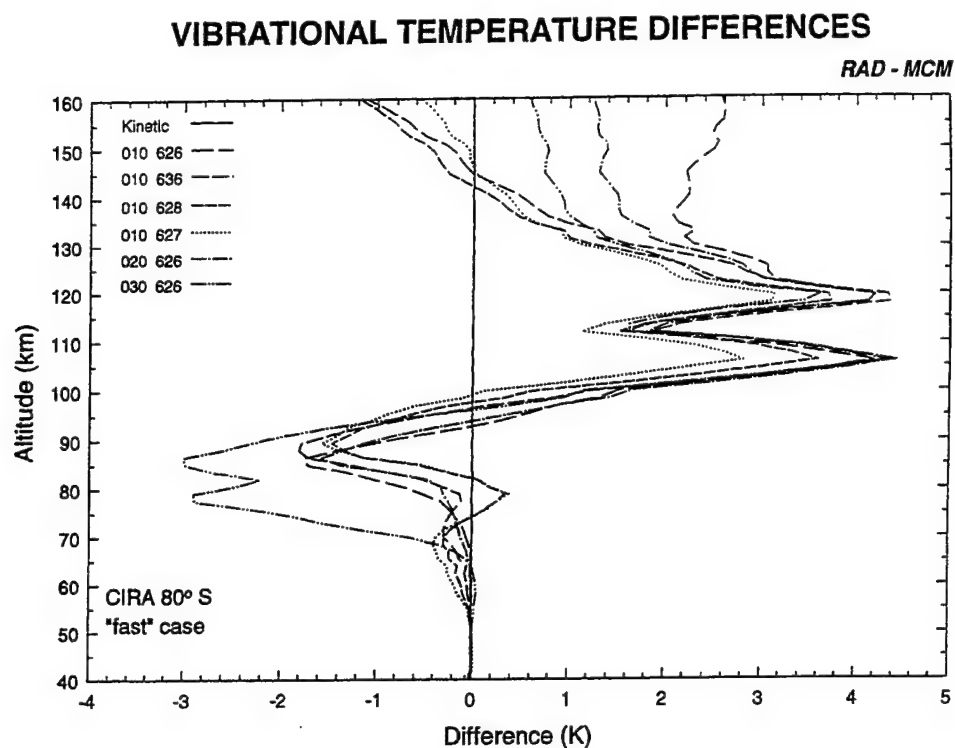
Figure 16. As Figure 12, but for the CIRA 80^0 S model atmosphere.

VIBRATIONAL TEMPERATURE DIFFERENCES

RAD - MCM
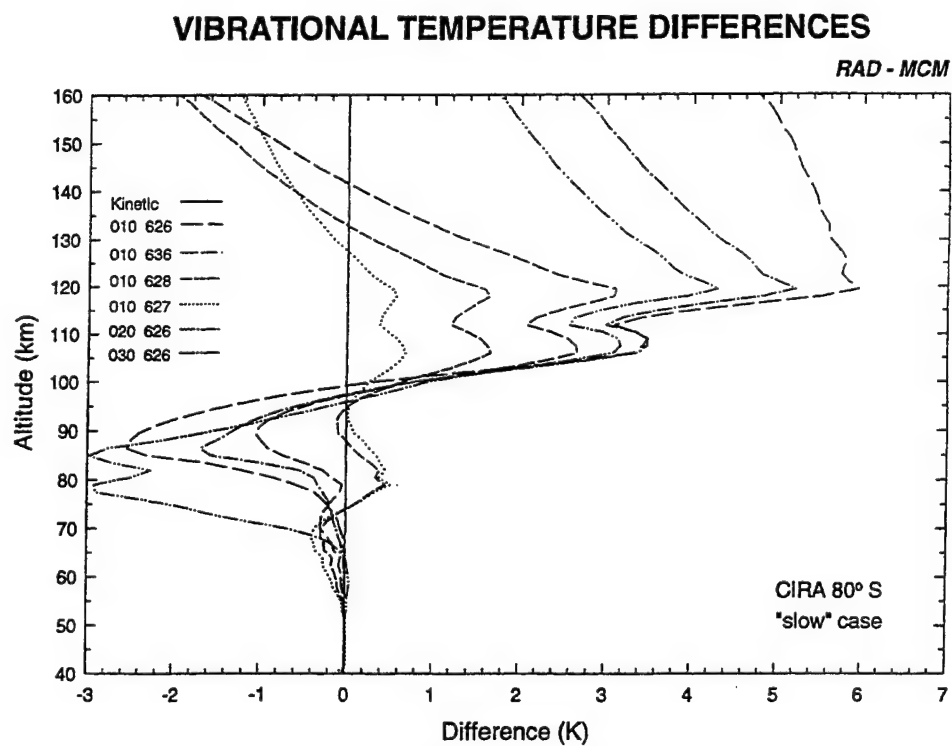
Figure 17. As Figure 16, but for the slow case.

km where retrievals would be attempted (and much less than 1 K for most of that). For the CIRA 80^0 S model, there were differences approaching 2 K near the cold summer mesopause for most states, and a difference near 3 K for the 03301 state. Both models find that the major-isotope 01101 state is quite close to LTE at mesopause, even the cold summer polar mesopause (80^0 S model). In the lower thermosphere the MCM calculation consistently predicts lower vibrational temperatures, the maximum discrepancies being typically 3 or 4 K in a region between 110 and 120 km, with smaller differences at higher altitudes.

For the slow cases, which provide the best tests of the radiative transfer algorithms, both models of course predict much lower thermospheric vibrational temperatures over-all. The discrepancies in the model results were somewhat greater than for the fast cases, as expected, but absolute differences were still less than 2.5 K for the midlatitude and 80^0 N models for all bands, and much less in the mesosphere for the band of prime interest for retrievals. For the stressing 80^0 S case, the largest absolute differences were less than 3 K in the mesosphere and 6 K in the thermosphere. The MCM model consistently predicts lower vibrational temperatures in the thermosphere and higher ones at the mesopause.

Cooling rates for the mid-latitude atmosphere are shown in Figures 18 and 19, the latter including a breakdown according to groups of bands. At low altitudes, the cooling is the same for the fast and slow cases, but in the thermosphere it is greatly elevated for the fast case. In the lower mesosphere, the absolute difference in total cooling between the models is less than 0.5 K/day, or 6 to 8%, for all atmospheres. In the upper meso-sphere and thermosphere, differences are not significant for the slow cases, and are less than 3 K/day at all altitudes for the fast cases. Percent differences on the order of 25% are seen, but only at altitudes just below the mesopause where the cooling itself is very small.

A number of significant conclusions can be drawn from this study. First of all, the two radiative transfer algorithms do give consistent results for both the vibrational popu-lations of the $CO_2(v_2)$ states and the cooling rates of the 15 μm bands originating in them. The agreement extends to strong and weak bands, to a large range of altitudes, to the most likely extreme temperature structures, and to a large range of atomic oxygen deactivation rate constants. This confirms the expectation that retrieval of kinetic temperature is feasi-ble at least up to the mesopause using the MCM approach, which of course runs faster than the line-by-line (LBL) calculation performed by RAD. It also corroborates results, first obtained from the ARC calculations, for greatly elevated vibrational temperatures and atmospheric cooling in the thermosphere due to collisions with atomic oxygen.
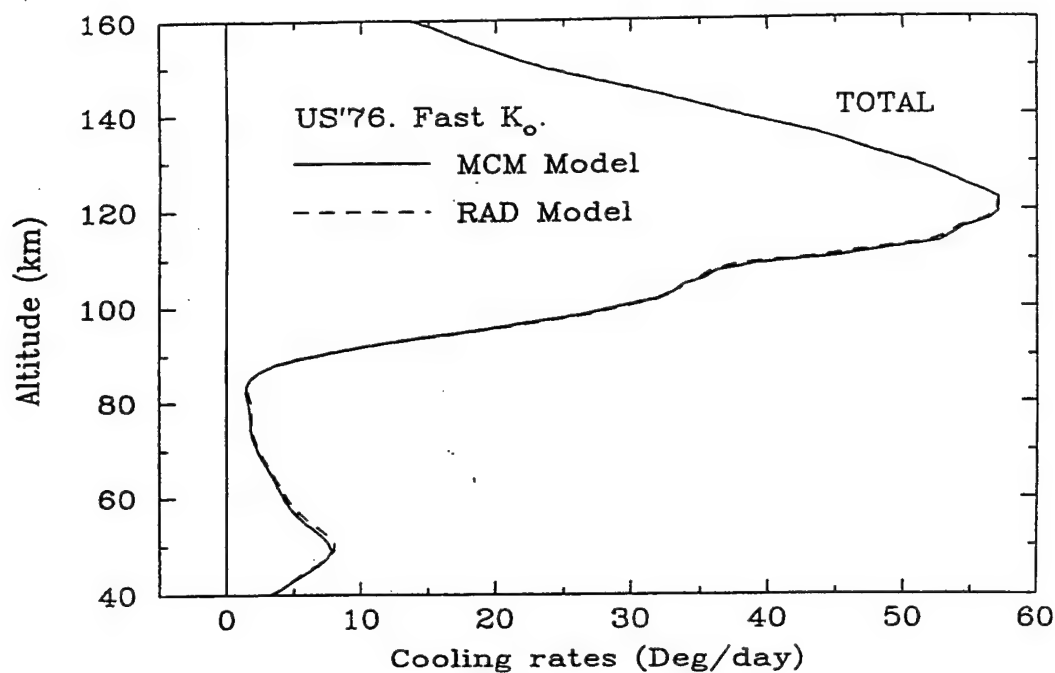
Figure 18. Comparison of total cooling rate due to 15 μm emission as calculated by MCM and RAD, for the mid-latitude model and the larger atomic-oxygen rate constant.
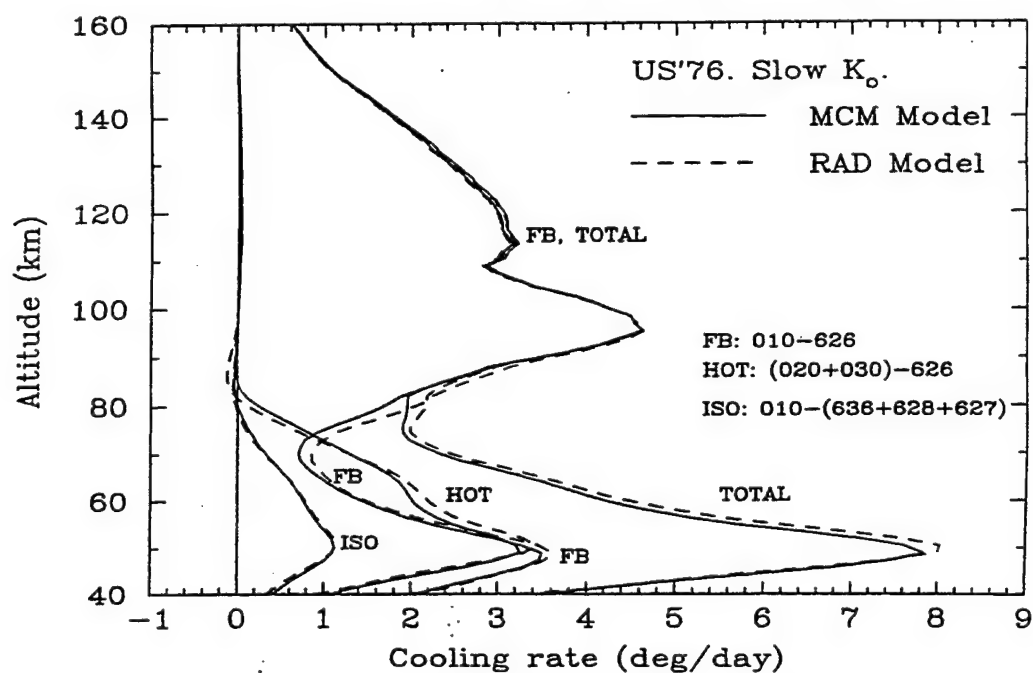
Figure 19. Comparison of the total cooling due to 15 μm emission as calculated by MCM and RAD for the mid-latitude model and the slow case. Contributions from the 626 fundamental band, the minor-isotope fundamentals, and the hot bands are also shown.

Another important conclusion has to do with the reasons for the discrepancies in vibrational temperature that did persist. By greatly reducing the size of the groups of lines used by MCM, that is by essentially performing a LBL calculation for the 626 fundamental band, discrepancies in the upper region of the calculation were reduced, but a general pattern of differences still persisted. More importantly, by studying the radiative contributions of the different atmospheric layers at several observation points in the MLT region, where RAD predicts greater absorption of upwelling radiation and therefore higher vibrational temperatures, we came to the conclusion that the residual discrepancies were due to the path-average lineshape that is used in the MCM algorithm, in contrast to the variable-lineshape approach in RAD. That is, the approximation of using mass-weighted pressures and temperatures to calculate the absorption lineshapes consistently results in small overestimates of Earthshine absorption (compared to the RAD calculation) at some altitudes and small underestimates at other altitudes, the amount and sign of the discrepancies being primarily dependent on the temperature structure above and below the altitude of interest. Thus, the larger discrepancies were observed for the CIRA 80^0 S model atmosphere, with its very cold mesopause largely responsible for greater differences in the absorption lineshapes at different altitudes than occur with the other model atmospheres.

To see this more clearly, we note that for observation points in the thermosphere, MCM generally calculates less absorption than RAD from layers below the mesopause and more absorption from layers above it. This is illustrated in Figure 20. In Figure 21 a similar pattern appears for a higher point in the thermosphere, although the changeover comes at about 80 km rather than the mesopause. At thermospheric altitudes the MCM path-weighted temperatures used for the absorption lineshapes are a little smaller than they should be, although the pressure is a little greater. The absorption lineshapes are therefore somewhat narrower, resulting in less absorption in the wings due to warmer lower-altitude source regions and more in the line centers due to colder higher-altitude regions. As a result, MCM calculates less total radiative excitation in the thermosphere and slightly lower vibrational temperatures than RAD does.

For observations near the mesopause, on the other hand, the MCM path-weighted temperature is greater than it should be, as is the pressure. The absorption lineshape is therefore broader than the RAD lineshape, resulting in more absorption in the wings and less in the line centers. Therefore, in this case MCM should calculate somewhat greater excitation rates than RAD, as it does.

Another conclusion, following from this observation, is that the models' differences are not due so much to their very different numerical schemes (inversion vs. iteration) but
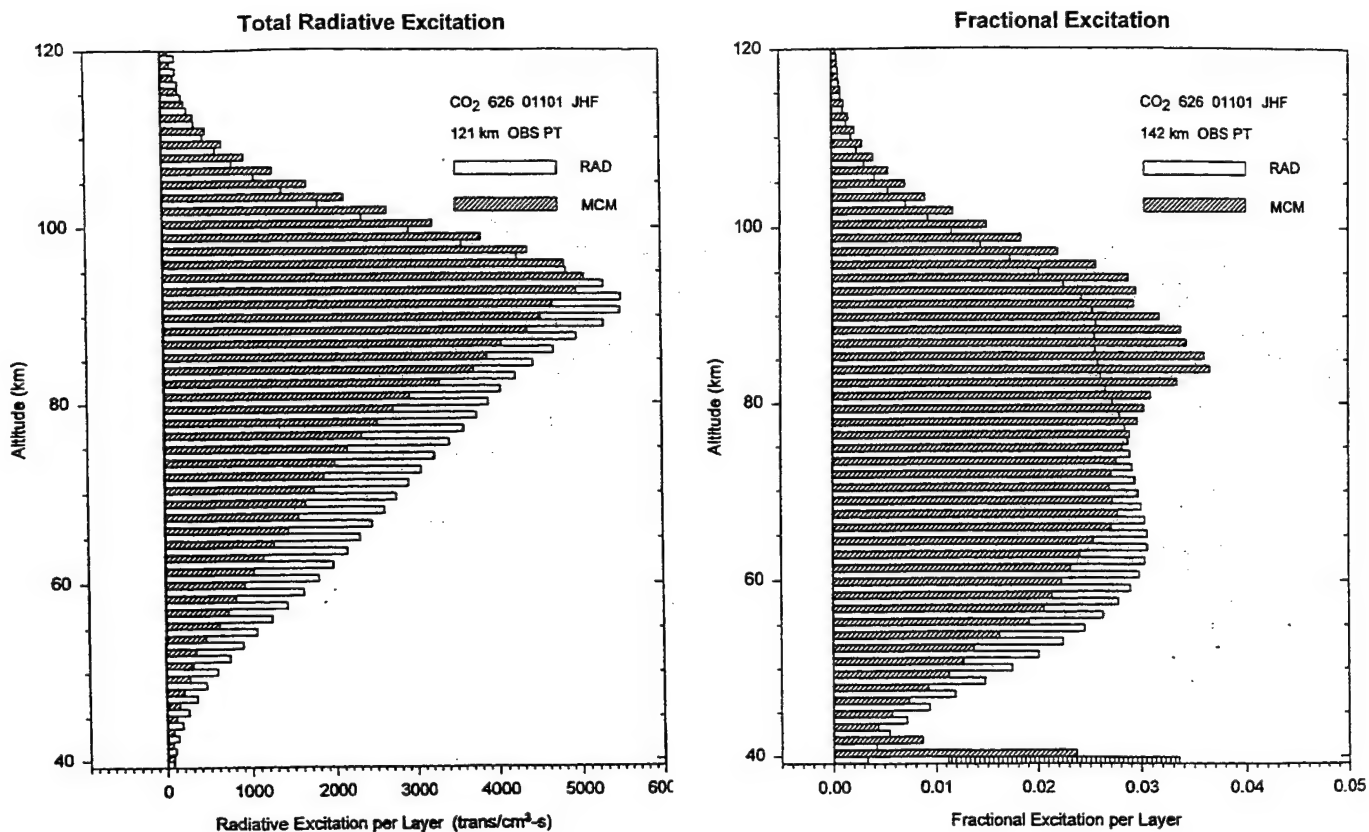
Figure 20. (left) Total radiative excitation rates due to layers between 40 and 120 km for the CO_2 626 01101 state, for an observation point at 121 km. The lower-boundary contributions are negligible. The calculation was for the slow case and the mid-latitude model.

Figure 21.(right) As in Figure 20, except the fractional radiative excitation is plotted for an observation point at 142 km. The lower-boundary contributions are shown below 40 km.

rather to a detail of the MCM algorithm. Yet another is that small altitude-dependent biases in kinetic temperatures retrieved using an MCM non-LTE model can be estimated from these patterns.

It is important to note that the magnitude of the discrepancies that we have identified is smaller than errors that we would expect to be induced by approximations built into both models, so the radiative transfer algorithms are validated as they stand. The discrepancies are also smaller than uncertainties that are inherent in characterizing the actual state of the atmosphere for most simulations, so it is fair to say the model formulations are valid as well. Last of all, the consistency of the cooling rates shows that the algorithms are accurate enough to be used in dynamical models of the middle atmosphere and the MLT region.

2.3 Gravity Waves and Atmospheric Cooling

Many studies have been, and are being, conducted to investigate detailed structure (as opposed to climatological or average structure) in the temperature profile of the mesosphere and lower thermosphere, and its role in determining the thermal balance and optical signature of the region. Upward-propagating gravity waves are one significant source of such structure, as is known from theoretical treatments, experimental observations, and extensive modeling. Using the ARC codes, we looked at the effect of gravity wave structure on infrared atmospheric cooling of the MLT region.

It is well known from modeling studies, using average climatology, that emission in the CO_2 15 μm bands constitutes the most important mechanism for cooling the lower thermosphere. It is less well known how this emission, and the resulting cooling, is perturbed by the presence of waves and other disturbances. The fact *(Goody and Yung, 1989)* that, under some conditions that are more descriptive of the stratosphere and lower mesosphere, the infrared cooling is proportional to the *curvature* of the kinetic temperature profile (regarded as a function of altitude) suggests that the large perturbations that accompany wave activity should produce very large changes in the instantaneous local cooling rates.

To evaluate this possibility, we made use of a realistic gravity-wave model (U.B. Makhlouf, private communication) to provide input for our ARC codes, and calculated the $CO_2(v_2)$ vibrational temperatures and cooling rates. The assumption implicit in submitting such a problem to the RAD code is that the horizontal wavelength of the disturbance is large compared to the vertical wavelength and the mean free path of photons in the horizontal direction, so that the 1-d formulation is adequate to handle the radiative transfer. Although the mean free path condition ultimately breaks down at the higher altitudes, the principal 15 μm bands are sufficiently optically thick that it is a good approximation throughout the region where the wave model is reliable. (Moreover, *all* the bands are optically thick in the regions where they individually contribute significantly to the total cooling.) At the higher altitudes, rather than simulating wave breaking, we used exponential damping to a maintain reasonable 1-d structure.

In conducting this study, we started with a model atmosphere similar to the U.S. Standard Atmosphere (1976), except that the temperature profile was smoothed to eliminate discontinuities in its gradient. We obtained gravity wave perturbations to the temperature and the density profiles of CO_2, N_2, O_2, and atomic oxygen. This was done for three separate cases, characterized by vertical wavelengths of 8, 13, and 25 km. We then

constructed input model atmospheres corresponding to eight different phases of each of the waves. The phases were equally spaced from 0 to 2π.

Figure 22 shows the ambient kinetic temperature profile, along with the perturbed temperature for four of the eight phases of the 13-km wave in the 80-130 km region where the maximum effects are seen. Above 130 km the wave damps out rapidly, and below 80 the perturbations are quite small.

In Figures 23 and 24 we plot vibrational temperature profiles for a single phase for the most important bend-stretch states. Figure 23 shows, as one expects, that the vibrational temperature of the 01101 state of the principal isotope tracks the kinetic temperature fairly closely up to the mesopause. Because the 626 fundamental band is optically thick, excitation due to absorption of radiation is primarily from local source regions. It thus mirrors the rate of absorption due to the thermal processes to a considerable extent, and despite the substantial perturbation of the emission rates within fairly short altitude ranges this maintains the 01101 level relatively close to LTE. Nevertheless the kinetic-temperature excursions due to the wave are not completely reproduced, and non-LTE conditions are considerably enhanced within the rather localized regions where the wave produces the greatest departure from ambient conditions.
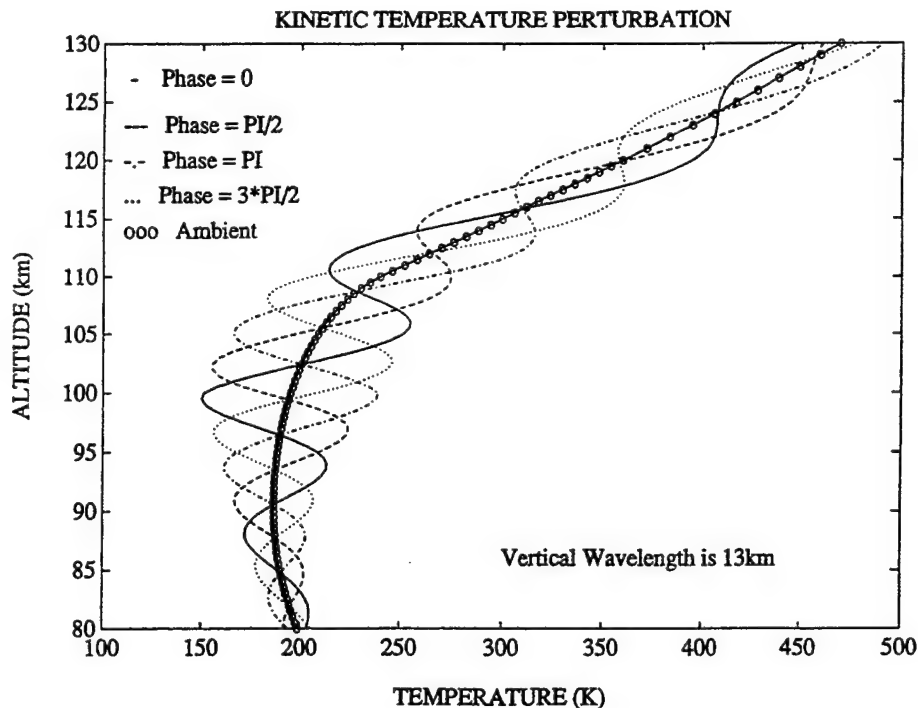
Figure 22. Gravity-wave perturbation of the kinetic temperature, for four phases of the wave with the 13-km vertical wavelength.

23
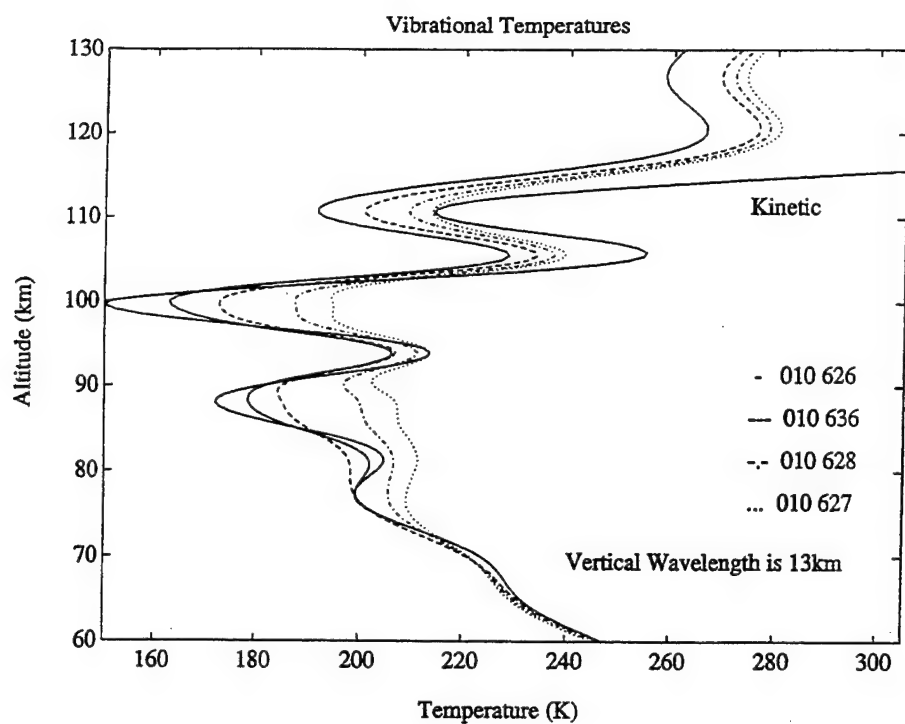
Figure 23. Vibrational temperatures of the CO_2 01101 state for one phase of the wave with the 13-km vertical wavelength, for four isotopes.
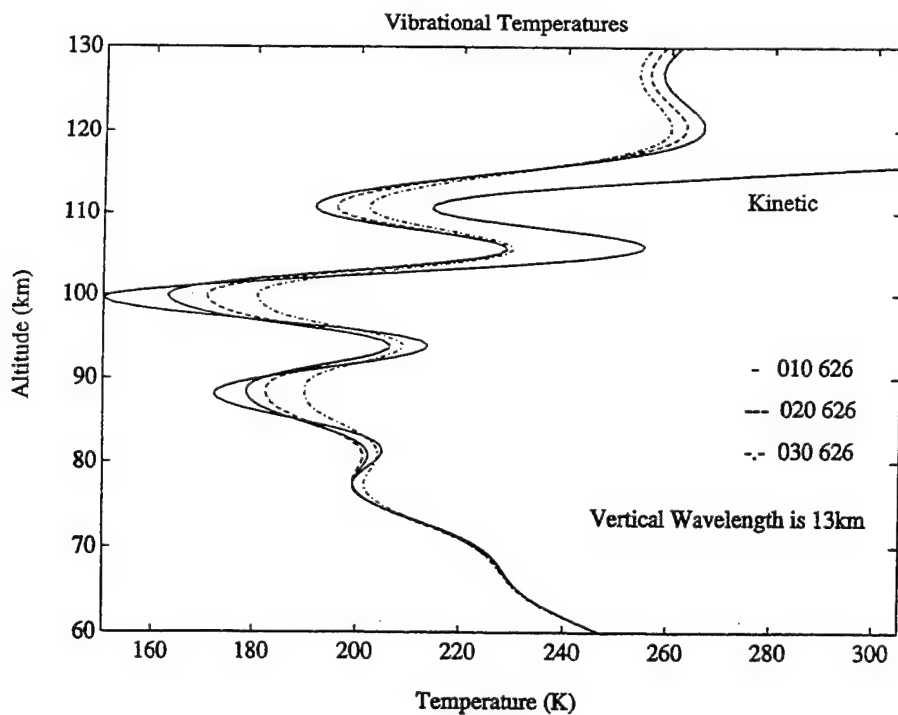
Figure 24. Vibrational temperatures of the CO_2 01101, 02201 and 03301 states for one phase of the wave with the 13-km vertical wavelength, for the 626 isotope.

The minor isotope 01101 states deviate much more from LTE than the 626 state does. Compared to the 626 case, the lower opacity of the infrared bands expands the source regions from which incoming photons are absorbed, primarily to lower altitudes. Thus a larger fraction of the absorption comes from a less strongly perturbed region, and in addition there is the effect of greater averaging over conditions of enhanced and diminished emission. This produces a smaller modulation of the radiative excitation, and one that has a different pattern from that of the thermal excitation, so the deviation from LTE is a lot greater.

Figure 24 shows the vibrational temperatures of the 626 higher excited states, as well as that of the 01101 state. Here the radiative excitation rate in each band is as strongly influenced by the vibrational population of the lower state as by the opacity of the hot bands, which are comparable to those of the minor-isotope fundamentals. Since the lower-state populations are strongly influenced by the wave in these cases, the 02201 and 03301 vibrational temperatures deviate from LTE less than the minor-isotope 01101 states do.

The behavior illustrated in Figures 22 through 24 is similar for waves with longer and shorter wavelengths, and also for different phases of the waves.

The total cooling due to the 15 μm bands for four phases of the 13-km wave is shown in Figure 25, where it is compared to the cooling calculated using the ambient profiles. Between 85 and 110 km, the excursions in this instantaneous cooling rate are truly enormous, ranging upwards of 50 K/day at some points. In fact, the excursions are greater than the absolute cooling over much of the MLT region, and at any moment nearly-adjacent regions are strongly heated and (more) strongly cooled.

It is important to note that our calculation cannot account explicitly for temperature feedback that might damp the wave and diminish these effects. Nor can it account for diffusion or dynamical effects that might mix the layers and alter the structure in other ways. Thus it does not provide a full description of the influence of a gravity wave on the MLT region, but rather indicates the approximate magnitude of effects that need to be accounted for. For waves with relatively short periods, the time available for competing processes to apply themselves may be too short to appreciably alter the cooling rates we have calculated, but we cannot test this hypothesis at the present time.

It also should be noted that the long-term effect of the passage of a wave cannot be determined by a snapshot view. As the wave propagates, regions of enhanced cooling become regions of diminished cooling, so the important quantity is not an instantaneous cooling rate, like what is shown in Figure 25, but rather the cooling averaged over the period of the wave. Figure 26 compares the ambient cooling with the average cooling for

INSTANTANEOUS COOLING

130 ┬
125 ┤
120 ┤
115 ┤

- Phase = 0
-- Phase = PI/2
-.- Phase = PI
... Phase = 3*PI/2
ooo Ambient

Vertical Wavelength is 13km

ALTITUDE (km)

130, 125, 120, 115, 110, 105, 100, 95, 90, 85, 80

COOLING RATE (K/day)
-20   0   20   40   60   80
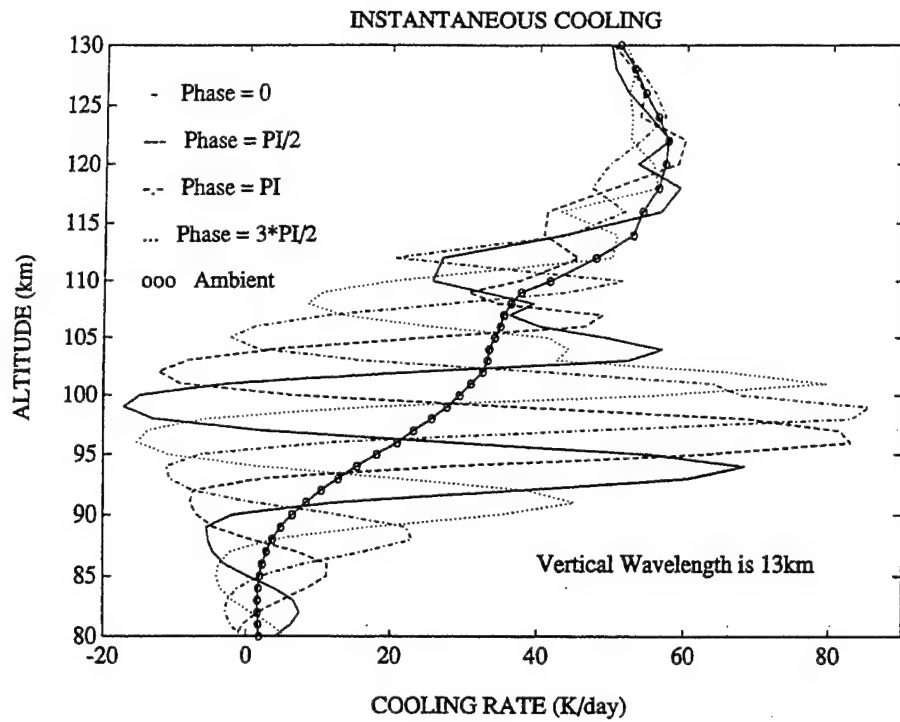
Figure 25. Instantaneous cooling due to the 15 μm bands, for four phases of the wave with the 13-km vertical wavelength.

AVERAGE COOLING

-- Vertical Wavelength = 8km
-.- Vertical Wavelength = 13km
... Vertical Wavelength = 25km
ooo Ambient

ALTITUDE (km)

130, 125, 120, 115, 110, 105, 100, 95, 90, 85, 80

COOLING RATE (K/day)
0   10   20   30   40   50   60
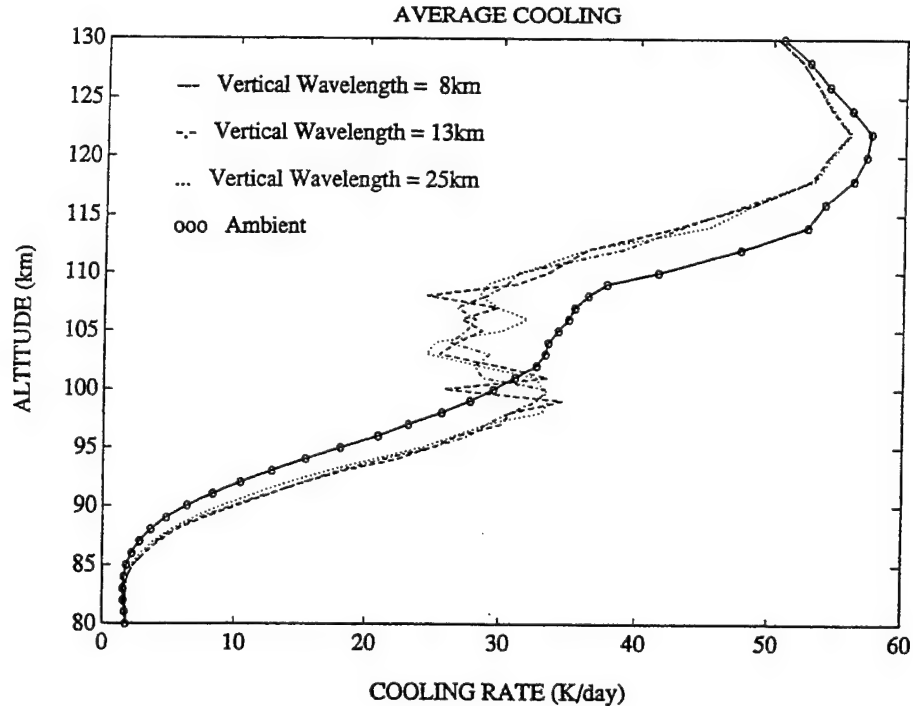
Figure 26. Cooling due to the 15 μm bands, averaged over the period of the wave, for the three modeled waves and for the ambient atmosphere.

26

the three waves we considered. (The latter was obtained by numerically integrating the cooling results for the different phases.) Although the average cooling is much more similar to the ambient cooling than to the instantaneous cooling at any moment, the effect of the wave clearly does not average out to zero. Rather, it enhances the cooling below approximately 100 km and diminishes it at higher altitudes, more or less independent of the wavelength. The amount of the change also appears not to depend on wavelength, and it exceeds 30% of the ambient cooling over a considerable portion of the altitude range between 90 and 115 km.

One can reasonably ask why a periodic disturbance, even one with an altitude-dependent amplitude, should produce changes that are so clearly asymmetric about the ambient cooling. In fact, the photon emission rates do not necessarily fluctuate in a symmetric fashion, and there is also a strong bias on the direction in which radiant energy is transported because of the density and opacity of the atmosphere. The exact reason for the behavior shown in Figure 5, however, remains an open question. We do think that these results indicate that radiative transfer in the 15 μm bands must be treated very carefully when the thermal balance of the MLT region is being evaluated.

As an addendum, we note that considerable effort was required to validate the cooling algorithm used by RAD before we were able to carry forward this work on gravity-wave structure. As noted above, in the limit of optically thick bands the cooling can be shown analytically to be proportional to the curvature of the temperature profile. In principal, then, a linear piece-wise continuous temperature profile with a discontinuous slope at each layer-boundary produces infinite cooling. In practice, numerical algorithms operating on thick (but not perfectly thick) bands do reflect the degree to which the slope of the temperature profile changes at the observation points, by producing sharply peaked cooling rates. (See Section 3.3.4.1 for a brief mention of observation points in RAD.) As a result, there can be unexpected consequences if the input temperature profile is not carefully chosen.

To further elucidate this point, consider the U.S. Standard Atmosphere in regions where near-LTE conditions prevail. The kinetic temperature profile is constant over a range of several kilometers at the stratopause and has constant slopes in the upper stratosphere and lower mesosphere. In a very thick ro-vibrational line the difference between the rates of photon emission and absorption, which is proportional to the cooling, is only affected by the two layers straddling the observation point. Each of these layers is characterized by its average temperature. If the slope is constant and negative, then the greater absorption of photons from the lower layer (due to the higher temperature there) and the lesser absorption from the upper one (due to a lower temperature) gives an overall ab-

sorption rate that is almost exactly balanced by the emission rate at the point in between, and there is no cooling. On the other hand, if the slope is zero on the lower side and negative on the upper side, then the lower layer's temperature is the same as that at the observation point, this balance is upset, and substantial cooling does occur.

Figure 27 illustrates the consequences of these facts. It shows the upper stratosphere and lower mesosphere temperature profiles for three model atmospheres, and the associated cooling calculated by RAD. The U.S. Standard Atmosphere produces the unphysical spiked profiles in the cooling rate. (Note the noise appearing at 73 km, where there is another discontinuity in the slope.) The "A65" profile, which is a carefully-smoothed approximation to it, produces a much more realistic result. The double peak resulting from the "A71" profile is a result of its flat stratopause.
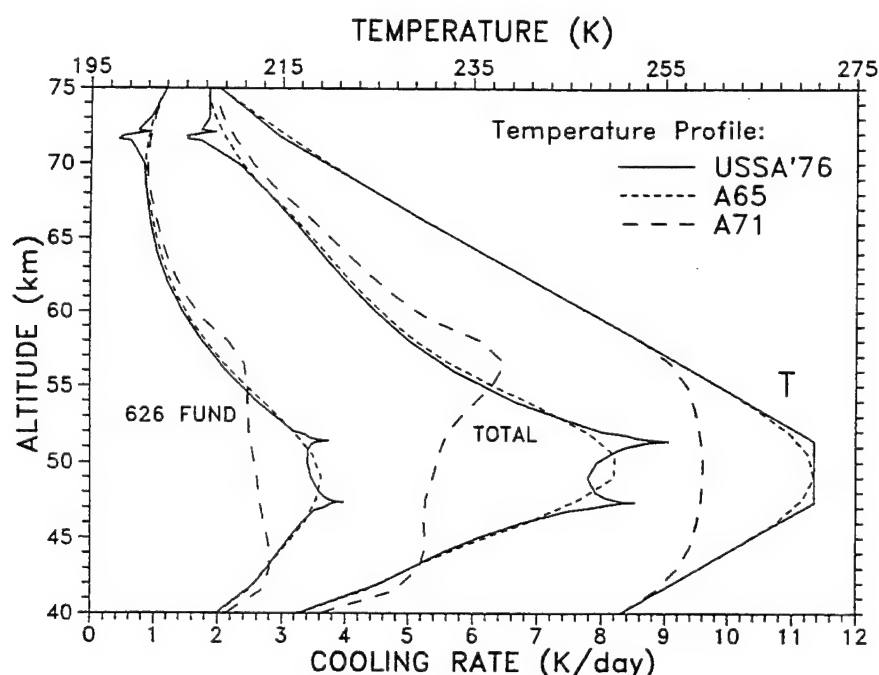
Figure 27. Kinetic temperature profile (upper scale) for three model atmospheres, and the associated CO_2 infrared cooling (lower scale). Both the total cooling and the contribution of the thick 626 fundamental are shown for all three cases.

It is important to note that the spikes are not the result of layering that is too coarse, but rather represent the actual cooling that an atmosphere with such structure would produce if it existed. The curve plotted in Figure 27 was done with very fine layering in the vicinity of those points. With much coarser layering one gets a jagged cooling profile with a big noise signal, in which case the results in fact do not represent an actual cooling rate very accurately.

28

While the U.S. Standard Atmosphere is an extreme example, one lesson of this is that temperature profiles with sharp breaks in slope can cause rather peculiar problems. Another is that difficulties can also arise even in physically realizable temperature structures if the layering is not sufficiently fine in comparison to the vertical dimensions of the structure. Both points are significant for calculations like those presented earlier in this section, but our validation efforts showed that they can also be important even for profiles with a much more benign appearance.

2.4 4.3 μm Data Analysis and Modeling

The CIRRIS database, obtained during the STS-39 mission in April 1991, provided a rich source of spectral infrared data in limb-viewing geometry. We looked at some of these data, both qualitatively and with quantitative model calculations. We also developed some spectral analysis techniques to evaluate certain features that cannot be modeled *ab initio*.

We examined CIRRIS data in the 2200-2450 cm^{-1} (4.3 μm) range, looking at limb paths through the mesosphere and thermosphere, up to tangent heights of almost 200 km where instrumental noise dominates the spectra. Up to about 140 km, this spectral region is dominated by $CO_2(v_3)$ emissions. Distinctly different physical processes are responsible for the bulk of the emission at night, in the daytime, and during auroral events. Nighttime scans in the mesosphere also include prominent OH transitions in the 9-8, 8-7, and 7-6 bands, and daytime spectra for limb paths with tangent heights above 100 km reveal very prominent lines of NO^+ that had not been seen prior to the CIRRIS observations. In fact, the $NO^+(1-0)$ signature appears strongly in the high-latitude dayglow and the auroral nightglow, less strongly in the low-latitude dayglow and the ambient nightglow. There are auroral enhancements of CO_2 and NO^+ emissions, as well.

2.4.1 Spectral Data Analysis

Infrared spectral data sets are often analyzed by fitting individual spectra using sets of basis functions to account for the contributions of different bands of different emitters. The normal process is to use weighted least squares techniques, which often have the capability of unraveling complicated spectra to reveal and identify even the less important components (e.g., *Dodd et al, 1994*). The relative contributions of different bands are determined from the factors multiplying the basis functions that are found to produce the best overall fit. For some conditions, excited-state emitter column densities can be extracted from these amplitudes.

One reason that the analysis of limb spectra can be quite complicated is that the basis functions, constructed *a priori* from forward models, may reflect atmospheric conditions that are at variance with the actual state of the atmosphere at the time and location of the data-taking. In particular, since the local temperature determines the rotational distribution of emitting states, the shape of the basis functions may be affected. Also, as a result of the viewing geometry, the data reflect the conditions of the atmosphere averaged over the path rather than the conditions at any particular altitude. For optically thin emissions, this is not such a great problem, because the altitudes near the tangent point are heavily weighted in this path average, both by the longer geometrical segments and by the greater atmospheric densities in the lower-lying regions (except for layered emissions like OH). But for optically thick emissions, this is not necessarily true.

A second complication is that, despite exhaustive efforts that are usually given over to calibrating the instruments, small wavelength shifts may still be found in the spectral data, producing offsets between the peaks in the data and the corresponding peaks in the basis functions. Such offsets can completely immobilize a fitting algorithm that is not prepared to deal with it, or—worse still—produce erroneous results. Moreover, shifts that do occur may be nonuniform, making it impossible to remove them with a simple adjustment of the independent variable. In earlier analyses of data from the Field Widened Interferometer *(Espy et al, 1988)*, shifts on the order of 0.2 cm^{-1} in data characterized by instrumental resolution of about 1.2 cm^{-1} made it impossible for us to fit many of the spectra that were available.

The CIRRIS data, having a resolution on the order of 1 cm^{-1}, were characterized by non-uniform wavelength shifts as great as 0.2 cm^{-1} throughout this region. In order to extract radiances due to the different bands and emitters from the individual spectra, it was therefore necessary to develop and implement a piece-wise fitting method that looked at small segments of the spectral region independently. First of all, basis functions were calculated for all bands that were expected to be significant. For CO_2 this was done by constructing a model atmosphere and running the ARC codes to produce synthetic spectra for each band. For the optically-thin OH and NO^+ emissions, HITRAN lines or (for NO^+) equivalent lines that we calculated on our own were used to construct spectra characterized by the modeled rotational temperature of the tangent point. The synthetic spectra were all normalized to unit band radiance. Then the spectral range was divided into blocks 40 cm^{-1} wide, and each such block was fit separately using a non-linear least squares algorithm. The blocks were actually chosen to overlap each other, so the centers of consecutive blocks differed by only 20 cm^{-1}. One of the parameters to be fit was a wavelength offset that allowed the basis functions to be shifted within each block by a

constant amount, constrained to be less than the typical separation of CO_2 rotational lines in this region.

Since, in principal, fits in different blocks produce different results for the same bands, it was necessary to iterate the process to insure a consistent set of results for the entire spectral region. After all the blocks were analyzed, then, the fit amplitudes of each band that was found to contribute significantly were themselves fit to functions that provided a smooth variation across the entire region, and the basis functions within each block were adjusted according to the value of this function at the center of that block. The process was then repeated using the new basis functions, until eventually a convergence criterion was satisfied and the calculation was cut off.

This procedure was quite successful in extracting integrated band radiances for the principal CO_2 and NO^+ bands, especially at high altitudes where the signal consisted of only a few principal components. The convergence was usually rapid, and the wavelength shifts varied consistently (smoothly) from block to block. The convergence is shown in Figure 28, where the $CO_2(\nu_3)$ fundamental band radiance extracted from a high-altitude spectrum by this algorithm is plotted as a function of the iteration number. This particular calculation was forced to run for 10 iterations.
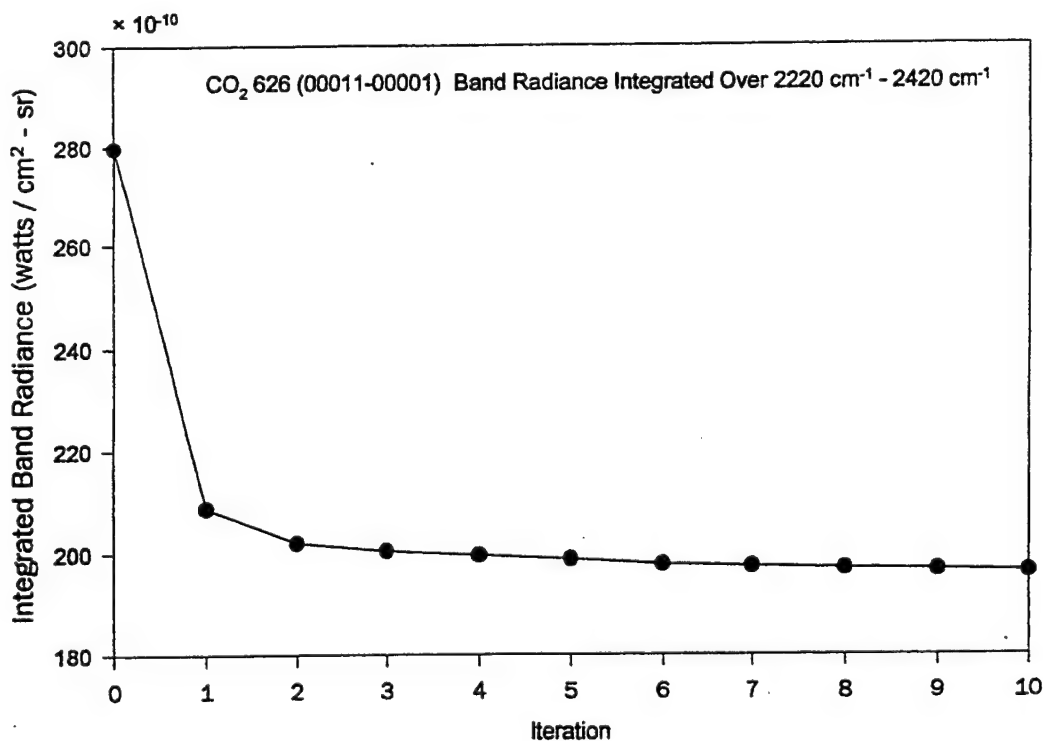
Figure 28. Convergence of iterative fitting algorithm for $CO_2(\nu_3)$ fundamental band.

31

As an example of the procedure, Figure 29a shows a set of 13 co-added daytime scans for a tangent height of approximately 120 km, with the P and R branches of the 626 $CO_2(\nu_3)$ fundamental appearing prominently about the 2349 cm^{-1} band origin and NO^+ lines superposed on the noise background at the long and short-wavenumber ends of the spectrum. (Note that co-adding spectra with similar tangent heights was often necessary for high-altitude scans to improve the signal to noise ratio.) The fit to this spectrum is given in Figure 29b, where the NO^+ lines are more obvious because of their regular spacing. The residuals are plotted in Figure 29c, and show that even with the wavelength shift implemented there are some features that are not totally accounted for. However, with the wavelength shift suppressed, the results are considerably worse, as can be seen from Figure 29d. One conclusion that may be reached is that the method is successful in extracting even fairly small signals (e.g., the NO^+ lines) from a noise background. Another is that correcting for the wavelength shift is important, but it appears to be insufficient to account for all the features of the experimental spectrum. In this particular case, the relatively large residuals result from the process of co-adding the individual spectra, which increases the signal to noise ratio of the observed radiance but also increases the noise in the wavelength dimension, thereby slightly broadening the peaks. The basis functions were calculated using the nominal instrumental apodization function, which was a Kaiser-Bessel function with a FWHM of 1.03 cm^{-1}, and we did not attempt to compensate for the smearing caused by the co-adding by using a broader apodization. However, the algorithm does achieve its goal, which is to extract band radiances for the principal radiators.

Figures 30 and 31 summarize some of the results that were determined from the examination of many CIRRIS spectra with tangent heights above 120 km, most of them taken at high latitudes. Figure 30 gives the CO_2 and NO^+ radiance for daytime conditions, plotted versus the tangent altitude. The high-latitude data clearly show that the NO^+ signal not only dominates the highest-altitude scans but also has a large scale height. The slow variation with tangent height is in accord with the slow variation in the density of this ion below 200 km. As expected, the CO_2 emission is much more prominent at the lower altitudes, but it has a much smaller scale height. At altitudes above 160 km the derived CO_2 radiance shows a lot of scatter, which reflects the low signal to noise ratio for this emitter above 160 km or so.

Although there are only two low-latitude points for each emitter in Figure 30, one can see from them that both the CO_2 and NO^+ radiances are substantially smaller at low latitudes. The weaker signals make it difficult to fit low-latitude spectra that have tangent altitudes above 140 km, and the low-latitude spectra are less numerous anyway. Nonethe-

Figure 29a (top) CIRRIS data in the 4.3μm region. Thirteen spectra were co-added; 29b (middle) Fit to the data in (a); 29c (bottom, top curve) Residuals from fit to the data in (a); 29d (bottom, bottom curve) Residuals from fit to the data in (a), with the wavenumber shift suppressed.

CIRRIS Spectral Fits - High Altitude
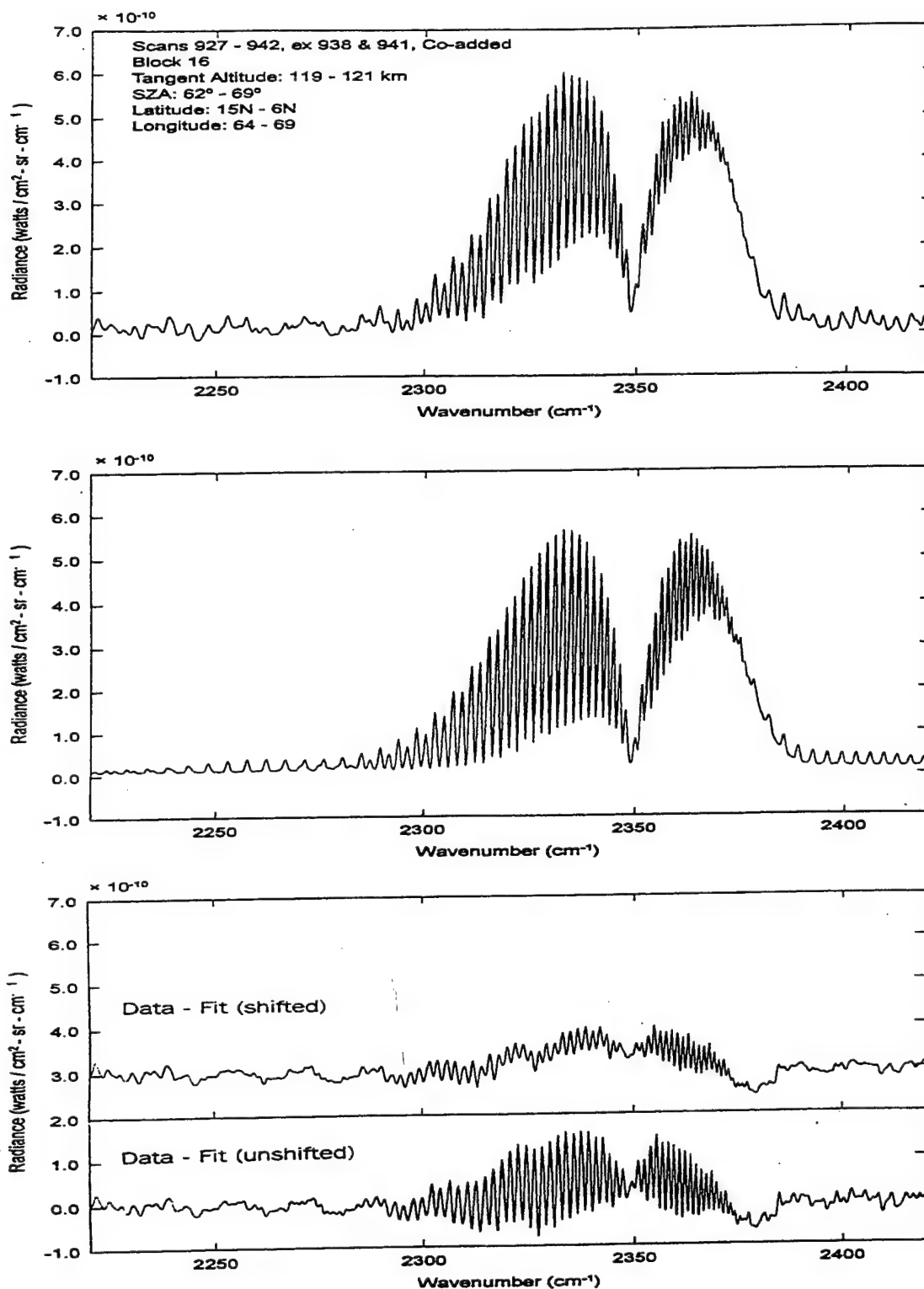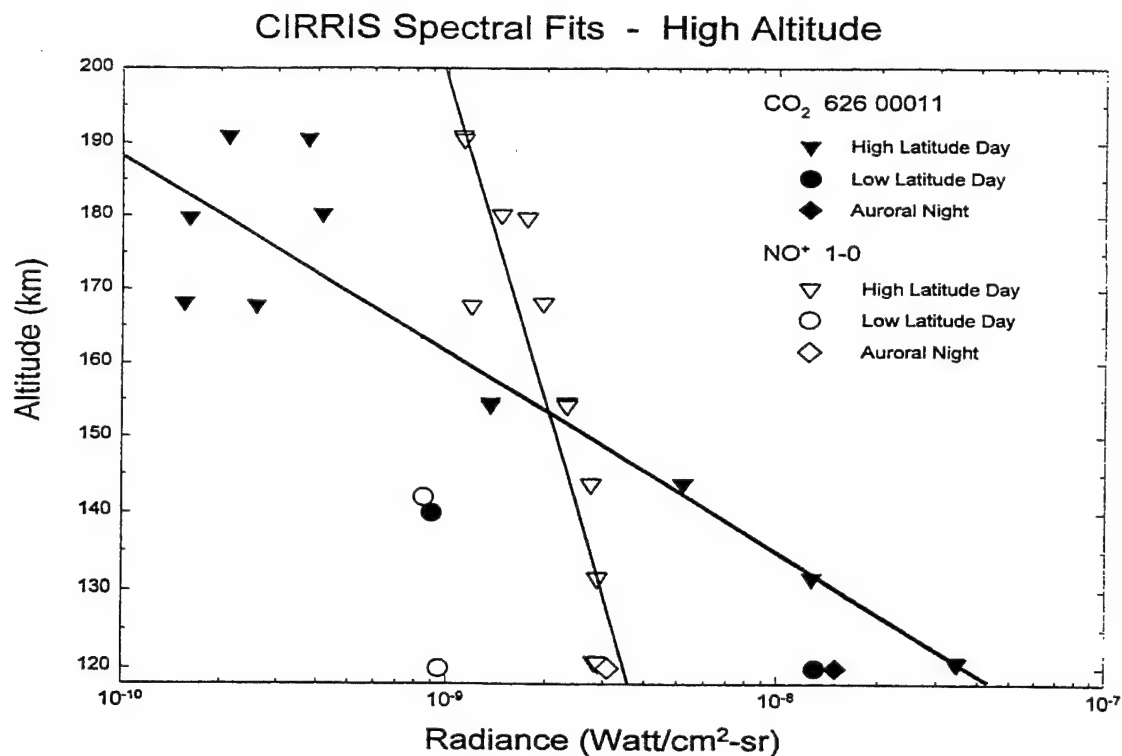
Figure 30. CO_2 and NO^+ band radiances from spectral fits to CIRRIS daytime data corresponding to tangent heights greater than 120 km. One nighttime spectrum with auroral activity is also included for comparison.
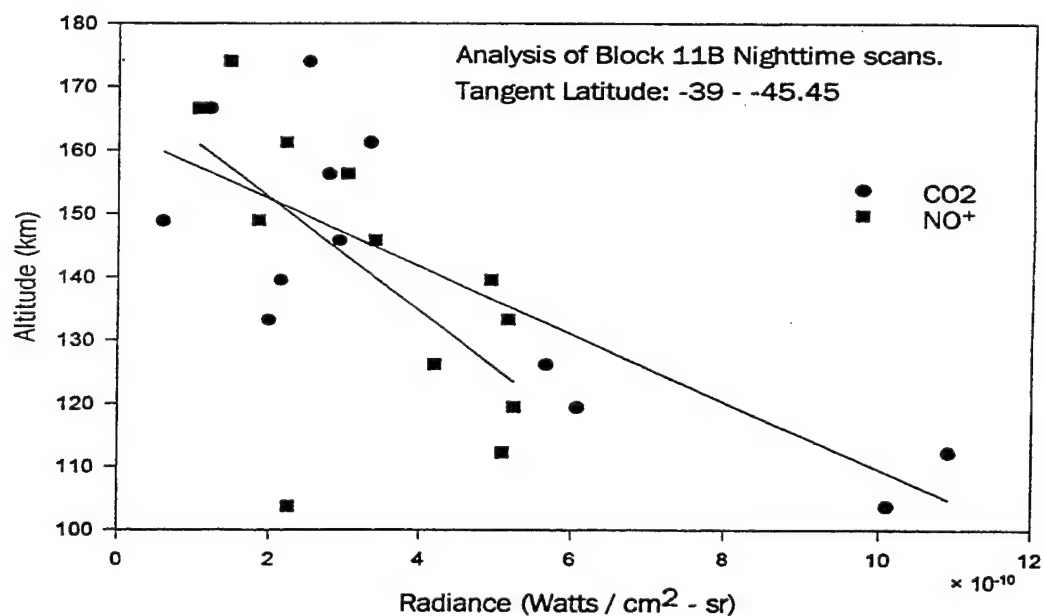
Figure 31. CO_2 and NO^+ band radiances from spectral fits to CIRRIS nighttime midlatitude data corresponding to tangent heights greater than 120 km

34

less, the high-to-low latitude differences (at least for CO_2 emissions) are consistent over the database, which includes a lot of radiometer data. Moreover, they are altitude dependent, as the limb radiance for high latitude scans is typically six to eight times that for low latitudes for tangent heights near 140 km, while the ratio is less than three near 120 km.

This variability in the radiance is, however, not in accord with climatological models, since these models do not predict latitudinal differences in CO_2 number density that are nearly this large. That is, to the extent that these optically-thin emissions reflect the density, the consistently larger high-latitude radiances cannot be explained except by a larger number of emitters. Therefore, the plots in Figure 30 constitute part of the evidence accumulated recently that CO_2 densities do have large geographical variations, and that the differences are altitude-dependent.

The emitter density is not the whole story, but it is the major reason the limb radiance varies with latitude. Another consideration, one that argues for larger rather than smaller radiances at the lower latitudes, is the solar zenith angle dependence of the upwelling 4.3 μm radiation, which results in greater excitation rates and hence more emission at high altitudes when the SZA is smaller.

Figure 31 also plots the CO_2 and NO^+ radiance against the tangent height, but for nighttime mid-latitude conditions. Because of the lack of solar pumping, the emission rate from both molecules is a lot lower than in the daytime. The NO^+ signal in particular is hard to discern, but the fitting program got significant results for some spectra down almost to 100 km.

Figure 32 gives an example of nighttime data at much lower tangent heights, a scan with a tangent height of 88 km. The primary signal is that of the $CO_2(v_3)$ 626 fundamental, with weaker CO_2 bands underlying it. The 636 fundamental contributes to the radiance in the 2250-2300 cm^{-1} region. The other noticeable feature is the presence of strong OH lines from the 9-8 and 8-7 bands. The contribution of these lines according to the ARC model is also shown. Lines from the 9-8 Q branch are seen at about 2230 cm-1, those of the 8-7 Q branch are at about 2410 cm-1, and the R and P branches of these bands, respectively, overlie the main CO_2 lines.

Figure 33 shows another nighttime spectrum, with a somewhat lower tangent height. The data are shown at the top (a), and the spectral fit results are in the middle panel (b). The fit gives significant contributions from six CO_2 bands, namely the v_3 fundamentals of four isotopes, and the first hot bands of the 626 and 636 isotopes. The in-band OH radiance for this example is about 10% of the total, which is typical for nighttime spectra with LOS passing close to the OH layer. For comparison, the bottom panel (c) shows the results of the ARC model simulation for this case.
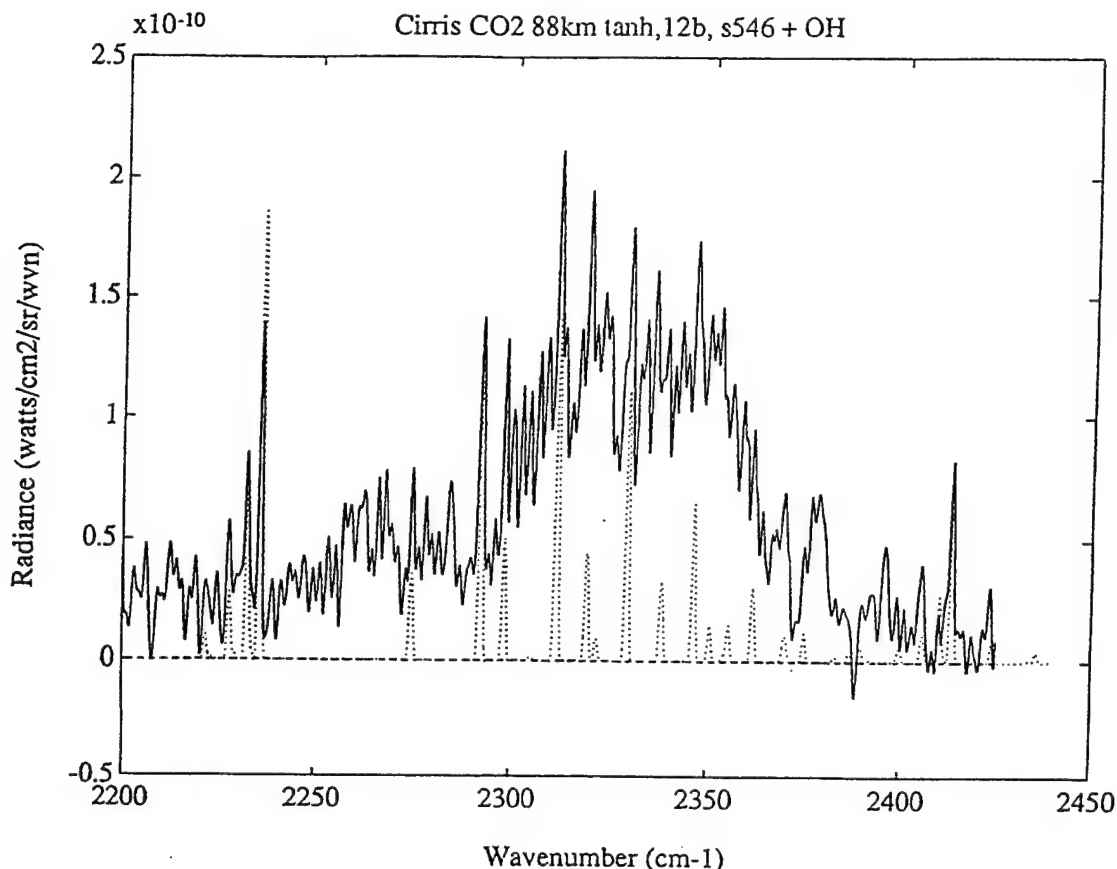
Figure 32. CIRRIS nighttime spectrum with tangent height at 88 km, with model results for OH lines superposed.

2.4.2 ARC Model Results

In addition to the spectral fitting, we did extensive modeling of the CIRRIS data and other 4.3 μm data sets. The CO_2 component of the modeling was carried out with the ARC radiative transfer codes. Most of the details of these calculations have been described by *Nebel et al (1994)* and will not be repeated here. The OH modeling used a one-dimensional dynamical photochemical model that produces the line intensities *(Makhlouf et al, 1995)*, plus the line-of-sight and synthetic spectrum codes described in Section 3.

As is well known, CO_2 4.3 μm emissions are much weaker at night than in the daytime because of the absence of solar pumping. The principal excitation mechanisms for the coupled CO_2-N_2 system are thermal processes and absorption of upwelling radiation, with the coupling effected by fast V-V transfer. Additional processes that directly excite N_2 vibration also raise the CO_2 vibrational temperatures and enhance the emission. These include auroral processes, excitation due to V-V transfer from high-lying vibrational states of nascent OH *(Kumer et al, 1978)*, and (for twilight conditions) quenching of $O(^1D)$. In addition, as noted above, the high-lying OH states themselves also emit into the 4.3 μm window.

36
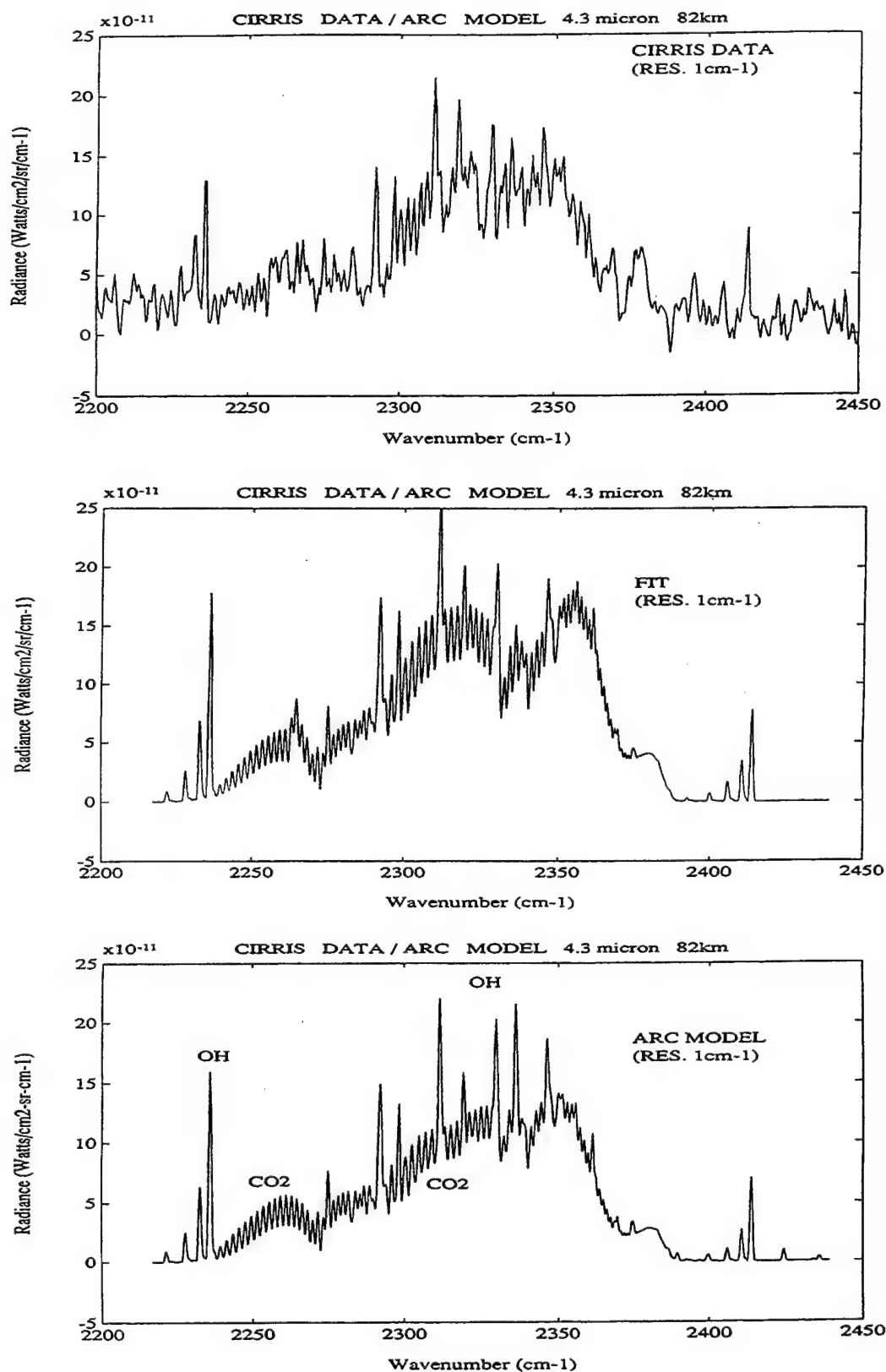
Figure 33a (top) CIRRIS nighttime spectrum for a tangent height of 82 km; 33b (middle) Spectral fit to the data in (a); 33c (bottom) ARC simulation.
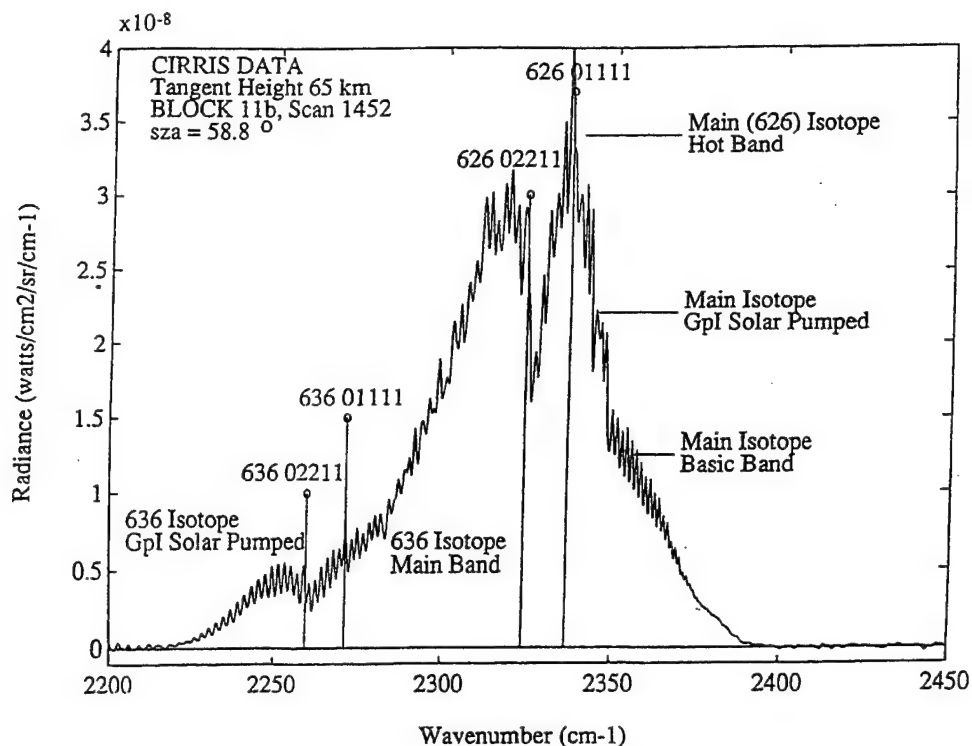
Figure 34. Daytime CIRRIS spectrum, with the principal features labeled. "GpI" refers to bands originating in the Group-1 states

In the daytime, direct solar pumping of CO_2 and $O(^1D)$ excitation of N_2 supplement the basic excitation processes. The CO_2 "group 1" states that are solar-pumped at 2.7 μm also emit at 4.3 μm. In addition, the relatively large populations in these states have some influence on the degree of excitation of N_2, and hence the other CO_2, states, because the V-V reaction proceeds strongly in that direction.

As a point of reference, some daytime spectra are shown in Figures 34 and 35. In Figure 34, the bands originating in the Group 1 states are dominant, as is typical in the mesosphere. The opacity of the 626 v_3 fundamental limits its prominence, but the R branch is clearly identified. Several hot-band Q branches are also clearly seen. Figure 35 compares spectra taken at successively greater tangent heights in the thermosphere.

Our modeling of the 4.3 μm region included assessments of the extent to which several of the supplementary mechanisms mentioned above are significant for the nighttime and daytime calculations. The following is a very brief synopsis of the results.

2.4.2.1 OH

The influence of OH on the 4.3 μm limb radiance is indicated in Figure 36. In this plot, the radiance due to CO_2 excited by the basic nighttime processes, as modeled by ARC for conditions appropriate for CIRRIS nighttime scans, is shown as a solid line. In addition, we show the radiance due to CO_2 with V-V transfer from nascent OH included
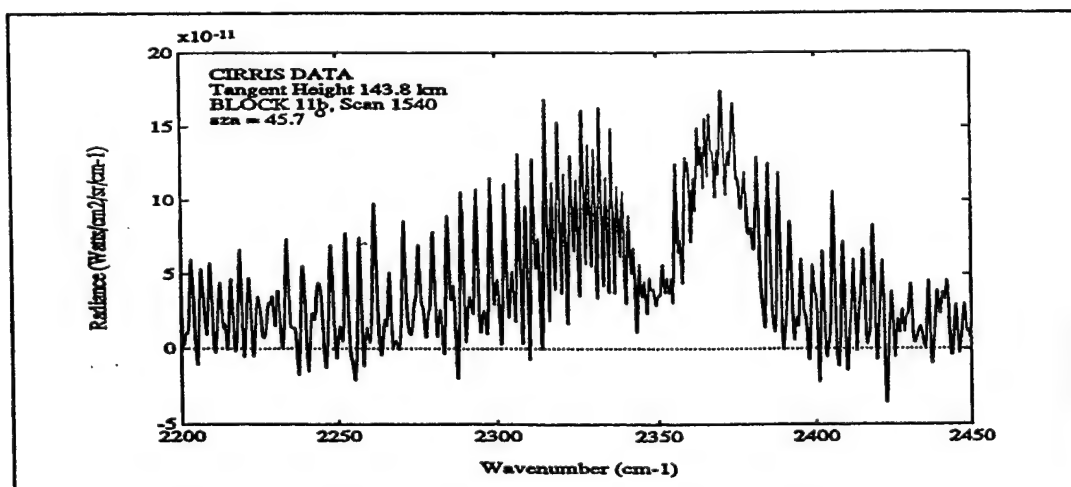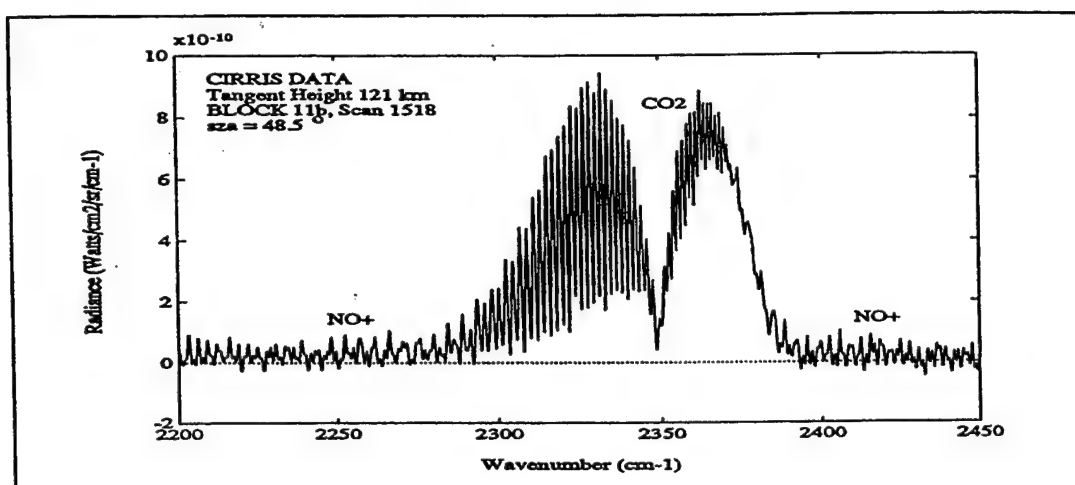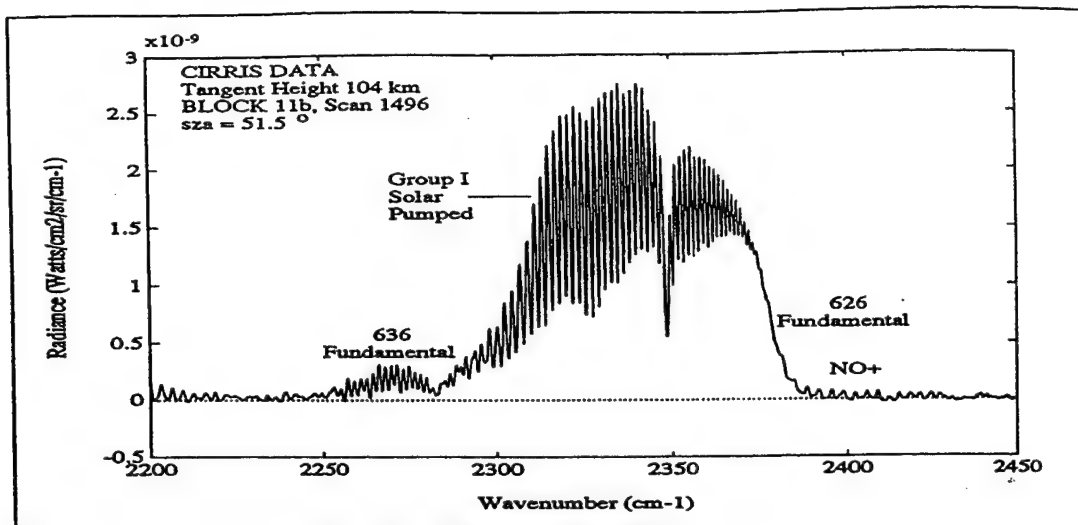
Figure 35. Three CIRRIS daytime spectra, corresponding to tangent heights of 104, 121, and 144 km.

Modeled Limb Radiance, 4.1-4.5 um
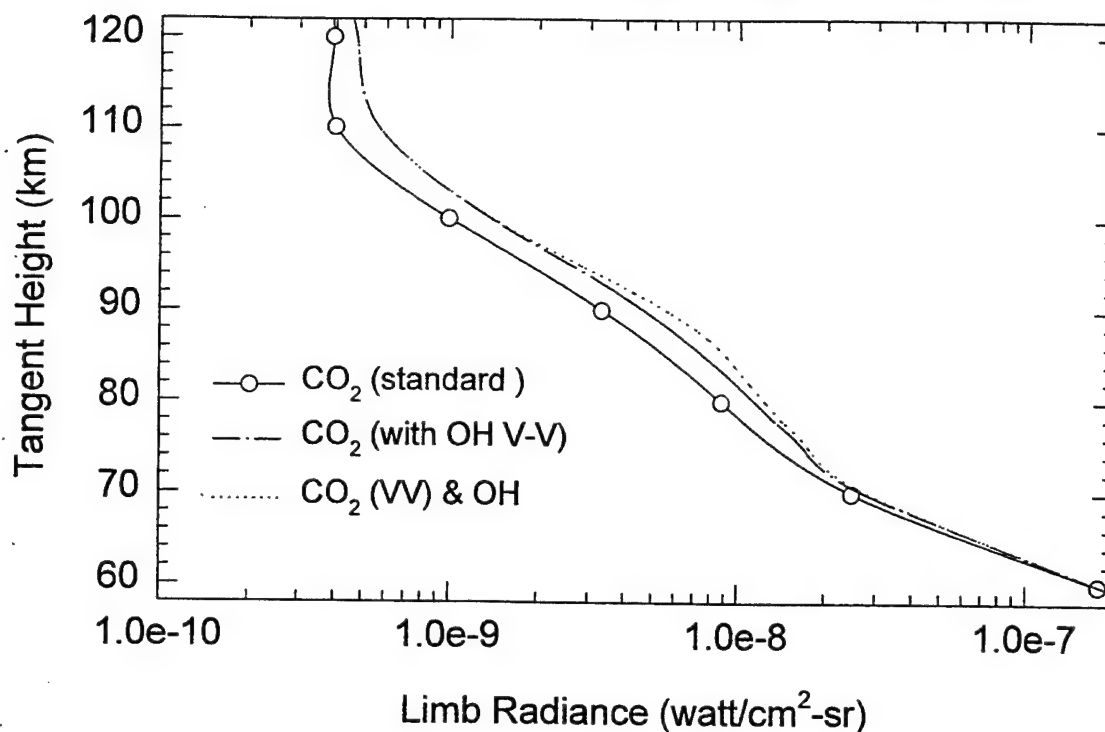
Figure 36. Limb radiance in the 4.1-4.5 μm range, as modeled for CO_2 using standard excitation processes, for CO_2 using V-V. transfer from nascent OH as an additional excitation mechanism, and for CO_2 with V-V excitation plus direct inband emission from OH.

as an excitation mechanism, and this plus the direct OH emission into the 4.1-4.5 μm region.

According to this calculation, the V-V transfer process affects the CO_2 limb radiance for paths with tangent heights between 80 and 130 km even though the OH layer near 88 km itself is only a few kilometers thick. The explanation for this is that the excitation of N_2 is large enough to greatly enhance the local CO_2 emission rate, which then results in increased excitation at higher altitudes by radiative transfer. The calculation shown in Figure 36 indicates a 40% increase in limb radiance for the 90 km tangent path. However, it is necessary to note that the rate constants that we used for the V-V. transfer into N_2 *(Streit and Johnson, 1976)* were actually extrapolated from experiments with O_2, which is expected to produce a faster reaction than N_2. Therefore, we regard the results shown here as an upper bound on the effect of this process.

Note also that the direct inband contribution from OH in this calculation peaks at about 20% of the standard CO_2 radiance, which is on the high side of model predictions for different conditions and is higher than what was found in most CIRRIS spectral-fit scans.

2.4.2.2 O(^{1}D)

O(^{1}D) is produced by photodissociation of ozone in the mesosphere and molecular oxygen in the lower thermosphere, and is rapidly quenched by collisions with N_2 and O_2. In collisions with N_2, 25% of the O(^{1}D) energy is thought to end up in N_2 vibration. Making the assumption that n quanta of N_2(v) from a single collision (n≤7) are rapidly converted to n molecules with one vibrational quantum, we modeled the effect of O(^{1}D) quenching on the 4.3 μm emission. The one-dimensional photochemical model mentioned earlier *(Makhlouf et al, 1995)* was used to simulate the conditions of interest and provide O(^{1}D) for different solar zenith angles.
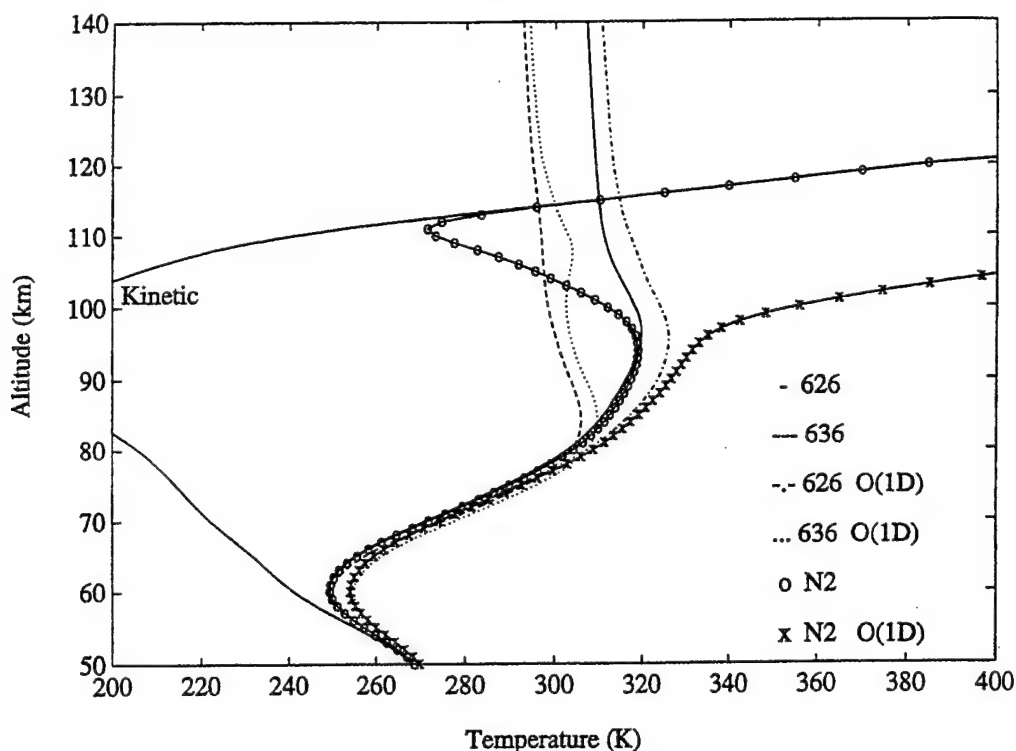
Figure 37. Vibrational temperatures of the CO_2 626 and 636 00011 state, and the N_2(v=1) state, for a solar zenith angle of 2.2^0, calculated with and without the O(^{1}D) excitation mechanism.

Figure 37 shows the vibrational temperatures of the CO_2 626 and 636 00011 states and the N_2(v) state for an overhead Sun, with and without the O(^{1}D) excitation mechanism *(Winick et al, 1993)*. One can see that there is a change of several degrees in the CO_2 vibrational temperatures at ~65 km and above 85 km. The lower enhancement is where O_3 photodissociation peaks. (One can also see that the N_2 vibrational temperature escalates tremendously in the lower thermosphere with the O(^{1}D) mechanism included.)

41
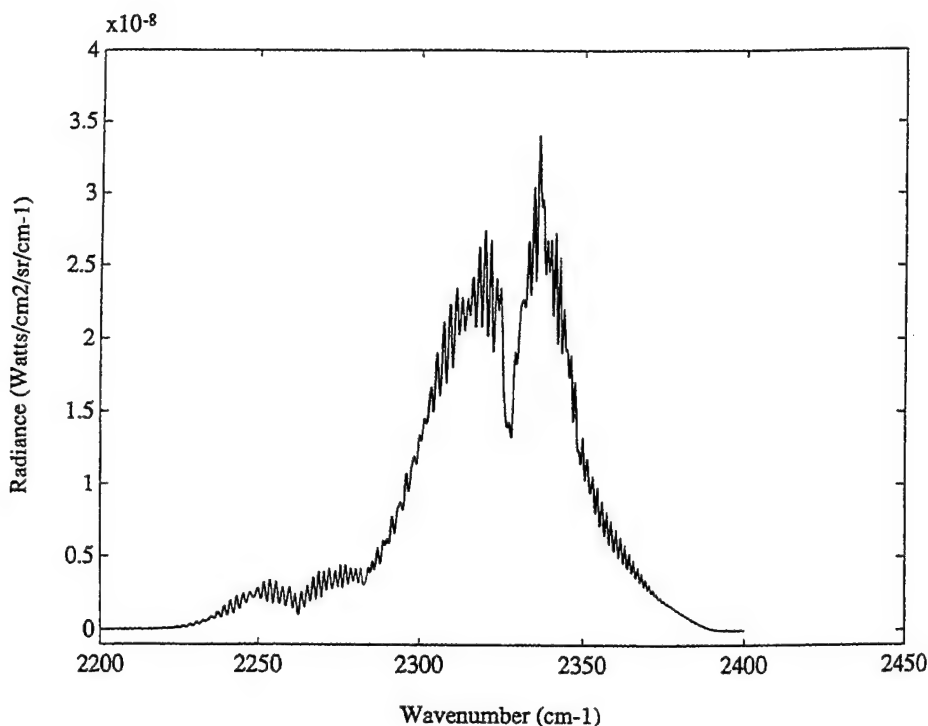
Figure 38. ARC simulation of the spectrum shown in Figure 34, a daylight scan with a tangent height of 65 km. $O(^1D)$ excitation was omitted. The model underpredicts the data even when $O(^1D)$ is included.

However, the resulting increase of ~30% in the CO_2 emission rates translates into much smaller increases in limb radiance (<10%) because of the opacity of the atmosphere.

Figure 38 shows the ARC-modeled spectrum corresponding to the data in Figure 34. Careful comparison of the figures reveals that the model calculation, which was done without $O(^1D)$ excitation, underpredicts the data substantially in the regions where the 626 and 636 fundamentals can be identified. The inclusion of $O(^1D)$ improves the result somewhat, but still leaves the prediction short of the experimental radiance level.

We also modeled 4.3 μm zenith data from the SISSI experiment that was discussed in Section 2.1 *(Winick et al, 1993)*. This case was quite different from the CIRRIS day-time experiments, because the data correspond to twilight conditions with the solar zenith angle greater than 90^0. In such circumstances there is practically no solar pumping of CO_2, the 4.3 μm signal is consequently much weaker, and the effect of $O(^1D)$ is much more apparent. That is, the production of $O(^1D)$ at the highest altitudes is not severely in-hibited by the passage of the solar photons through lower regions of the atmosphere, but the pumping of the CO_2 states is, so the $O(^1D)$ excitation can be thought of as being added to the roster of nighttime, not daytime, excitation mechanisms. This is reflected in Figure 39, which plots the vibrational temperature profile of the 626 00011 state, with

42

and without $O(^1D)$ excitation. Both curves show a transition from typical nighttime behavior in the lower mesosphere to daytime behavior in the thermosphere, but the $O(^1D)$ clearly produces more "daylike" conditions in the upper mesosphere.

Figure 40 shows the modeled radiance (again, with and without $O(^1D)$ excitation) together with the spectral radiance data from the rocket experiment. Clearly there is a great improvement of the very large discrepancy that obtains when $O(^1D)$ is not used. The model also produces a peak in the zenith radiance profile which is similar to that seen in the data. But the peak occurs at a considerably lower altitude, and as a result the model still substantially underpredicts the SISSI data. Several possible explanations have been considered *(Winick et al, 1993)*. Among them is that the $O(^1D)$ profile is very sensitive to the solar zenith angle, which means that the one-dimensional calculation used to generate this profile may not be sufficient for twilight conditions because it cannot account for changing conditions (removal of O_3) along the optical path through the atmosphere to the Sun. At this point, the reason for the discrepancy between model and data is unresolved.
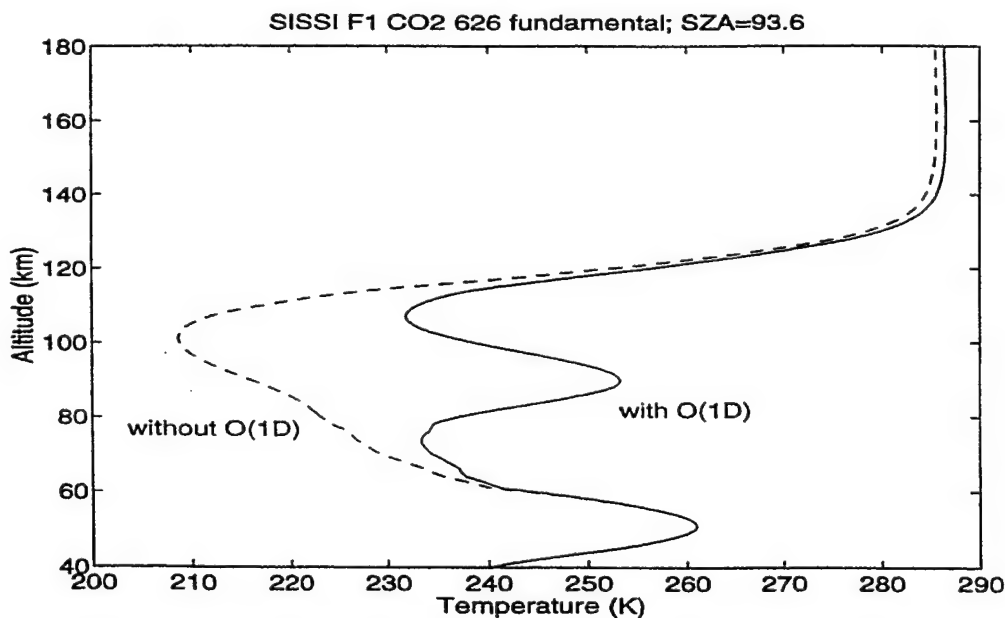
Figure 39. Vibrational temperature of the CO_2 626 00011 state, modeled for the conditions of the SISSI experiment with and without excitation due to $O(^1D)$, for a solar zenith angle of 93.6^0.

Despite the failure to perfectly reproduce the CIRRIS and SISSI radiance profiles, some useful conclusions may be drawn from this study. One is that the non-LTE daytime enhancement of CO_2 4.3 μm emission is a significant effect, but the increases in total in-limb band radiance are still fairly small. For morning twilight conditions, however, there

is a very great enhancement of radiance in the mesopause region that probably varies quite rapidly as the Sun rises.
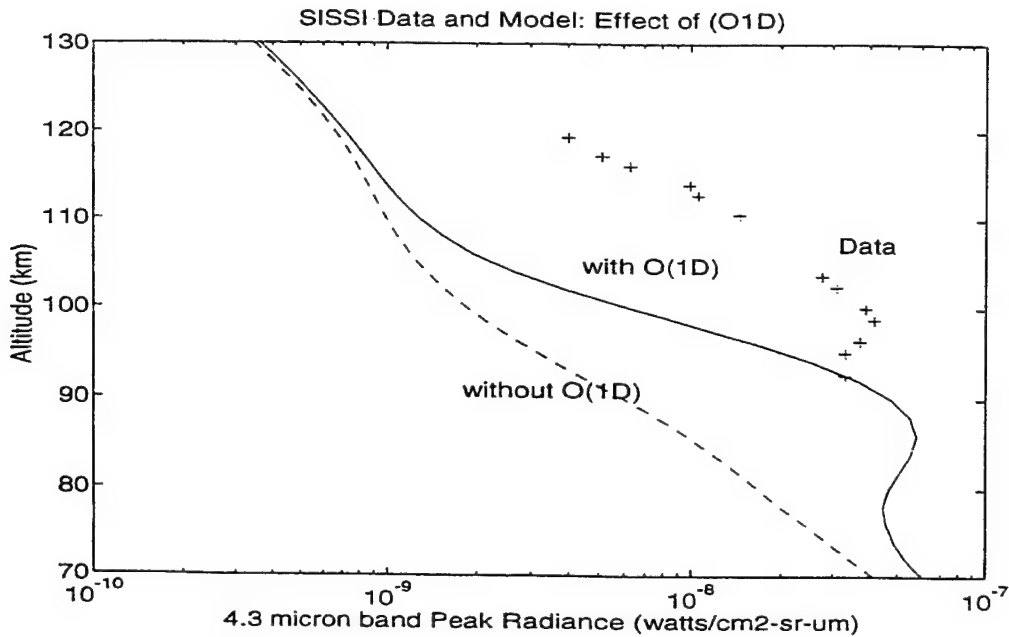
Figure 40. Zenith radiance modeled for the conditions of the SISSI experiment, with and without $O(^1D)$ excitation, compared to data from the rocket.

2.4.2.3 V-V Processes

We considered the likelihood that, for daytime conditions, the excitation of the Group 1 states by solar pumping at 2.7 µm produces a sufficiently great population to affect the rate of N_2 excitation through near-resonant V-V transfer. Vibrational quanta can be exchanged with high probability between N_2 and any excited $CO_2(v_3)$ state, and the reaction can be skewed in one direction or the other by an elevated population of one reactant. Therefore, with Group 1 states having vibrational temperatures considerably above that of N_2 in the upper mesosphere *(Sharma and Wintersteiner, 1985)*, the net effect of including them in the calculation is to augment the production of N_2 vibration.

We included this process in the RADC calculation that determines the $CO_2(00011)$ and $N_2(v)$ vibrational temperatures. Assuming that the effect of this addition on the N_2 vibrational temperature is relatively small, we did not couple the calculation of the Group 1 states explicitly with that of the 00011 states. Rather, we iterated by first calculating the Group 1 states (using a fixed provisional N_2 vibrational temperature profile), then determining the N_2 and 00011 states with the V-V transfer from Group 1 as an excitation-mechanism, and in the end repeating both calculations.

44

The effect of including this additional V-V process in the calculation of coupled CO_2 and N_2 state populations has a small but nonnegligible effect. This is illustrated in Figure 41, which shows the 626 00011 vibrational temperature, and that of N_2, assuming daytime conditions and a solar zenith angle of 78^0. Three pairs of curves (N_2, CO_2) show the daytime calculation done without either the additional V-V excitation due to Group 1 or the excitation due to $O(^1D)$; the same calculation including the V-V; and the same calculation including both. The effect of including the additional V-V interaction is to raise the 00011 vibrational temperature a few degrees at all altitudes between about 60 and 95 km. As with the $O(^1D)$ mechanism, this will only translate into a small increase in limb radiance, due to the opacity of the atmosphere.

Note that the $O(^1D)$ increases the vibrational temperatures only slightly more for this low-Sun case than for the high-Sun case plotted in Figure 37, despite the contrary appearance resulting from the different scales used in the two figures.
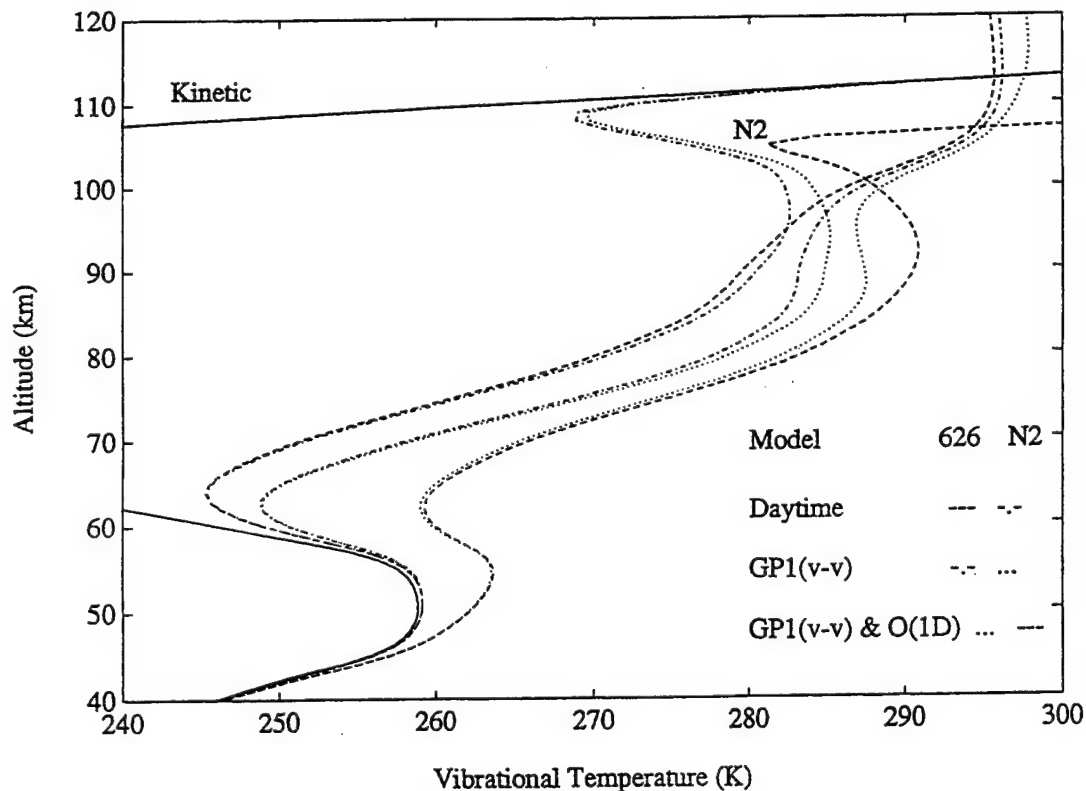
Figure 41. Daytime vibrational temperatures of the CO_2 626 00011 state and the $N_2(v=1)$ state. Calculations were done using only the basic excitation mechanisms, these plus the V-V interaction with the Group 1 states, and both of these plus excitation due to $O(^1D)$.

3. ATMOSPHERIC RADIANCE CODE

3.1 Overview

Development and maintenance of the Phillips Laboratory Atmospheric Radiance Code (ARC) have been ARCON's responsibility during the period covered by this report. The physical models and the algorithms underlying each of the several components of ARC have been described in past papers and reports, referenced below, so this section concentrates on a detailed discussion of how to use them. Several research problems to which ARC has recently been applied are presented elsewhere in this report.

Atmospheric Radiance Code consists of several stand-alone FORTRAN codes that are used, collectively, to model non-LTE processes affecting the infrared signature of the upper atmosphere. The distinguishing feature of these codes is the use of line-by-line (LBL) methods to deal with radiative processes, in particular, the radiative excitation of vibrational states by transfer from within the atmosphere. The principal objectives are to predict non-LTE vibrational populations, expressed as vibrational temperatures, and to determine the resulting line-of-sight (LOS) radiances. An important ancillary result, in the case of the vibrational temperature calculations, is the rate of atmospheric cooling due to transitions in infrared-active bands.

The current status of ARC was reviewed at the 18th Annual Conference on Atmospheric Transmission Models *(Wintersteiner et al, 1996).*

The principal components of ARC are programs known as SABS, RAD, RADC, VPMP, NLTEA, and CONV. SABS calculates the rate of solar flux absorption in infrared bands for different conditions. When daytime conditions are being simulated, its results are used as input for RAD, RADC, and VPMP, which determine the vibrational populations (temperatures) of various infrared-active states. NLTEA performs line-of-sight calculations, using these vibrational temperatures, and CONV generates synthetic spectra using the results of NLTEA. Each of these programs is described in a separate subsection, below. As indicated therein, short auxiliary programs may be used to support the I/O procedures of some of the main ARC codes.

3.2 Common Features of ARC Codes

Although the programs described below serve quite different purposes, they are generally structured in a similar fashion. In particular, there is much that is common about the codes' input requirements, not so much the quantities that comprise the input but

rather the means of organizing and reading them. In the interest of avoiding redundancy in the subsections that follow, we present a discussion of some of these similarities here.

3.2.1 Input File Structure

All input files for ARC codes consist of a two-part header followed by data records. ARC input file headers consist of two parts: "comment lines" followed by "directive lines". Comment lines are lines that begin with a "C" in column 1 and consist of character strings that are read and echoed but not processed in any other way. Directive lines are lines having a "D" in column 1. Some (not all) input modules will search the character strings comprising these lines for particular substrings. The substrings are used for setting program options or locating data, but not for reading data *per se*. For example, a substring might set options flags to enable extra print output or restrict a calculation to LTE conditions, or it might indicate what data reside in the following data records. When a directive substring is recognized, one of several possible functions is enabled; otherwise the line is treated like a comment line, with no substantive action taken.

All ARC codes will read headers structured in this way. "C" lines are always optional. "D" lines are usually optional, but some codes require them for locating atmospheric input data, a procedure that is explained below in the discussion of "column directives". The other directives that are effective are different for different codes, and are listed in the respective subsections. The order always is that all "C" lines precede all "D" lines, which in turn are followed by data records.

3.2.2 Program Directives Files

Most of the ARC codes, being computationally-intensive, were designed to run in a batch or background mode rather than interactively. Except for CONV, each code reads a so-called "program directives file" to tell it what files to read and write, what calculations to perform, and what parameters to use in so doing. This file is always associated with logical unit 1 in the FORTRAN code and hence is called the "unit-1 file". In order for it to be recognized by the code, it must be given a specific filename. For NLTEA it is called NLTEA001, and program directive files for other codes are named similarly.

Unlike the other input data files, where numerical data records are usually constructed in column format, the data records on the program directives files are free-format records read by list-directed read statements. Therefore, list elements are separated by a delimiter character (usually a comma), character variables must be enclosed in single quotes, each record must be terminated with a slash (/), and records may extend over more than one line. Moreover, any list element that is read as a null retains its previously

47

set (default) value. [A null is encountered when two consecutive delimiters appear in the record.] Lists of the contents of the data records on the unit-1 files are given for each of the ARC codes in the respective subsections of this report, as are example program directive files.

All the ARC program directives files contain one or more "filenames records" that tell the program where to find input data and write output data. The filenames can be up to 60 characters in length. Note that, in the examples in later sections, slash characters appearing *within* the single quotes that delimit these character variables are part of the UNIX path, and are to be distinguished from the list-directed read terminator that appears at the end of each data record.

Several ARC codes need one or more infrared bands to be specified on the unit-1 file. This is done with a 3-character molecule code, an integer isotope code, and an 8-character vibrational state code, all in the notation defined for use in the HITRAN database *(McClatchey et al, 1973)*. Trailing blanks in the state codes can be omitted on the input records.

3.2.3 HITRAN Data Files

Most of the ARC codes also use line data taken from the HITRAN database *(Rothman et al, 1992)*. These data are normally read from a "unit-3 file", which always has the 80-column format used in the pre-1986 releases of HITRAN (e.g., *McClatchey et al, 1973*). Except where noted, individual input linefiles may contain transitions from many bands and/or many isotopes of a single radiating molecule, listed in any order. Except for NLTEA, all required transitions must appear on the same input file.

3.2.4 Atmospheric Data Files and Column Directives

The ARC codes also need input data to construct model atmospheres. These data are always given in column format on one or more atmospheric data input files, and an altitude grid is always in the first column. The primary atmospheric data input file is always associated with unit 2, and provides the altitude grid upon which the calculation is performed. Some of the codes specifically require a secondary atmospheric data input file associated with unit 9, and sometimes yet another file associated with another logical unit. (NLTEA uses multiple files, but uses them sequentially and calls them all "unit-2 files".) When a second or third file is used, the altitude grid on that file does not necessarily have to be the same as that on the primary file, because the input data are interpolated onto the latter, but it is recommended that the altitudes at least span the original range to avoid extrapolation at either end.

In some of the ARC input modules, the formats for reading the columns of atmospheric data are fixed, in which case the required specifications are given in later subsections. However, some codes determine appropriate formats for individual files by reading the first data record, which eases the job of preparing the files.

Except for NLTEA, all the ARC modules for reading atmospheric data recognize a default order for the required columns of data. That is, the altitude grid may be followed by the kinetic temperature profile, the radiator number density profile, and then specific other profiles in a predefined sequence. This is normally repeated for the secondary atmospheric data file as well, with different profiles. However, the required data and the required sequences can be different not only for different programs but also for different runs of the same program, so we have adopted a procedure using so-called "column directives" to let the codes determine on their own which columns contain required data. This procedure has not been implemented in all ARC codes, and because of the defaults it doesn't always have to be used even when it is implemented. But it does simplify input requirements and should be used when possible.

A column directive is identified when the keyword string "COLUMN", followed by a three-digit integer field, is located on a directive line in a file header. The code then extracts a column number from the integer field, and looks for subsidiary strings on the same line to identify the data in that column. The number and content of the subsidiary strings necessarily depend on the data sought, but—for each of the required data fields that the program knows it needs to locate—whenever all the identification criteria are met a flag is set and the code stops looking for that profile.

For atmospheric data input, four types of data are sought: altitudes, temperatures, number densities, and mixing ratios. There are four corresponding substring identifiers, three of which are not, by themselves, sufficient to locate any sought-after quantity. The first of these is "ALTI", which does determine the column with the altitude grid. The second is "TEMP", identifying some kind of temperature that can then be completely specified by the additional string "KINETIC" or partially specified by the additional string "VIB". In the latter case, vibrational temperatures of required states are located unambiguously only if strings including the 3-character molecule code, the 4-digit integer isotope code, and the 8-character vibrational state code are also matched.

The third substring identifier is "DENS", which suggests a number density of some sort and initiates a search for further substrings, including "TOTAL" for the total density of all species and molecule codes such as "CO2" and "N2 ". (In the case of atomic oxygen and $O(^1D)$, "OATOM" and "O1D" are recognized.) The fourth substring identifier is

"MIX", which identifies a mixing ratio if the correct molecule code accompanies it on the directive line.

Examples of column directives are given in Section 3.7.5 where NLTEA, which requires their use, is discussed. Note that although the order of the strings is immaterial, except for the integer field following the keyword, they must always be in upper-case characters. Also, the programs match the entire 8-character vibrational state codes with the substrings in the header, so in this case (unlike the unit-1 input) trailing blanks must be retained. And finally, the mixing ratio is used as an alternative to the actual number density of radiating species (but not major species like N_2 and O_2) so once a mixing ratio is located the search for the number density is terminated, and vice versa.

Mixing ratio data are always given in ppmv, while number densities are in molecules/cm^3, altitudes in kilometers, and temperatures in degrees Kelvin.

Column directives can be used to locate data other than the basic model atmosphere, for example solar flux absorption coefficients, and are further discussed at the appropriate places in this report.

3.2.5 Output Files

Most ARC codes produce three output files intended for disposition to a printer. The "unit-4 files" echo the input data and contain most of the primary program output, including the band radiances. The "unit-5 files" provide more detailed intermediate results, much of which can usually be suppressed for production runs. The "unit-6 files" echo input file headers, list progress messages as the modules successively complete their functions, include tables indicating where different input data are found, and give warning or fatal-error messages whenever possible. The unit-6 files are, in effect, reports on the progress of the runs. They are intended to highlight any anomalous or unexpected conditions, and thus should be examined at the end of each run. These files have default names (such as NLTEA004 for the NLTEA unit-4 file) that cannot be changed at run time except by use of a script.

Each program also produces one or more output files with the principal results of its calculations, provided that filenames are specified for them on the program directives file (which normally they are). These files are naturally different for each code, and so are described in later subsections. Some of the codes, notably SABS, will take output files from one run and read them on the next run in order to append the new results to them. Other codes, such as RAD, require separate programs to copy sets of output data to a common summary file.

All the standard output files are ASCII. However, RAD and RADC do write interpolation tables to one binary file, which is used to avoid repetitive calculations and is intended to be read only by those codes.

3.2.6 Source Files

All the ARC codes are written in FORTRAN77. They each consist of several source files, which must be compiled and linked. The names of the files include the version number and a FORTRAN extension, such as "f" or "FOR". The codes are easily portable from one platform to another, as the only system-dependent calls are the ones returning the run date, run time, and CPU exec time. The modules EXECT and DATT contain alternate versions of these calls for different operating systems, with all but one set commented out. One or two system-dependent statements, all of them flagged in column 73 of the source code, are left over from past versions of the codes, but have no effect on the 32-bit machines that are commonly in use nowadays.

3.3 RAD

3.3.1 Introduction

The purpose of program RAD is to calculate vibrational populations of certain infrared-active states of CO_2 and CO for which absorption of radiation is a significant excitation mechanism. Its application is limited to states which are so weakly coupled to other excited states that a two-level approximation is suitable, or to groups of states that are so tightly coupled that they can be regarded as being in mutual equilibrium and thereby also susceptible to analysis with the two-level approximation. Among those for which RAD has been used, the CO_2 01101 and 01111 states qualify in the former category, as does the $CO(v=1)$ state. The CO_2 {10002-02201-10001} and {11102-03301-11101} states are examples of the latter.

The basic RAD algorithm has been explicated in the open literature (*Wintersteiner et al, 1992*), which may be consulted for details. Here we give a detailed description of how to use the code.

There are different specific requirements for each of the separate applications of RAD. The discussion is therefore specialized in later subsections to the $CO_2(v_2)$ states, the $CO_2(01111)$ state, and the $CO(v=1)$ state. The first requirement for running the code in all its manifestations, however, is to specify the basic model atmosphere (including profiles of kinetic temperature, total density, and major-species densities), the number density or mixing ratio profile for the radiating molecule, and any other profiles that may be necessary for evaluating the excitation rates of the state in question. It is also necessary

to provide the HITRAN data for the band(s) in which radiative transfer takes place, and construct a program directives file to direct the calculations that are to be performed.

The RAD output consists of vibrational temperature profiles for the state(s) being considered. The rates of excitation and de-excitation due to all collision and radiative processes are calculated and are also written to one of the output files, as is the atmospheric cooling rate in the case of the $CO_2(v_2)$ states.

3.3.2 Source Files

RAD consists of seven FORTRAN source files which must be compiled and linked. Since different kinetic processes are involved in calculating the balance of production and loss for the different states to which the code is applied, some of the source modules are used only for one of the possible calculations. Therefore, in each of its incarnations, RAD consists of six common modules linked together with one other module that does the actual vibrational-temperature calculation for the state in question.

The names of the six common modules are RAD_x.ext, DIREC_x.ext, ATMPR_x. ext, ITERAT_x.ext, TABLES_x.ext, and RADSUB_x.ext, where "x" is the version number (presently 35) and "ext" is an extension indicating a FORTRAN source file.

For the CO_2 (01101) state, the seventh module is named VER010_x.ext.When the compilation is done and the link is complete, the executable has a name that distinguishes it from the executables that treat other states, e.g. RAD_010. For the CO_2 {10002-02201-10001} and {11102-03301-11101} states, the seventh modules are VER020_x.ext and VER030_x.ext, respectively. For CO_2 (01111), the other module is VER011_x.ext, and for the CO vibrational state it is VERCOV_x.ext.

3.3.3 I/O Files

In order for any version of RAD to run, four input files must be accessible. The program directives file, RAD001, tells the program what to do and where to find other input data. A "unit-2 file" and a "unit-9 file" (both named on the program directives file) provide the atmospheric profile input data. RAD does not recognize column directives or determine format specifications, so these files must be prepared exactly as described below. A "unit-3 file" (also named on unit 1) contains the HITRAN data giving the rovibrational transitions in the infrared band(s) to be processed. There are also three output files intended for disposition to a printer, as described earlier.

A "unit-10 file" is used under most normal circumstances. This file contains interpolation tables for the Voigt lineshape function, and for E_2, the exponential integral of order two. Since both functions are used extensively, interpolation saves a lot of time.

Whenever RAD runs for the first time in a particular directory space, it generates the tables and writes this file, which has the default name of TABLES.DAT. The file is read at the beginning of subsequent runs, provided that the proper unit-10 filename is given. Otherwise, RAD will recreate the table at the beginning of each run.

For the CO_2 (01111) and $CO(v)$ calculations, input files associated with units 11 and 12 may also be required. These are discussed in the subsections dealing specifically with those calculations.

The output is normally written to a file associated with logical unit 7. This file will contain six columns of data: the altitude grid, the kinetic temperature, the radiator density, the vibrational temperature of the lower state of the radiative transition, the vibrational temperature of the upper state (which is the sought-after quantity), and the vibrational temperature of the lowest excited state (01101 for CO_2, $v=1$ for CO). For calculations in which the lower state is the ground state, the fourth column is identical to the fifth. Note that there may be considerable redundancy: for example, for CO_2 (01101) all three vibrational temperature profiles are the same.

All input files have the simple structure discussed in Section (3.2.1), namely headers followed by data records. For the purposes of RAD, directive lines ("D" lines) are the same as comment lines because RAD does not process any directives.

The requirements for the input files depend on which calculation is being performed, and so are given in the respective subsections.

3.3.4 Application of RAD to $CO_2(v_2)$ states

The standard way of generating $CO_2(v_2)$ vibrational temperatures with RAD is described here. Normally nine profiles are generated in nine separate runs. Each run generates several print output files and one data output file to which RAD does not append successive results. Each run has its own program directives file to tell RAD what to do. These give the names of the other input and output files, specify which state is to be processed, give the reaction rate constants that are to be used, and set the program parameters that RAD needs. The program parameters are normally the same for all nine runs.

The first four profiles are the vibrational temperatures of the 01101 state for the four principle CO_2 isotopes, 626, 636, 628, and 627. The excitation mechanisms are either thermal (V-T collisions with the major atmospheric constituents) or radiative (in the v_2 fundamental band, 01101-00001). Rate constants for the V-T processes are normally taken to be the same for all isotopes, although it is possible to vary them.

The next four profiles correspond to the {10002-02201-10001} states, or the {02201} states as we shall abbreviate them. These are coupled strongly enough by collisions that they can be assumed to be in mutual equilibrium and thus be characterized by the same vibrational temperature. As before, profiles are generated separately for each isotope. Each calculation requires the 01101 population for that isotope as input. As described in *Wintersteiner et al (1992)*, the excitation mechanisms are V-T collisions with major atmospheric constituents, V-V collisions in which a v_2 quantum is transferred between two CO_2 molecules, and radiative transitions. The radiative transitions occur in the three bands connecting these states with the lower-lying 01101 state.

The ninth vibrational temperature profile is that of the 626 {11102-03301-11101} states, or {03301} states, also assumed to be in mutual equilibrium. This calculation could be done for the minor isotopes, but usually isn't. The excitations are completely analogous to those used for the {02201} calculation, which must precede it, except that the radiative transitions are those of seven bands instead of three.

It is necessary to note the process whereby the calculation of three strongly-coupled states' populations is reduced to a two-level problem (with a single upper level). If one assumes mutual equilibrium among 10002, 02201, and 10001, one makes virtually no error in treating all the radiative transitions in the three actual bands as lines of a single band with an upper-state energy equal to that of 02201. That is, if one takes the HITRAN data for all three bands and relabels all the upper states as 02201 (making no other change, including the individual lower-state energies), and uses the RAD algorithm with that linefile to calculate the radiative absorption, the result is the same to within an extremely small fractional error as the sum of the absorption rates that one would get if the three bands were treated individually. Moreover, when RAD uses the thermally-averaged band Einstein coefficient calculated from this modified HITRAN linefile, the radiative loss rate turns out to be exactly the sum of the radiative loss rates of the three states when they are calculated separately using their correct upper-state energies. As a result, the calculation of the vibrational temperature of these three levels is accomplished using all the radiative transitions, and also all the individual collision processes except those interconnecting the three upper states (which are assumed to be very fast, thereby enabling this shortcut). Lumping all the transitions into a single band does not reduce the computational effort, because all the lines are still there, but it greatly simplified the code development.

Similar comments apply to the {11102-03301-11101} calculation.

The 01101 runs all use a file with kinetic temperature and [CO_2] as the primary atmospheric data input file on unit 2. The {02201} runs use the unit-7 output from the

Table 1. Sequence of Operations for $CO_2(v_2)$ Calculations
1. Copy the program directives file for the 626-01101 calculation to RAD001
2. Run RAD_010
3. Repeat steps 1 and 2 for 636, 628, and 627
4. Copy the program directives file for the 626-{02201} calculation to RAD001
5. Run RAD_020
6. Repeat steps 4 and 5 for 636, 628, and 627
7. Copy the 626-{02201} output data file to a file called RNU2.DAT
8. Run DFDF
9. Copy the program directives file for the 626-{03301} calculation to RAD001
10. Run RAD_030
11. Run VTSUMM
12. Run SCOOLEX
13. Run COOLSUM

01101 runs for their unit-2 input. The {03301} run uses the output file from the 626 {02201} run. In the {03301} case it is necessary to exchange two columns of data in the unit-2 file before beginning the run, to get the lower-state vibrational temperature in the proper column. This exchange is accomplished by copying the {02201} output file to a new file called RNU2.DAT and then running the simple routine DFDF. The latter routine produces a file called R030002.DAT, which should be used as the unit-2 input for the {03301} run.

After the nine runs are complete, a vibrational temperature summary file can be created by running the interactive FORTRAN program VTSUMM. This program reads the nine data output files and writes a new file containing the kinetic temperature, the CO_2 number density, and the nine vibrational temperatures. If the data output files have been given names that include the level and isotope designations (for example, Axx_CO2_010_626_yyy.DAT) VTSUMM will anticipate the names of all the files it needs to read once the first one has been entered. Vibrational temperature summary files are written with headers and column directives in place, and can be used as atmospheric data input files for NLTEA, RADC, SABS, and VPMP without further changes.

To get the infrared cooling in the 15 μm bands, it is necessary to run two other short interactive programs. Program SCOOLEX searches the RAD unit-4 output files for the excitation and deexcitation rate tables and copies them to an "excitation rate summary file". Program COOLSUM extracts the cooling rates from the excitation rate file and writes them to a "cooling-rate summary file". SCOOLEX requires nine unit-4 filenames, and like VTSUMM it may be able to anticipate the last eight once it has been given the first one. COOLSUM only needs the excitation rate file from SCOOLEX as input, plus a name for the cooling-rate summary file. Neither of these programs writes a header to the output file it produces, so it is good practice to add some comments or append a standard header for any file that will be kept.

Table 1 lists the set of operations for performing the $CO_2(v_2)$ calculations that has just been described.

3.3.4.1 Program Directives File for the $CO_2(v_2)$ Calculation

Table 2 lists the contents of the five input data records on the program directives file for the RAD $CO_2(v_2)$ calculation. Table 3 gives sample files for the 01101, {02201}, and

---

Table 2. Unit-1 Input Data Records for RAD [$CO_2(v_2)$ Calculation]

A. Filenames Record:
    FLNM2, name of the principal atmospheric data input file
    FLNM3, name of the linefile with the required CO_2 transitions
    FLNM7, name of the output file with the desired vibrational temperature profile
    FLNM8, unused (but leave a null or blank field here)
    FLNM9, name of the secondary atmospheric data input file
    FLNM10, name of the file with Voigt and E_2 interpolation tables

B. Band Record:
    MOL = molecule code = 'CO2'
    ISO = isotope code
    UST = upper vibrational state code
    LST = lower vibrational state code

C. Observation Heights Record
    HGTS = array of observation altitudes (km)

D. Program Parameters Record:
    HMIN = lower boundary of the atmosphere (default = 50 km)
    HMAX = upper boundary of the atmosphere (default = 1000 km)
    ACC = precision required for the vibrational temperatures (default = .05 K)
    INIT = initial vibrational-temperature code (0, 1, 2, or 3; default = 0)
    NPTS = # of integration points per panel (2, 4, or 8; default = 2)
    NDP = code for the Voigt lineshape algorithm (-1, 0, or 1; default = 0)
    CTF = cutoff parameter for uplook and downlook sums (default = .01)
    TAB = parameter with interpolation-table spacing (default = .01)
    NITR = maximum # of iterations (default = 3)
    ITAC = maximum # of accelerated iterations (default = 50)
    VMIN = lower end of the range searched for HITRAN data (default = 0 cm^{-1})
    VMAX = upper end of the range searched for HITRAN data (default = 20,000 cm^{-1})

E. Reaction-Rate Constants Record:
    NOR = Reaction numbers
    CF = Six parameters for each reaction

Table 3. Sample Program Directives Files for the RAD $CO_2(\nu_2)$ Calculations

CRAD001_1.DAT---UNIT-1 INPUT FOR RAD RUN #1
C
'~/atm67/a67_co2d.dat','~/lnfl/L010000.DAT', 'A67_CO2D_010_626_FJF.DAT',,
 '~/atm67/a67_tnd.dat','TABLES.DAT'/
'CO2', 626, '01101','00001'/
40,42,44,46,48,50,52,54,56,58,60,62,64,66,68,70,
 71,72,73,74,75,76,77,78,79,80,81,82,83,84,85,86,87,88,89,90,
  91,92,93,94,95,96,97,98,99,100,101,102,103,104,105,106,107,108,
   109,110,112,114,116,118,120,122,124,126,128,130,135,140,145,150/
40,180,.001,1,4,0,.0005,.001,3,100/
1, 0.0, 3.5E-13, 0.5, 2.32E-09, 76.75, .333333,
2, 0.0, 7.0E-17, 0.5, 6.70E-10, 83.80, .333333,
3, 0.0, 7.0E-17, 0.5, 1.00E-09, 83.80, .333333/

CRAD001_5.DAT---UNIT-1 INPUT FOR RAD RUN #5
C
'A67_CO2D_010_626_FJF.DAT','~/lnfl/l222010.dat','A67_CO2D_020_626_FJF.DAT',,
 '~/atm67/a67_tnd.dat','TABLES.DAT'/
'CO2', 626, '02201','01101'/
40,42,44,46,48,50,52,54,56,58,60,62,64,66,68,70,
 71,72,73,74,75,76,77,78,79,80,81,82,83,84,85,86,87,88,89,90,
  91,92,93,94,95,96,97,98,99,100,101,102,103,104,105,106,107,108,
   109,110,112,114,116,118,120,122,124,126,128,130,135,140,145,150/
40,180,.001,1,4,0,.0005,.001,3,100/
1, 0.0, 3.5E-13, 0.5, 2.32E-09, 76.75, .333333,
2, 0.0, 2.1E-16, 0.5, 2.01E-09, 83.80, .333333,
3, 0.0, 2.1E-16, 0.5, 3.00E-09, 83.80, .333333,
4, 1.1E-11, 0.0, 0.5, 0.0, 0.0, .333333/

CRAD001_9.DAT---UNIT-1 INPUT FOR RAD RUN #9
C
'R030002.DAT','~/lnfl/l333222.dat','A67_CO2D_030_626_FJF.DAT',,
 '~/atm67/a67_tnd.dat','TABLES.DAT'/
'CO2', 626, '03301','02201'/
40,42,44,46,48,50,52,54,56,58,60,62,64,66,68,70,
 71,72,73,74,75,76,77,78,79,80,81,82,83,84,85,86,87,88,89,90,
  91,92,93,94,95,96,97,98,99,100,101,102,103,104,105,106,107,108,
   109,110,112,114,116,118,120,122,124,126,128,130,135,140,145,150/
40,180,.001,1,4,0,.0005,.001,3,100/
1, 0.0, 3.5E-13,   0.5, 2.32E-09, 76.75, .333333,
2, 0.0, 3.15E-16, 0.5, 3.00E-09, 83.80, .333333,
3, 0.0, 3.15E-16, 0.5, 4.50E-09, 83.80, .333333,
4, 1.1E-11, 0.0, 0.5, 0.0, 0.0, .333333/

{03301} calculations for the 626 isotope. Some miscellaneous comments about the information in these tables follow.

The observation heights, which are the altitudes at which the radiative absorption calculations are performed, can be spaced evenly throughout the desired altitude range by entering an altitude minimum, maximum, and spacing (in km). Alternatively, they can be specified with a list of seventy or fewer entries, entered in ascending order. The latter option enables the radiative transfer calculation to be more accurate in regions with large temperature variations or large changes in excitation rates, as one may space the observation points are more closely there.

Except for the altitude range, most quantities in the program parameters record are criteria for convergence or cutoff of sums used in the radiative transfer calculation, or else affect some other detail of the calculation in some way. The default values were chosen for speed, not accuracy. Most of them were included as input parameters in order to make adjustments during code validation tests. More information can be found in comments in subroutine DIREC. However, for most purposes the values used in the sample program directives files in Table 3 are satisfactory, and probably superior to the default values.

The quantity HMAX defaults to 1000 km, but the actual top of the atmosphere will be the highest altitude found on the primary atmospheric data input file unless another (lower) explicit value is read.

The lineshape code, NDP, selects one of three algorithms for calculating the Voigt profile. The default selection, using the interpolation tables, is the fastest, while choosing -1 gives a slightly more accurate result at considerable cost in time.

The initial vibrational temperature code is used because it is necessary to start the iterative process of determining the unknown vibrational temperature with a guess profile, and different choices can be made for that profile. The normal procedure is to choose INIT=1, thereby using the kinetic temperature profile (except in the thermosphere, where the guess profile is held at 230 K). Further discussion of the guess profiles is given in the next section.

Each of the reaction-rate constants used in a given run is specified by six parameters. The parameterization for the forward rate for the ith reaction has the form

$$k_i(T) = C_{i1} + C_{i2} T^{C_{i3}} + C_{i4} \exp(-C_{i5} / T^{C_{i6}})$$

and the reverse rate is calculated automatically using the principal of detailed balance. The rate constants are read as an array CF(i,j), where j is the index running from 1 to 6. For each reaction, a line giving the reaction number and these six constants must be provided. The three reactions used for the 01101 calculation and the four used for the other

58

two are described in Tables 2a and 2b of Wintersteiner et al (1992), and the corresponding input parameters are given in the examples in Table 3.

The atomic oxygen rate (reaction 1), being controversial, is often varied. The parameters in Table 3 derive from the analysis reported by Sharma and Wintersteiner (1990).

3.3.4.2 Atmospheric Data Input Files for the $CO_2(\nu_2)$ Calculations

The requirements for the primary and secondary atmospheric data input files for the $CO_2(\nu_2)$ calculation, associated with units 2 and 9 respectively, are given in Table 4.

For the 01101 calculation, the unit-2 file normally contains just the altitude grid, the kinetic temperature, and the CO_2 number density or mixing ratio, as shown in Table 4. For the {02201} calculation, the 01101 output file is usually used for unit 2. For the {03301} calculation, the {02201} output file, modified by swapping two columns as indicated earlier, becomes the unit-2 file. An initial "guess" profile is always required for the vibrational temperature that is to be determined. If the program parameter INIT is read as 0 or 1, this profile is determined automatically. In that case, any data that may appear in the fourth column of the unit-2 file for the 01101 calculation, or the fifth column for the other calculations, are ignored. If INIT is read as 2 or 3, however, RAD will

Table 4. Atmospheric Input Data for RAD $CO_2(\nu_2)$ Calculations

Unit 2 for 01101:   FORMAT(F5.0,F10.3,E12.5)

Column 1:	Altitude
Column 2:	Kinetic Temperature
Column 3:	CO_2 Density or Mixing Ratio

Unit 2 for {02201}:   FORMAT(F5.0,F10.3,E12.5,3F12.3)

Column 1:	Altitude
Column 2:	Kinetic Temperature
Column 3:	CO_2 Density or Mixing Ratio
Column 4:	CO_2(01101) Vibrational Temperature
Column 5:	CO_2(02201) Vibrational Temperature*
Column 6:	CO_2(01101) Vibrational Temperature

Unit 2 for {03301}:   FORMAT(F5.0,F10.3,E12.5,3F12.3)

Column 1:	Altitude
Column 2:	Kinetic Temperature
Column 3:	CO_2 Density or Mixing Ratio
Column 4:	CO_2(02201) Vibrational Temperature
Column 5:	CO_2(03301) Vibrational Temperature*
Column 6:	CO_2(01101) Vibrational Temperature

Unit 9 (all):   FORMAT(F5.0,4E12.5)

Column 1:	Altitude
Column 2:	Total Number Density
Column 3:	N_2 Density
Column 4:	O_2 Density
Column 5:	Atomic Oxygen Density

* indicates guess profiles; see text

take data from those columns for this profile. The latter situation is not illustrated for the 01101 case in Table 4.

3.3.4.3 HITRAN Data Input Files for the $CO_2(v_2)$ Calculations

RAD, like the other ARC codes, obtains HITRAN data from files generated using the 80-column format of the pre-1986 releases of HITRAN. The file used for the 01101 calculation contains data taken straight from the database using this format, and the same file may be used for transitions of all isotopes.

The files for the {02201} and {03301} calculations need to be constructed a little differently because of the considerations outlined in Section 3.3.4. That is, the linefile for the {02201} calculation is a concatenation of three files that would normally describe three vibrational transitions, modified only by labeling the upper vibrational state of each line as 02201. This file is called L222010.DAT. A similar modification produces the linefile used for the {03301} calculation, which is called L333222.DAT; here the concatenated files include lines from seven bands.

3.3.5 Application of RAD to the $CO_2(01111)$ state

The process of running the $CO_2(01111)$ calculation, which evaluates radiative transfer in the first v_3 hot band, has some important differences from that for the v_2 states. Normally four separate runs are done, one for each of four isotopes. Vibrational temperatures of several CO_2 states are needed from previous calculations to evaluate the collision reactions that help populate 01111. Also, to account for solar pumping in the 01101-01111 band for daytime simulations, it is necessary to read solar flux absorption coefficients, as calculated by SABS. As a result, there are either one or two additional input files. Requirements that are different from those for the v_2 calculation are described in this section.

One assumption that underlies the 01111 calculation is that the populations of other CO_2 states are known, and that the effect of changes in the 01111 state do not affect them. The kinetic scheme has been discussed in some detail by *Nebel et al (1994)*. To run this calculation, it is necessary to read vibrational temperatures of the 01101 state, the {02201} states, and the $N_2(v=1)$ state. The latter is calculated using the RADC code, described later. RAD also wants the vibrational population of the so-called {04401} states, a sextuplet of closely-coupled states near 2600 cm^{-1} that have the equivalent of four quanta of bending mode (v_2). There is no explicit calculation of these states, but the coupling of 01111 with them is weak enough that it could be neglected without much error. instead of neglecting them entirely, however, the standard procedure is to use the {02201} or {03301} vibrational temperatures to characterize them. RAD will automati-

Table 5. Sample Program Directives File
for the RAD CO2(01111) Calculation

```
CRAD001_1.DAT---UNIT-1 INPUT FOR RAD RUN #14
'a67_co2d_010_626_fjf.dat','~/lnfl/L011010.DAT',
 'a67_co2d_011_626_fjf.dat',, '~/atm67/a67_tnd.dat',
'TABLES.DAT', 'A67_N2V_020.DAT', 'sab_a67_011_626.dat '/
'CO2', 626, '01111','01101'/
40,42,44,46,48,50,52,54,56,58,60,62,64,66,68,70, 71,72, 73,74,
 75,76,77,78,79,80,81,82,83,84,85,86,87,88,89,90, 91,92,93,94,
  95,96,97,98,99,100,101,102,103,104,105,106,107,108, 109,110,
   112,114,116,118,120,122,124,126,128,130,135,140,145,150/
40,180,.001,1,4,0,.0005,.001,3,100/
/
```

cally substitute one of these in place of the {04401} temperature if the input data column in which the latter profile is expected turns out to be empty.

The quantities to be read from the program directives file for the 01111 calculation are exactly the same as those listed in Table 2, except filenames FLNM11 and (for a daytime calculation) FLNM12 are also required. Table 5 gives a sample unit-1 file. The four reactions used for this calculation are reactions 11-14 in Table 2 of *Nebel et al (1994)*. The default reaction rates set in RAD are satisfactory for this calculation, so the last record may simply consist of a terminal slash as shown in the example.

The atmospheric input data for the 01111 calculation are listed in Table 6. Files associated with logical units 2, 9, and 11 are needed. Note that the 01111 vibrational temperature to be read is a guess profile, ignored (as in the v_2 calculation) unless the INIT parameter on the program directives record of the unit-1 file is 2 or 3. In most

Table 6. Atmospheric Input Data for RAD
CO2(01111) Calculation

Unit 2: FORMAT(F5.0,F10.3,4E12.5)

Column 1:	Altitude
Column 2:	Kinetic Temperature
Column 3:	CO_2 Density or Mixing Ratio
Column 4:	CO_2(01101) Vibrational Temperature
Column 5:	CO_2(01111) Vibrational Temperature
Column 6:	CO_2(01101) Vibrational Temperature

Unit 9:   FORMAT(F5.0,4E12.5)

Column 1:	Altitude
Column 2:	Total Number Density
Column 3:	N_2 Density
Column 4:	O_2 Density
Column 5:	Atomic Oxygen Density

Unit 11: FORMAT(F5.0,3F10.3)

Column 1:	Altitude
Column 2:	N_2(v=1) Vibrational Temperature
Column 3:	CO_2(02201) Vibrational Temperature
Column 4:	CO_2(04401) Vibrational Temperature

61

Table 7. Solar Flux Absorption Input Data
RAD CO_2(01111) Calculation
Unit 12: FORMAT(F8.2,E12.4)
Column 1: Altitude grid
Column 2: SFA, 01101-01111 Band

cases, then, the output file from the RAD calculation of CO_2(01101) can be used directly for unit-2 input in this case.

For daytime calculations only, a file containing solar flux absorption coefficients from SABS is required to account for pumping in the 01101-01111 band. This file is associated with logical unit 12. Since absorption of solar flux is what distinguishes the day and night conditions in RAD, the absence of this file (either because of the omission of a unit-12 filename from the filenames record on the program directives file or because the file can't be found or opened) results in a nighttime calculation. Table 7 lists the requirements for this file, which of course must contain different data for each CO_2 isotope. A SABS output file with the correct absorption coefficients in column 2 can be read directly.

3.4 RADC

3.4.1 Introduction

The purpose of program RADC is to calculate vibrational temperatures of the 00011 state of the four most populous isotopes of CO_2 and that of $N_2(v=1)$, to which they are closely coupled by exchange of vibrational quanta. As the code is a derivative of RAD, there are many similarities between them. The principal difference is that several states must be calculated simultaneously, so the simplifications inherent in the two-level formulation cannot be utilized.

The physical model underlying the calculation is described in detail *by Nebel et al (1994)*. Radiative transfer in the four v_3 fundamental bands is evaluated exactly as it is in the individual bands treated by RAD. Collision processes and explicitly-calculated excitation rates are included in the steady-state equations, which are solved by matrix inversion. The collision mechanisms are parameterized by rate constants that are expressed in exactly the form used by RAD. Input file requirements are similar to the RAD requirements, and the output consists of the vibrational temperature profiles of the four 00011 states and that of $N_2(v=1)$.

Day or night calculations can be run. The primary difference is solar pumping in the four main 4.3 μm bands, but the effect of excitation of N_2 vibration due to quenching of $O(^1D)$ is also usually used for the daytime calculation. The latter is treated like a normal collision process even though there is no reverse reaction—that is, there is no production of $O(^1D)$.

The solar flux absorption coefficients constitute one of the "explicitly-calculated" excitation rates mentioned above. Other one-way processes resulting in excitation of N_2, rather than CO_2, may also be accommodated. These include excitation by auroral processes and by collision with vibrationally-excited nascent OH *(Kumer et al, 1978)*. They must be determined off-line, in terms of transitions (from v=0 to v=1) per molecule of N_2 per second. In the case of aurora, such quantities are calculated directly by AARC, the Phillips Lab Auroral Atmospheric Radiance Code *(Winick et al, 1987)*. In the case of OH, they must be determined from the relevant rate constants (e.g., *Streit and Johnson, 1976*) and the OH(v) populations *(Makhlouf et al, 1995)*.

3.4.2 I/O Files

As with the other ARC codes, RADC calculations are directed by quantities read from a program directives file, associated with the name RADC001. Atmospheric data are read from three other files, named in that file and associated with logical units 2, 8, and 9. Column directives are recognized for the unit-2 and unit-9 files. The HITRAN data for all four bands are found on a single "unit-3" file.

In addition to these five files, two other input files may be needed. The solar flux absorption coefficients for a daytime calculation, from program SABS, are found on the "unit-12 file". If this file is not named, or cannot be found, RADC will automatically run without the solar pumping and thus produce results that are more in accord with nighttime conditions. In addition, excitation of N_2 by auroral processes and/or nascent OH will be accounted for if a "unit-11 file" containing the production rates for these mechanisms is named, located, and read. As with the solar absorption coefficients, if an error occurs they will simply be omitted and the calculation will run without them.

Detailed descriptions of how to prepare all the input files are given below.

RADC may also use a "unit-10 file" with interpolation tables in exactly the same manner as RAD does, according to the description in Section 3.2.2.

The output file will contain eight columns of data: the altitude grid, the kinetic temperature, the CO_2 density, the four 00011 vibrational temperatures, and the N_2 vibrational temperature, in that order.

3.4.3 Program Directives File

Table 8 lists the contents of the input data records for the RADC program directives file. The band records identify the four bands in which radiative transfer is calculated, and should be exactly as shown. As with RAD, the observation heights can be spaced evenly throughout the altitude range by giving an altitude minimum, maximum, and spacing, or they can be specified with a list of seventy-five or fewer entries, entered in ascending order. The program parameters record is exactly like that in RAD, and comments pertaining to it can be found in that section. The reaction-rate constants record is also similar, but of course the reactions are different. They are found in Tables 2a and 2b of *Nebel et al (1994)*.

Table 8. Unit-1 Input Data Records for RADC

A. Filenames Record:
    FLNM2, name of the principal atmospheric data input file
    FLNM3, name of the linefile with CO_2 00011-00001 transitions
    FLNM7, name of the output file with the desired vibrational temperature profiles
    FLNM8, name of the file with group-1 vibrational temperatures
    FLNM9, name of the secondary atmospheric data input file
    FLNM10, name of the file with Voigt and E_2 interpolation tables
    FLNM11, name of the file with direct excitation rates for $N_2(v)$
    FLNM12, name of the file with solar-flux absorption coefficients

B. Bands Records
    'CO2', 626, '00011','00001'/
    'CO2', 636, '00011','00001'/
    'CO2', 628, '00011','00001'/
    'CO2', 627, '00011','00001'/

C. Observation Heights Record
    HGTS = array of observation altitudes (km)

D. Program Parameters Record
    (Same as in Table 2)

E. Reaction-Rate Constants Record
    NOR = Reaction numbers
    CF = Six parameters for each reaction

A sample program directives file for RADC is given in Table 9. This file is set up for a nighttime calculation, since no unit-12 filename is named. The presence of the unit-11 filename means that some external source of N_2 vibrational excitation is being provided. On the program parameters record, values used for the number of iterations (NITR) and

Table 9. Sample Program Directives File for RADC

CRADC001---UNIT-1 input for RADC_5B
C
'~/atm67/a67_co2d_fjf_summ.dat','~/lnfl/L001000.DAT',
 'a67_co2d_001_all_n_fjf_caseE.dat',
  '~/atm67/a67_co2d_g1_626_n_fjf.dat',
   '~/atm67/a67_tnd.dat',
    'TABLES.DAT','excr_caseE.dat'/
'CO2', 626, '00011','00001'/
'CO2', 636, '00011','00001'/
'CO2', 628, '00011','00001'/
'CO2', 627, '00011','00001'/
40,42,44,46,48,50,52,54,56,58,60,62,64,66,68,70,71,72,73,74,
75,76,77,78,79,80,81,82,83,84,85,86,87,88,89,90,91,92,93,94,
95,96,97,98,99,100,101,102,103,104,105,106,107,108,109,110,
112,114,116,118,120,122,124,126,128,130,135,140,145,150/
40,160,.001,1,4,0,.0005,.0001,3,500/
/

the maximum number of accelerated iterations (ITAC) are greater than what is normally used for the RAD calculations because the bands considered here are optically thicker. The slash comprising the last line of the file indicates that the default values are accepted for all the collision rate constants.

3.4.4 Atmospheric Data Input Files

Three files are used for reading atmospheric data profiles. Unlike the case with RAD, formatting requirements are eased for two of them by use of column directives, but these are not required. Table 10 gives the default requirements for RADC, assuming column directives are not used. We later indicate how to make use of them to simplify the input.

The primary atmospheric data input file is, as usual, associated with unit 2. The quantities read from it are listed in Table 10; one can see that the RAD $CO_2(\nu_2)$ calculation must be run before RADC. The format for reading this file is determined automatically.

The secondary atmospheric data input file is associated with unit 9. This file contains number densities for the major atmospheric constituents, plus a profile for $O(^1D)$. All are required, even though $O(^1D)$ is not sufficiently abundant at night to influence the N_2 populations. In the absence of a realistic $O(^1D)$ profile, it is sufficient to provide a column of small numbers (not zeroes) in its place. The format for reading this file is also determined automatically.

The third atmospheric data input file, associated with unit 8, is reserved for the vibrational temperatures of the CO_2 10012, 02211, and 10011 states, referred to as "group 1" *(Nebel et al, 1994; Sharma and Wintersteiner, 1985)*. Only the major-isotope popula-

tions are used by RADC. These states are strongly pumped by solar flux during the day and directly influence the coupled CO_2-N_2 vibrational populations through V-V transfer. The required temperatures are calculated by program VPMP, described in Section 3.5, and RADC is set up to directly read the output file from that program. Several columns of data appearing there are redundant for RADC and therefore are not read, which accounts for the 50X field in the fixed format specification given in Table 10.

As mentioned earlier, requirements for the primary and secondary atmospheric input data files (units 2 and 9) can be relaxed by use of column directives. By including directive lines in the file header, with the character string COLUMN followed immediately by a three-digit integer field, any column of the file can be associated with particular data that RADC uses, and as a result those data are not restricted to the locations indicated in Table 10. In particular, the order of the columns can be different, and columns of data that do not need to be read can still appear on the file. Moreover, all of the data that would, in the default configuration, be read from unit 9, can actually be read from unit 2 if column directives are used. In such a case, the unit-9 file is not used.

Since RADC does not decipher column directives that may appear on unit 8, the group-1 vibrational temperatures must be provided in the default format.

Table 10. Atmospheric Input Data for RADC (Default Requirements)
Unit 2:
Column 1: Altitude
Column 2: Kinetic Temperature
Column 3: CO_2 Density or Mixing Ratio
Column 4: CO_2 626 01101 Vibrational Temperature
Column 5: CO_2 636 01101 Vibrational Temperature
Column 6: CO_2 628 01101 Vibrational Temperature
Column 7: CO_2 627 01101 Vibrational Temperature
Column 8: CO_2 626 02201 Vibrational Temperature
Unit 8: FORMAT(F7.2,50X,3F9.3)
Column 1: Altitude
Column 2: CO_2 626 10012 Vibrational Temperature
Column 3: CO_2 626 02211 Vibrational Temperature
Column 4: CO_2 626 10011 Vibrational Temperature
Unit 9:
Column 1: Altitude
Column 2: Total Number Density
Column 3: N_2 Number Density
Column 4: O_2 Number Density
Column 5: Atomic Oxygen Number Density
Column 6: $O(^1D)$ Number Density

3.4.5 Direct-Excitation Input Files for RADC

The two optional input files may contain excitation rates, calculated off-line, for the CO_2 states (solar-flux absorption coefficients, unit 12) and the N_2 state (unit 11). Table 11 gives the requirements for these files.

Table 11. Direct-Excitation Input for RADC
Unit 11: FORMAT(F10.2,4E12.5)
Column 1: Altitude
Column 2: N_2 Excitation Rate #1
Column 3: N_2 Excitation Rate #2
Column 4...
Unit 12: FORMAT(F8.2,1X,4E12.5)
Column 1: Altitude
Column 2: SFA Coefficients for CO_2 626 00001-00011
Column 3: SFA Coefficients for CO_2 626 00001-00011
Column 4: SFA Coefficients for CO_2 626 00001-00011
Column 5: SFA Coefficients for CO_2 626 00001-00011

The file containing N_2 excitation rates may be used for up to four separate mechanisms. That is, excitation rate profiles due to auroral excitation, excitation from nascent OH, and up to two other possible mechanisms, may be read from columns 2-5 of this file. RADC will simply sum these quantities, so the order in which the columns appear, in case more than one process is included, is immaterial. For these profiles, the units are transitions per cm^3 per second.

The solar flux absorption (SFA) coefficients are given in units of transitions per molecule per second, as calculated by program SABS. "Per molecule" refers to total CO_2.

3.5 VPMP

3.5.1 Introduction

VPMP serves the purpose of calculating the vibrational temperatures of specific high-lying CO_2 states for which infrared radiative transfer is not regarded as an important excitation mechanism. The code treats groups of states that are coupled strongly, but not so strongly that (like some of those treated by RAD) they can be assumed to be in mutual equilibrium. The states comprising the four groups that we consider are listed in Table 12. They are primarily excited by solar pumping in the daytime. Exchange of vibrational quanta with N_2 also connects them to lower-lying bend-stretch states and has some influence on the N_2 vibrational population by serving as a conduit for energy absorbed from the solar flux. The daytime model has been described by *Sharma and Wintersteiner (1985)*.

In the absence of solar pumping, the high-lying states are not significantly populated

Table 12. High-Lying CO_2 States Treated by VPMP
Group 1: 10012, 02211, 10011
Group 2: 11112, 03311, 11111
Group 3: 20013, 12212, 20012, 04411, 12211, 20011
Group 4: 30014, 22213, 30013, 22212, 30012, 22211, 30011

above the stratopause and thus are not very important for nighttime simulations. For the sake of completeness, however, we do make provision for nighttime calculations, in which case it is necessary to account for Earthshine pumping due to radiative transfer in the 2.7 and 4.3 μm bands that populate Group 1. (In the daytime, this absorption can be neglected because it is overwhelmed by that resulting from solar flux.) This accounting is not carried out by the detailed algorithms applied in RAD, but rather with a very rough calculation that assumes that only upwelling radiation from the lower boundary is absorbed, and moreover that there is no attenuation in the atmosphere. With these rather poor approximations, the resulting nighttime vibrational temperatures depend on the location of the lower boundary of the model, and for that and other reasons can be regarded as accurate only to about ten degrees Kelvin. The justification for doing this is that the nighttime emissions are so low that they produce a very small fraction of the 2.7 and 4.3 μm radiance, and that the influence of these states on the other CO_2 states through V-V transfer and N_2 is also negligible. The need for the nighttime profiles comes about because the current version of RADC requires them, much as it requires the daytime profiles.

VPMP requires that solar-flux absorption coefficients calculated by SABS be read in for the daytime calculation. For the nighttime case, the approximate earthshine pumping is calculated by a short program called NIGHT_PUMP, which produces output (in the same format as that of SABS) that is read by VPMP in place of the solar coefficients. The way to perform this calculation is described below.

3.5.2 I/O Files

To run VPMP, several input files must be accessible. These include the program directives file, a primary atmospheric data input file and possibly a secondary file, and files associated with units 3 and 4 containing the solar flux absorption coefficients (for the night-time case, the simulated earthshine pumping). No HITRAN data are used, however.

Only two output files are written specifically for disposition to a printer. The principal program results are on the unit-5 file, and as usual the unit-6 file is a progress report for the run. The principal data output file is written to unit 7. Its contents include the altitude grid, the kinetic temperature, and the CO_2 density, followed by the vibrational temperatures of the 01101, 02201, and 03301 states of the relevant isotope and then by the vibrational temperatures of the states in the group under consideration. The bend-stretch states' vibrational temperatures are simply the profiles read at the beginning of the calculation. The format in which the file is written is (F7.2,F10.3,1PE12.4,1X,0P,10F9.3). The header on the output file contains column directives that are recognized by some of the ARC codes.

3.5.3 Program Directives File

The program directives file must be associated with the name VPMP001. The three unit-1 directives that affect the run are exactly the same as for SABS, and are given in Table 19, in the next section. Table 13 gives a list of data records that VPMP reads from this file, and Table 14 gives an example of such a file.

Some miscellaneous comments about the input data records are as follows. On the filenames record, files that are not used should be entered as blank names or nulls, except for the last names before the terminating slash. The unit-4 and unit-9 files may fall into this category, and the unit-8 file, which is not used, always does. Even the unit-7 output file can be omitted if desired; in that case the calculations are performed anyway but the results are only written to the print output files.

Table 13. Unit-1 Input Data Records for VPMP

A. Filenames Record
  FLNM2, name of the primary atmospheric data input file
  FLNM3, name of the first SFA coefficients file
  FLNM4, name of the second SFA coefficients file
  FLNM7, name of the output file
  FLNM8, unused (blank filename)
  FLNM9, name of the secondary atmospheric data input file

B. Group Record
  MOL = molecule code = 'CO2'
  ISO = isotope code
  IGP = group code

C. Program Parameters Record
  SZA = solar zenith angle (degrees)
  HMIN = lower boundary of the atmosphere
  HMAX = upper boundary of the atmosphere

D. Reaction Rate Constants Record
  NOR = reaction number
  CF = Six parameters for each reaction

On the group record, the molecule identifier is always 'CO2'. On the program parameters record, the solar zenith angle (SZA) is used to retrieve the correct solar flux absorption (SFA) coefficients from the SABS output file. VPMP accepts coefficients that correspond to SZAs

---

Table 14. Sample Program Directives File for VPMP

```
CVPMP001_10.DAT---unit-1 input for VPMP run #10
C Group 1 626 calculation
D BRIEF
'~/atm67/a67_co2d_fjf_summ_s80.dat',
 '~/atm67/SAB_A67_CO2D_G1A_FJF.DAT',
  '~/atm67/SAB_A67_CO2D_G1B_FJF.DAT',
   'A67_CO2D_G1_626_FJF_S17_2.DAT',,
    '~/atm67/a67_tnd.dat'/
'CO2', 626, 1
80, 40, 180/
/
```

within one degree of the quantity read from the unit-1 file.

The rate constants record is read exactly as it is for RAD. That is, the reaction is specified by a reaction number and the corresponding rate constants are specified by six coefficients, as indicated in Section 3.3.2. The reaction numbers and the parameterization of the rate constants is given by *Sharma and Wintersteiner (1985)*.

The sample program directives file in Table 14 directs the 626 group-1 calculation. The BRIEF directive has no effect since the default is to not write out extra program results. Two atmospheric data input files, two SFA coefficients files are named, and the unit-8 filename is entered as a null. The terminating slash indicates that the default reaction-rate constants are satisfactory for the calculation at hand.

3.5.4 Atmospheric Data Input Files

The atmospheric data needed for a VPMP run is obtained from a primary input file associated with unit 2 and possibly from a secondary file on unit 9. Table 15 gives the quantities VPMP uses (except as noted below), as well as the required order of the columns in case column directives are not used. (Note that for this default configuration there are columns of data that are read but not used at all.) The format for reading these files is determined by the code. The 03301 vibrational temperature is not always available, and if it is absent the 02201 vibrational temperature is substituted.

The use of column directives simplifies the procedures for reading atmospheric data. The primary atmospheric data input file can then contain all required data, with columns in any order, so vibrational temperature profiles for different isotopes can be read from the same file. Column directives can be used on both the primary and secondary files, or alternatively all the data listed in Table 15 can appear on the unit-2 file, making the other one unnecessary.

Table 15. Atmospheric Input Data for VPMP (Default Configuration)	
Unit 2:	
Column 1:	Altitude
Column 2:	Kinetic Temperature
Column 3:	CO_2 Number Density or Mixing Ratio
Column 4:	Vibrational Temperature of CO_2 01101
Column 5:	Vibrational Temperature of CO_2 02201
Column 7:	Vibrational Temperature of CO_2 03301
Column 9:	Vibrational Temperature of $N_2(v=1)$
Unit 9:	
Column 1:	Altitude
Column 2:	Total Number Density
Column 3:	N_2 Number Density
Column 4:	O_2 Number Density
Column 5:	Atomic Oxygen Number Density

70

3.5.5 SFA Coefficients Files

In order to run, VPMP requires solar flux absorption coefficients as calculated by SABS in at least some of the possible pumping channels, for all four groups of high-lying CO_2 states. For the nighttime calculation, which is usually executed only for the 626 Group 1 states, data simulating the earthshine pumping is required in the same format.

Table 16 lists the bands in which solar pumping is usually provided for each of these cases. Some bands are optional, as indicated.

Since data for a lot of bands may be used, and since SABS may write coefficients for more than one SZA to the same output file, VPMP has the facility to search two files for the coefficients it needs. These files are associated with units 3 and 4. VPMP will look on the first one for data corresponding to the right bands and the right SZA, and unless it finds all the information it can use it will then go on to the other file (provided that a file-name is given). It will use all coefficients it finds that satisfy its criteria, but it will not perform the calculations if any required bands are missing.

VPMP uses special column directives to identify which columns of data contain co-efficients for the required bands and the specified solar zenith angle. These column directives are constructed in a manner similar to the column directives used to locate vibra-

		Group 1	Group 2	Group 3	Group 4
	Table 16. Solar Pumping Bands for High-lying CO_2 States				
1	*	00001-10012	* 01101-11112	* 00001-20013	* 00001-30014
2	*	00001-10011	* 01101-11111	* 00001-20012	* 00001-30013
3		10002-10012	11102-11112	* 00001-20011	* 00001-30012
4		02201-02211	03301-03311	00001-12202	* 00001-30011
5		10001-10011	11101-11111	00001-12201	-
6		-	-	10002-20013	-
7		-	-	10002-20012	-
8		-	-	10001-20012	-
9		-	-	10001-20011	-
10		-	-	02201-12212	-
11		-	-	02201-12211	-
* indicates bands required for VPMP calculation					

71

```
Table 17. Beginning of SABS output file, including header
CSAB_A67_CO2D_G1A_FJF.DAT                    SABS11 OUTPUT
C
C FORMAT(F8.2,1X,1P,11E11.4)
D COLUMN  1 ALTITUDE (KM)
D COLUMN  2 SFA COEFFS CO2 626 00001  10012   SZA = 17.00
D COLUMN  3 SFA COEFFS CO2 626 00001  10012   SZA = 60.00
D COLUMN  4 SFA COEFFS CO2 626 00001  10012   SZA = 80.00
D COLUMN  5 SFA COEFFS CO2 626 00001  10011   SZA = 17.00
D COLUMN  6 SFA COEFFS CO2 626 00001  10011   SZA = 60.00
D COLUMN  7 SFA COEFFS CO2 626 00001  10011   SZA = 80.00
D
D  ALT    SFA       SFA       SFA       SFA       SFA       SFA
D
  40.00  1.0066E-06 7.8007E-07 5.2515E-07 1.2597E-06 9.8645E-07 6.5652E-07
  41.00  9.8080E-07 7.4928E-07 5.0634E-07 1.2149E-06 9.4516E-07 6.3665E-07
```

tional temperature data, as described in Section 3.2.4, but there are two differences. The first difference is that since the directives specify a band rather than a state, both upper and lower vibrational state codes are needed instead of a single state code. The second is that the strings "SFA COEFFS" and "SZA =" must be found on the same directive line, and the latter must be immediately followed by a solar zenith angle that can be read in F7.2 format. That is, a seven-digit field with the SZA used when the calculation was performed must immediately follow the "=". When these conditions are satisfied, VPMP will try to match the identifiers in the directive with the bands and the solar zenith angle it needs for its calculations, and assign the column of data accordingly.

SABS writes these column directives onto the header of each file it produces, so its output files can be used directly by VPMP without changes. Table 17 gives an example of such a header. Note, however, that if a file should be constructed without directives in the file header, VPMP will use whatever data are in the first five columns of the unit-3 file (or the first eleven, for Group 3) for the required solar pumping coefficients. Since there is then no check on what is read, incorrect coefficients are not rejected and one must be careful to get exactly the right data in the right columns.

Table 18. Atmospheric Input Data for NIGHT_PUMP	
Column 1	Altitude
Column 2	Kinetic Temperature
Column 3	CO_2 Number Density
Column 4	CO_2 626 01101 Vibrational Temperature
Column 8	CO_2 626 02201 Vibrational Temperature

For nighttime simulations, program NIGHT_PUMP mentioned earlier produces the requisite file for the 626 Group 1 calculation. This program runs interactively. It only requires the user to provide one input file, plus filenames for that file and the one that is to be produced for VPMP to read. Table 18 lists the information that is expected on this file, which, being assumed to have the form of a RAD ν_2 vibrational temperature summary file (see Section 3.2.3), has columns of data that are not used for the present purposes. NIGHT_PUMP does not write a header with directives to its output file, but the format is such that VPMP can use it as it stands.

3.6 SABS

3.6.1 Introduction

The purpose of program SABS is to calculate the rate of absorption of solar flux in infrared bands, in order to enable the calculation of populations of vibrational states that are affected by it. These results for specific bands are used by other ARC programs, namely RAD, RADC, and VPMP. However, it can be applied to any band for which HITRAN data are available..

The algorithm used by SABS was originally described when the code was used to help calculate the vibrational temperatures of high-lying CO_2 states *(Sharma and Wintersteiner, 1985),* but recent updates make it possible to automate the calculations. SABS still processes only one band at a time, but during each run it will add results for new bands to output files from preceding runs. During each run it may evaluate the absorption for several different solar zenith angles (SZAs), as well. The normal procedure is to create a set of program directive files, one for each band under consideration, and then prepare a script to run the program as many times as necessary.

The SABS output consists of sets of solar flux absorption coefficients given as a function of altitude. The coefficients have units of in-band transitions per second per molecule, "per molecule" referring to the total density of the absorbing molecule rather than the density of whatever isotope may be under consideration. The output files contain the altitude grid followed by columns of coefficients for SZAs and bands in the order they are calculated, with up to eleven sets of coefficients. When one output file is full, SABS will close it and proceed to write the remaining results to a new one.

3.6.2 I/O Files

For each SABS run, at least three input files must be available. The program directives file tells the program what to do and names the other input and output files. One or

two atmospheric data input files provide the information to construct the model atmosphere. The primary file is associated with unit 2, and the secondary one, if used, is on unit 9. Also, a "unit-3" file containing the HITRAN data for the band in question must be accessible.

As with most of the other ARC codes, three output files are written for disposition to a printer. Two data output files, associated with units 7 and 8, can also be named for each run. If the first of these files exists (and is in the proper format), SABS will append columns of solar flux absorption coefficients to whatever data already are found there. If it doesn't exist, SABS will create it. In either case, it will write only eleven columns of coefficients to the first file, and then close that file and open the other one to write the remaining data. If the unit-8 file is not named but is needed, a default filename (BACKUP) is used. In the event that the altitude grid on an existing output file is different from that used in the current calculation, the new results are interpolated onto the original grid. The format in which the files are written is (F8.2,1X,1P,11E11.4).

The headers on the data output files include column directives that are recognized by some of the ARC codes. A sample header is shown in Table 17, as part of the discussion of input requirements for VPMP.

As with the other ARC codes, the input files consist of comment lines, directive lines, and data, in that order. The directive lines are optional but are particularly useful for reading atmospheric input data. Requirements for all the input files are given below.

3.6.3 Program Directives File

There are only three unit-1 directives that can influence the SABS calculation or the program output. The relevant character strings are listed in Table 19. Table 20 gives a list of the data records that SABS reads from the program directives file, and Table 21 gives an example of such a file.

Table 19. Unit-1 Directive-Line Strings for SABS	
"NOBRIEF"	causes detailed program results to be written that otherwise would be suppressed
"LTE CALC"	requires an LTE calculation to be performed.
"KEY ="	allows the ten characters following the = to be used as a keyword. The keyword is written onto the output files, but has no other function.

74

```
Table 20. Unit-1 Input Data Records for SABS
```

A. Filenames Record
    FLNM2, name of the principal atmospheric input data file
    FLNM3, name of the linefile with absorption lines
    FLNM7, name of the first output file
    FLNM8, name of the second output file (for overflow)
    FLNM9, name of the secondary atmospheric input data file

B. Band Record
    MOL = molecule code
    ISO = isotope code
    UST = upper vibrational state code
    LST = lower vibrational state code

C. Observation Heights Record
    HGTS = array of observation altitudes (km)

D. Solar Zenith Angles Record
    SZ = array of solar zenith angles (degrees)

E. Program Parameters Record
    HMAX = upper boundary of the atmosphere (default = 1000 km)
    ACC = fractional error allowable in absorption coefficients (default = .01)
    NPTS = # of integration points per panel (2, 4, or 8; default = 4)
    NDP = code for the Voigt lineshape algorithm (-1, 0, 1; default = 0)
    VMIN = lower end of the range searched for HITRAN data (default = 0 cm-1)
    VMAX = upper end of the range searched for HITRAN data (default = 20,000 cm-1)
    SFX = fixed solar flux (default = 0 ph/sec-cm^2-cm^{-1}; see text)

It is useful to note that the observation altitudes read from this file, HGTS, serve to define discrete altitudes at which the absorption calculation is actually performed. These altitudes generally are not the same as the altitudes read from the primary atmospheric data input file, which constitute the grid defining the atmospheric layers and also the grid onto which the observation-height results are interpolated in the end. The reason for making the distinction is to avoid unnecessary computation. One can prepare input files with relatively fine layering (such as might be needed for other calculations using the same model atmosphere), but calculate

Table 21. Sample Program Directives File for SABS

```
Csabs001_10.dat---UNIT-1 FILE FOR SABS
C CO2 GROUP 1 SOLAR FLUX ABSORPTION
C
D NOBRIEF
'~/atm67/a67_co2d_fjf_summ.dat',
 '~/lnfl/L101000.DAT',
  'SAB_A67_CO2D_G1_FJF.DAT',' ',
   '~/atm67/a67_tnd.dat'/
'CO2', 626, '10012','00001'/
40, 160, 2/
20,60,80/
160, .0001, 4, -1/
```

the absorption explicitly at only every fourth or fifth point. Or one could minimize the effort spent on high-altitude regions where there is little or no absorption. Since the absorption in a band is generally a smoothly-varying function, very small errors result from the final interpolation step. The observation heights may be read either as a minimum altitude, maximum altitude, and a spacing, or else as an explicit list of up to 100 altitudes entered in increasing order.

Some miscellaneous comments regarding the input data records are as follows. The unit-8 filename may be omitted. There may be up to 10 solar zenith angles processed for each band. If one or more of them is greater than 90 degrees, SABS will determine the lowest altitude required for the model atmosphere from the lowest line of sight path to the Sun; otherwise the lowest altitude required is simply the altitude of the lowest observation point. HMAX defaults to 1000 km, but the actual maximum altitude for the calculation will in that case be determined by the highest altitude on the primary atmospheric data input file. The lineshape code has three possible values: -1, 0, and 1. If NDP is read as -1 or 0, a Voigt profile is used, with 0 (the default) giving the faster but less accurate result. If NDP is 1, a Doppler profile is used.

The last comment concerns SFX. When this quantity is left at its default value of zero, as it normally is, SABS will specify the solar flux at the top of the atmosphere based on the wavenumber of each line in the band, interpolating between data points originally given by *Thekaekara (1971)*. As an alternative one may enter a fixed value for the flux, SFX, presumably a value appropriate to the middle of the spectral region covered by the band, and use that for all lines.

The sample program directives file that is given in Table 21 directs one of several runs that are necessary to calculate the solar flux absorption in the bands populating the CO_2 626 10012, 02211, and 10011 states, the so-called "group 1" states. Note that the NOBRIEF directive will require SABS to write a lot of information to the print files that is usually not necessary for production runs. Both primary and secondary atmospheric input data files are used. The first output file is named but the second is blanked. The band under consideration is a strongly pumped 2.7 μm band. Observation points evenly spaced at 2 km between 40 and 160 km will be used for the calculation, which will consider solar zenith angles of 20, 60, and 80 degrees. The program parameters record shows that no layers above 160 km will be used, and the more accurate Voigt routine will do the lineshape calculation.

3.6.4 Atmospheric Data Input Files

The atmospheric data needed for a SABS run is obtained from a primary input file associated with unit 2 and possibly from a secondary file on unit 9. Table 22 gives the default setups for these two files, including the required order of the columns of data in case column directives are not used. The format for reading these files is determined by the code. Note that the vibrational temperature of the lowest excited state is used only to calculate the vibrational partition function. Also, the upper-state vibrational temperature is normally of no importance for the absorption calculation, since it is used only to calculate stimulated-emission contributions to the linestrength. Therefore, arbitrary profiles can be used when a proper upper-state profile is unavailable.

Although the default setup shown in Table 22 works whether or not column directives are found, it is much easier to use files that do have them. In such cases, the primary atmospheric input data file can contain all the data listed in Table 22, making the secondary file unnecessary. When the lower state of a hot band is also the lowest excited state, SABS does not require redundant columns if column directives are used. Most important, the columns of data can appear in any order, so a single file can be used for many of SABS runs without regard to the placement of the different vibrational temperature profiles. Column directives can be used on both the primary and secondary atmospheric input files. The only restriction is that if two files are used, the secondary file must contain only the total number density.

Table 22. Atmospheric Input Data for SABS (Default Configuration)	
Unit 2: (Regular Bands)	
Column 1:	Altitude
Column 2:	Kinetic Temperature
Column 3:	Absorber Number Density or Mixing Ratio
Column 4:	Upper-state vibrational temperature *
Column 5:	Lowest excited state's vibrational temperature
Unit 2: (Hot Bands)	
Column 1:	Altitude
Column 2:	Kinetic Temperature
Column 3:	Absorber Number Density or Mixing Ratio
Column 4:	Lower-state vibrational temperature
Column 5:	Upper-state vibrational temperature *
Column 6:	Lowest excited state's vibrational temperature
Unit 9:	
Column 1	Secondary Altitude Grid
Column 2:	Total Number Density
* Arbitrary profile acceptable; see text	

When an LTE calculation is requested with a unit-1 directive, SABS does use any vibrational temperatures, so they can be omitted from the atmospheric data input files.

3.7 NLTEA

3.7.1 Introduction

The purpose of program NLTEA is to calculate the line-of-sight (LOS) radiance in infrared bands in the terrestrial atmosphere. It was specifically designed to deal with lines of sight encountering non-LTE emissions that vary in the horizontal direction. NLTEA was originally an extension of program NLTE, which performed the same line-by-line calculations in a one-dimensional (1-d) atmosphere. The algorithms used to determine the radiance are the same as those in NLTE and were documented by *Wintersteiner and Sharma (1985)*. However, the input, output, and geometry modules are substantially improved. As a result, NLTEA is now used to do the 1-d calculations as well as those involving horizontal structure, making NLTE obsolete..

To run NLTEA, it is necessary to specify the lines of sight, the bands of interest, and the state of the atmosphere—including the vibrational populations, expressed as vibrational temperatures, of all the emitting states. A program directives file is used to direct the calculations and to name the other input and output files. All the input requirements are given in later subsections. Various options for running the program, accessible by manipulating the input parameters on the program directives file, are also outlined below.

The NLTEA program output consists of (1) the overall band radiance for each line of sight; and (2) integrated line radiances, also for each LOS, that can be used to generate synthetic spectra. The latter function is performed by program CONV. In addition, the program can calculate contributions to the total radiance on a layer-by-layer basis, enabling a detailed study of the sources of observed emissions.

NLTEA can also be used in a "single-line" mode, in which case the program output includes the lineshape and the path optical depth calculated on a monochromatic basis as a function of wavenumber, from the center of the selected ro-vibrational transition.

3.7.2 Usage

NLTEA processes many lines-of-sight in a single run. The geometry can be a limb view or an outward view. However, downlooking paths are not accommodated.

For limb looking a "footprint" option allows NLTEA to simulate the smearing in the vertical (tangent-height) direction that results from the finite angular field-of-view that characterizes all real detectors.

NLTEA also processes many bands in a single run. Within each band the radiances are calculated on a line-by-line basis, using the no-overlap assumption. Each line is therefore treated independently of all others. The band radiance is the sum of the individual lines' contributions, and the total radiance is the sum of all the bands' contributions.

NLTEA permits two alternate descriptions of horizontal variations along viewing paths. One allows for *continuous variations* in the emission rates, appropriate for conditions that change gradually along the LOS as, for example, might be found near the terminator where relatively small changes in solar zenith angle may affect the excitation of emitting states considerably. The other specifies *discrete regions* within which non-LTE processes may be considerably different from those in adjacent regions. This option is useful for calculations involving auroral emissions, sprites, and other phenomena resulting from localized excitation processes.

Descriptions of how to specify all the required input parameters are given later. Certain options require some detailed explanation, however; these explanations appear in the following subsections.

3.7.2.1 Horizontal Variations

The two options for specifying horizontal variations were mentioned earlier, and are each illustrated schematically in Figure 42.

For Option 1, the emitting states' densities vary continuously along the LOS. This is achieved by reading upper-state vibrational temperatures as a function of altitude for two or more discrete locations and interpolating these temperatures onto the primary altitude grid at its intersections with the LOS. For Option 2, the atmosphere is regarded as having been divided into discrete regions, each of them characterized by a single vibrational temperature profile throughout its volume. In that case, NLTEA determines which segment of each path traverses each region, and chooses the upper-state vibrational temperatures accordingly. There is no restriction on the variation of the emission rate across the boundaries, so the vibrational temperatures may change discontinuously in the horizontal direction.

In both of these cases, NLTEA will read more than one profile for each emitting state's vibrational temperature. That is, several 1-d profiles are used one way or another to get the proper description of the emission along each of the viewing paths. In both cases the horizontal variations are restricted to the emitting states' populations (which are parameterized by their vibrational temperatures). That is, the emitting states' populations at given altitudes may be different for different paths or different segments of a single

limb path, but the kinetic temperature, the total densities of the emitting molecules, and other properties of the atmosphere are assumed not to change except with altitude.
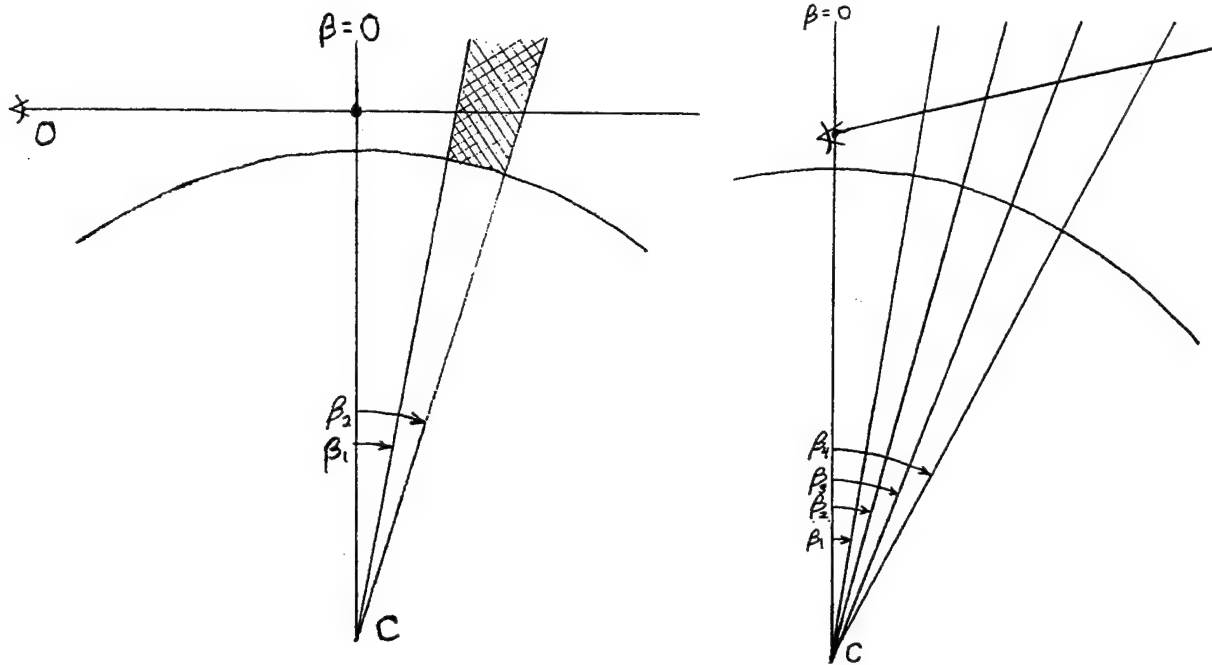
Figure 42a (left): Illustration of Option 1 (see text) for a limb-viewing line-of-sight (LOS) path intersecting a single discrete structure (cross-hatching) located on the side of the tangent point (heavy dot) away from the observer (O). The locus of points on the LOS is parameterized by the Earth-centered angle, β, with the tangent point corresponding to $\beta=0$, the structure being located by $\beta_1 < \beta < \beta_2$, and $\beta>0$ characterizing the portion of the path beyond the tangent point.

Figure 42b (right): Illustration of Option 2, where the atmosphere is assumed to vary continuously along a LOS. NLTEA reads separate model atmospheres corresponding to five Earth-centered angles (β_1-β_5) and interpolates onto the LOS at intermediate angles. In this case, $\beta=0$ is defined by the location of the observer, but Option 2 may also apply to limb viewing just as Option 1 (discrete segments) may apply to endoatmospheric views.

To correlate path segments with vibrational temperatures, each 1-d profile is associated with an "earth-centered angle" (ECA), or a pair of such angles, that is read from the program directives file. The angles are in the plane defined by the center of the earth and the viewing paths. For limb view, the angles are referenced to the line running from the center of the earth to the lowest tangent point. In this case, a negative angle refers to a 1-d profile closer to the exoatmospheric observer than the tangent point, while a positive angle specifies one that is farther away. For an observer within the atmosphere, negative angles are not permitted. In both cases, angles greater than 16 degrees are not allowed. For continuous variations along the paths (Option 1), there is a single ECA for each 1-d vibrational temperature profile that is to be read. For the discrete region case (Option 2) ECAs represent the boundaries between the regions, so the number of ECAs is one less than the number of regions and there must be one profile for each region. Thus, in Figure 42a, three profiles are required to specify the emission rates in the three regions defined by two ECAs (although if the profiles are the same in regions 1 and 3 it is not necessary to read duplicate files). In Figure 42b, five profiles corresponding to five ECAs are indicated.

The intended purpose of the discrete-region option is to enable calculations of phenomena originating in localized regions, for which the approximation represented by the sharp boundary may not be a totally unrealistic one. The continuous-variation option may be more generally applicable and (although requiring more individual 1-d profiles to be used) may thus be used for localized structures whenever variations across the boundaries can be modeled properly.

3.7.2.2 LOS Geometry

For limb-viewing lines-of-sight the required path parameters are the altitudes of the tangent points. These may be specified either by a range of equally-spaced altitudes (minimum, maximum, and spacing) or by a list of up to 50 individual altitudes in ascending order.

For outward-viewing lines-of-sight, the required path parameters are the observer's altitudes and the angle of the upward-looking LOS with respect to local zenith at the location of the observer. The altitudes are specified in the same way tangent heights are specified for limb geometry, and the angle is the same for all paths.

NLTEA distinguishes between the exo- and endo-atmospheric observing cases by the sign of the zenith angle that is read. A negative angle, which is the default, forces limb-look geometry, while an angle in the range 0-90 degrees assumes the observer is within the atmosphere. Other values are not acceptable.

3.7.2.3 Footprint Calculation

The footprint calculation is enabled for limb-look geometry if a directive line containing the character string "FOOTPRINT" is found on the program directives file. In such a case, a data record that is otherwise not present on the unit-1 file specifies the altitude of the exoatmospheric observer and the angular footprint of the detector. The desired views are specified by mean tangent altitudes, and for each view four separate LOS paths to represent the instrument field-of-view are generated and processed. In the end the radiance levels are determined by averaging over these four paths. No more than 12 views can be accommodated when the footprint option is enabled.

3.7.2.4 Single-Line Runs

The normal objective is to calculate the band radiance and the spectral radiance for a broad spectral region covered by the bands of interest. An alternative application is a so-called "single-line" run, which processes only a single ro-vibrational transition. This is useful for examining the transmission of the atmosphere in a very detailed fashion and for studying the emission on various segments of the LOS.

The single-line option is enabled if a directive line with the string "SINGLE" is encountered on the unit-1 file. The code then processes only the one transition per band and calculates and prints detailed information pertaining to it. The chosen line is the first line corresponding to the band of interest that appears on a specified HITRAN data file, or else the first line appearing at a wavenumber greater than the value VMIN which is read from the "program parameters record" (described below) on unit 1. Normally VMIN retains its default value of zero, which enables NLTEA to search linefiles from the beginning, but this is not a requirement for either regular runs or single-line runs.

3.7.3 I/O Files

At least three input files must be accessible in order for NLTEA to run. The unit-1 file contains program directives that tell NLTEA what to do and where to find other input data. One or more "unit-2 files" (named on the unit-1 file) provide the atmospheric profile input data. One or more "unit-3 files" (also named on unit 1) contain the HITRAN data describing transitions of each infrared band to be processed. Requirements for each of these are listed below.

Several optional output files are used to retain the program results. For the normal mode of operation a "unit-8 file" contains all the individual integrated line radiances. (The integrated line radiances, taken together, are known as "stick spectra", and can be degraded using selected scanning functions to produce synthetic spectra. This function is

carried out by program CONV.) This file accommodates results from at most twelve LOS paths. A "unit-9 file" contains the "band radiance summary" consisting of the radiance in each band plus the total radiance.

These two files will be written if and only if non-blank filenames are specified for them on the unit-1 file. Each of them can also be read and rewritten in successive NLTEA runs to append additional results, if necessary. They usually are not requested for single-line runs.

For the single-line mode of operation, one may request a "unit-7 file" and/or a "unit-10" file, also by simply specifying filenames. The former contains the monochromatic spectral radiance and the latter the path optical depth, each for up to twelve LOS paths. These may not be requested unless the single-line mode is in effect.

As with most other ARC codes, NLTEA also produces three files intended for disposition to a printer, including a unit-6 file that comprises a progress report on the run.

3.7.4 Program Directives File

The purpose of the program directives file is to tell NLTEA what calculations to perform, how to do them, and what other files to use. The header contains directives that invoke various options, and the data records give filenames and numerical information that is used directly.

Table 23 lists all the directive character strings that have a substantive effect on calculations performed by NLTEA or the information it writes to output files.

Table 24 lists the data records that are read from the program directives file, in the required order. As noted above, these data records follow the directive line-images and are read with list-directed reads. Defaults are provided for many of the list elements, but for NLTEA to operate properly data must be read into those elements for which no default is indicated below. More information can be found in the comments in subroutine DIREC.

Table 25 gives a sample NLTEA program directives file. In this example, eleven bands are being processed using seventeen limb paths, equally spaced in tangent height between 50 and 130 km. All the vibrational temperatures, as well as the kinetic temperature, CO_2 density, and total density, are assumed to reside on one of the four atmospheric data input files named. All the lines in each of the eleven bands are assumed to reside on one of the four HITRAN linefiles named. Stick spectra will be written to the unit-8 file, but for only twelve of the seventeen paths because twelve is the maximum number allowed. A band radiance summary will be written to the unit-9 file. If either of

Table 23. Unit-1 Directive-Line Strings for NLTEA	
"FOOT"	activates the footprint option; default is no footprint calculation.
"LAYER"	causes layer contributions for each path to be written to unit 5.
"NOBRIEF"	causes detailed program results to be written to units 4 & 5 that otherwise would not be written.
"FULL"	has the same effect as "NOBRIEF".
"LTE CALC"	requires an LTE calculation to be performed. The LTE option is not useful except for one-dimensional calculations, since no vibrational temperatures are used and therefore no regions can be distinguished.
"USE USST"	requires use of the U.S. Standard Atmosphere kinetic temperature.
"USE USSD"	requires use of the U.S. Standard Atmosphere total number density.
"USE USS"	followed (anywhere on the same line) by "TEMP" and/or "DENS" has the same effect as "USE USST" and/or "USE USSD".
"KEY ="	allows the 10 characters following the = to be used as a keyword. The keyword is written to the band radiance summary output file, but has no other function.

these two files exists as a valid file of the same type containing results from previous NLTEA runs, then the results of the present run will be added in or appended to the existing results. Of the six program parameters, only HMAX is reset from its default value because the other two quantities that are read happen to be the same as the respective defaults. No unit-1 directives have any effect. Since the FOOT directive is not found, the footprint calculation is not enabled and record F does not appear on the file.

Three discrete regions are being processed using Option 2. The first lies between the observer and a point 3.47 degrees closer to the observer than the 50-km tangent point. The other two lie beyond this point, and beyond a point 3.20 degrees closer than the tangent point, respectively. This is a case with a narrow intermediate region, which happens to intersect each limb path over a distance of only about 30 km, relatively near to the observer and falling between two much broader regions that might be described as "background". (In fact, regions 1 and 3 could have the same upper-state vibrational temperature profiles. To assure this, one would put two separate column directives on the same atmospheric data input file for each column, identifying the column with region 1 and also with region 3; see the discussion below.)

Table 24. Unit-1 Input Data Records for NLTEA

A.   Atmospheric Data Input Files Record: a list of files on which *any* of the required atmospheric data may be found. Character variables with up to 60 characters are read.

B.   HITRAN Data Files Record: a list of files on which HITRAN transitions of *any* of the specified bands may be found. Character variables with up to 60 characters are read.

C.   Output Files Record: names of the unit-7, -8, -9, and -10 files, in that order. Default is blank fields. Character variables with up to 60 characters are read.

D.   IR Bands Record: a list of bands to be processed by NLTEA. A band is specified by giving the molecule, isotope, upper vibrational state, and lower vibrational state. The molecule is given as a 3-character variable, the isotope as an integer, and the vibrational states as 8-character variables. The four-variable sets are entered sequentially. No more than 25 bands can be processed in a single run.

E.   LOS Paths Record: a look angle (default = -90 degrees) followed by a list of tangent altitudes or observer altitudes, in kilometers. A negative look angle triggers the limb calculation; a non-negative angle must be no greater than 90 degrees. The altitudes, no more than 50 in number, must be listed in increasing order. Alternatively, a range of equally-spaced altitudes may be specified by three quantities following the look angle: a minimum altitude, maximum altitude, and spacing.

F.   Footprint Record: the altitude of the exoatmospheric observer (default = 300 km) and the angular footprint of the detector (default = 0.01 radians). This record is included only if the footprint calculation is enabled with the FOOT directive; otherwise, it is omitted.

G.   Region Definition Record: the number of distinct atmospheric profiles being considered, an integer specifying Option 1 or 2, and a set of Earth-centered angles (ECAs) in degrees to identify the profile locations (1) or delineate the regions that are desired (2). The number of profiles cannot be greater than 10. For a 1-d calculation, which is the default, this record can be entered simply as "1/".

H.   Program Parameters Record: six program parameters:

HMAX = highest altitude to be considered (default = 1000 km or highest altitude encountered on the first atmospheric input data file)

ACC = allowable fractional error, integrated intensity in each line (default = .001)

NPTS = number of integration points per integration panel (2, 4, or 8; default = 4)

NDP = lineshape code: 0 = Voigt, 1 = Doppler (default = 0)

VMIN = lower end of range searched for HITRAN data (default = 0 cm^{-1})

VMAX = upper end of range searched for HITRAN data (default = 20,000 cm^{-1})

A region-definition data record like "5, 1, -3.0, -1.5, 0.0, 1.5, 3.0/" illustrates Option 1. The five angles correspond to five 1-d vibrational temperature profiles. For all seg-

```
Table 25. Sample Program Directives File for NLTEA

CNLTE001A.DAT---UNIT-1 INPUT FOR NLTEA
C
D BRIEF
D
'~/atm67/a67_co2d_fjf_summ.dat','~/atm67/A67_CO2D_001_ALL_FJF_N.DAT',
        '~/atm67/a67_tnd.dat', '~/atm67/A67_CO2D_G1_626_FJF_N.DAT'/
'~/lnfl/l001000.dat', '~/lnfl/l011010.dat', '~/lnfl/l101100.dat','~/lnfl/l021020.dat'/
' ', 'STK_A67_CO2D_FJF_NU3_N.DAT','BRS_A67_CO2D_FJF_NU3_N.DAT'/
'CO2', 626, '00011','00001',
'CO2', 636, '00011','00001',
'CO2', 628, '00011','00001',
'CO2', 627, '00011','00001',
'CO2', 626, '01111','01101',
'CO2', 626, '01111','01101',
'CO2', 626, '01111','01101',
'CO2', 626, '01111','01101',
'CO2', 626, '10012','10002',
'CO2', 626, '02211','02201',
'CO2', 626, '10011','10001'/
-90, 50, 130, 5/
3, 2, -3.47, -3.20/
180, .001, 4/
```

ments of all paths closer to the exoatmospheric observer than 3.0 degrees, the upper-state vibrational temperature for a given altitude is directly taken from the first 1-d profile. For segments between 3.0 and 1.5 degrees closer the temperature is linearly interpolated between profiles 1 and 2, and the same process applies for more distant segments except that past 3.0 degrees on the far side there is no interpolation, just as for the nearest segments. Thus, the five angles really define six "regions" within which a certain algorithm is applied to determine the emission rate along the paths, but unlike Option 2 the regions are not discrete in the sense of having discontinuities across the boundaries.

3.7.5 Atmospheric Data Input Files

Atmospheric data input files are associated, one by one, with logical unit 2. For each band being treated, NLTEA must have the radiating molecule's number density or mixing ratio, plus the vibrational temperatures of the upper state, the lower state (unless it is the ground state), and the first excited state (used to calculate the partition function). The upper-state temperature needs to be supplied for all requested regions. Also, the kinetic temperature and the total number density, which are the same for all bands, are needed.

NLTEA searches the headers of all the listed atmospheric data input files until it finds column directives locating the data that are required for all the bands. If certain profiles are missing, then NLTEA will not process that band and will print a message to that effect on unit 6. For each file it will use whatever column format is in effect on the first data line to read the entire file. If the columns are not consistent with the information in the column directives, the file will be discarded.

NLTEA cannot function without the "COLUMN" and "REGION" directives (except when only one region is specified; then only column directives are needed). The former identifies the contents of a given column of data, while the latter identifies the region corresponding to a given column of data. Both of these directives work in conjunction with subsidiary strings, and both require a three-digit integer field immediately following the keyword to give a column or region number.

Column directives were described in Section 3.2.4. To give an example, a line consisting of "D COLUMN 2 KINETIC TEMPERATURE" identifies the data in column 2

Table 26. Sample Atmospheric Data Input File for NLTEA

```
CA67_CO2D_001_ALL_N_FJF_XCC.DAT              RADC5 OUTPUT
C                                            CO2 626 00011  00001
C                    .                       CO2 636 00011  00001
C                                            CO2 628 00011  00001
C                                            CO2 627 00011  00001
C                                            10-May-96 10:37:52
C FORMAT(1X,F6.2,F10.3,1P,E12.4,0P,1X,5F9.3)
CD COLUMN  1 ALTITUDE (KM)
D COLUMN  2 KINETIC TEMPERATURE (K)

D COLUMN  3 CO2 DENSITY (MOL/CM3)
D COLUMN  4 VIBRATIONAL TEMPERATURE CO2 00011   626 REGION  2
D COLUMN  5 VIBRATIONAL TEMPERATURE CO2 00011   636 REGION  2
D COLUMN  6 VIBRATIONAL TEMPERATURE CO2 00011   628 REGION  2
D COLUMN  7 VIBRATIONAL TEMPERATURE CO2 00011   627 REGION  2
D COLUMN  8 VIBRATIONAL TEMPERATURE N2(V=1)
D
D  ALT    T       [CO2]    001-626 001-636 001-628  001-627 N2(V=1)
D
 40.00  250.350  2.7415E+13  250.349 250.349 250.352 250.360 250.349
 41.00  253.114  2.3715E+13  253.128 253.127 253.128 253.130 253.128
 42.00  255.878  2.0548E+13  255.858 255.855 255.854 255.849 255.858
 .
 .
```

of whichever file is being processed with the kinetic temperature, and further searches for kinetic temperature data will not be conducted. Column directives for number densities and lower-state vibrational temperatures are constructed as indicated earlier.

In the case of upper-state vibrational temperatures, an additional requirement is that the region be specified with the string "REGION" followed by a three-digit integer field giving a valid region number. Thus, a region directive can be, and usually is, part of a column directive line. However, a different form of the region directive is as a stand-alone (that is, not a part of a column directive). This requires the string "ALL PROFILES" to be located, and indicates that all data on the file in question are associated with the region identified. A line consisting of "D ALL PROFILES ARE FOR REGION 3" satisfies this requirement. This is useful if upper-state vibrational temperatures for a lot of different bands are stored on the same file. A directive of this type should precede all column directives, which are still needed to tell what data are found in which columns.

Note that REGION directives are required regardless of whether the horizontal variations are specified by Option 1 (continuous variations) or Option 2 (discrete regions). In the former case the "regions" identified in the directives refer to the locations associated with each 1-d upper-state vibrational temperature profile.

The order in which the strings appear on the directive lines is immaterial, except for the three-digit fields following the keywords. The vibrational state strings are matched with 8-character left-justified strings, so a sufficient number of trailing blanks must exist to permit a comparison. As an example, the line "D COLUMN 4 CO2 626 00011 VIB TEMP REGION 2" is sufficient to identify the data in column 4, but without three blanks following "00011" the state identification could not be made.

Table 26 gives an example of the beginning of an acceptable atmospheric data input file, with some of the comments and most of the data removed.

3.7.6 HITRAN Data Input Files

HITRAN data input files are associated, one by one, with logical unit 3. The only requirement for the linefiles that is different from the requirements of the other ARC codes is that band directives must be found in the headers. These lines contain the string "BAND" plus strings identifying the radiating molecule, the isotope, the upper vibrational state, and the lower vibrational state. They allow NLTEA to determine which of the many possible linefiles contains the ro-vibrational transitions it needs to process for each specified band. The order in which the strings appear is immaterial. Table 27 gives an example of the beginning of a CO_2 linefile.

Table 27. Sample HITRAN Input Data File for NLTEA							
Cl001000.dat							
C LINEFILE HITRAN92		11/30/93					
D BAND CO2 626 00011	00001	NU3 FUNDAMENTAL 109 LINES					
D BAND CO2 636 00011	00001	NU3 FUNDAMENTAL 98 LINES					
D BAND CO2 628 00011	00001	NU3 FUNDAMENTAL 193 LINES					
D BAND CO2 627 00011	00001	NU3 FUNDAMENTAL 179 LINES					
D							
2182.0352 7.47E-27.0563 3622.3413	00011	00001			P 96	636	2
2184.6850 1.50E-26.0565 3474.1983	00011	00001			P 94	636	2

3.8 CONV

3.8.1 Introduction

The purpose of program CONV is to generate synthetic spectra from the LOS radiance data produced by NLTEA, or from output that is written in the proper fashion by other programs (e.g., AARC).

If the proper option is invoked, NLTEA produces an output file containing "stick spectra" from all the bands it has processed. For a given band, a stick spectrum is simply a list of the integrated line radiances for a given line-of-sight (LOS) path for all of the individual ro-vibrational transitions in the band, each such radiance being associated with the position (in cm^{-1}) of the center of the line. That is, after NLTEA has processed a given transition by integrating the monochromatic spectral radiance over the entire line profile, the result is a single radiance assigned to that position. CONV convolves these quantities, treated as infinitesimally-narrow "delta-function" profiles, with selected response functions to produce the synthetic spectrum. The assumption underlying the calculation is that the response functions are much broader than the true line profiles of the individual transitions, which makes the delta-function approximation valid.

Unlike the other ARC codes, CONV runs interactively, and makes use of a set of ten menu options instead of a program directives file. It processes stick spectra from either one LOS or all the LOS appearing on the input file, and produces an output file with an equal number of synthetic spectra. The output units can be watts/(cm^2-sr-cm^{-1}) or watts/(cm^2-sr-μm). Details on using the code are given below.

3.8.2 I/O Files

CONV uses three input files and produces one output file, all of them ASCII files.

One input file is a "defaults file", having the name DEFLTS8.DAT. This file contains the input parameter settings used during the most recent CONV run, and is needed to populate the menu with default settings for all quantities that the code reads. The normal procedure is for the user to update these settings and then run the synthetic spectral calculation, but this file is rewritten every time a user quits the menu, with or without actually doing the main calculation. A backup file, DEFLTS8.BAK is also written every time the main defaults file is changed. If DEFLTS8.DAT cannot be found, then CONV will create it once input data for all menu items have been entered.

Another input file is a helpfile, named DAARCZ8.HLP. CONV will run without this file, but the help function, invoked by typing "H" at the main menu, will not work.

The third input file is the required stick spectrum file, the direct unit-8 output from NLTEA. This file is written with the line position in wavenumbers in column 1 and the integrated line radiances in watts/(cm^2-sr) in successive columns starting with column 2. Each column corresponds to a different LOS, and there may be stick spectra from as many as twelve LOS. It begins with a header that lists, among other things, all the LOS and all the bands that have been processed. This is followed, in succession, by the stick spectra from the first band, a delimiter line consisting of the string "CXXXXX", three comment lines, and then more stick spectra for the next band. The end of the file is indicated by a line consisting of "C$$$$$$". CONV is the only ARC code that permits an input file having comments interspersed with data records.

The output file is written in column format, with the first column containing the wavenumber or wavelength and the others giving the synthetic spectra that were calculated. Its header includes an echo of the input file header, followed by a list of parameters used in the calculation. The latter include the type of spectrometer response function, its full width at half maximum (FWHM), the units, and the names of files that were used.

3.8.3 Usage

Table 28 lists the items found on the CONV menu. Whatever options may be available are presented when one types the number of a menu item followed by a "return". One then enters suitable quantities, and control returns to the main menu to enable another choice. CONV will run the main calculation when a zero is entered in place of a menu item number, or the user can exit the menu by typing "Q". The units chosen for the calculation are indicated on the screen, as are the current parameter values.

The first item on the menu is a toggle between the possible choices for units, so in that case there are no further choices. That is, typing "1" followed by "return" switches the expression of all parameters from cm^{-1} to μm or vice versa. Everything that depends

90

on the units, such as the range for the synthetic spectra, is recalculated each time this switch is enacted.

The second and third items are simply the intended bounds of the spectra. The fourth item determines the number of points in the synthetic spectra. Three options are available here. The first is simply to enter the number of points, in which case CONV will determine the spacing required to span the interval specified by items 2 and 3. The second is to specify the spacing itself, in whatever units are in use. The third option is to read the individual points from a file, whose filename must then be provided. This file, if used, just consists of a column of wavenumbers or wavelengths.

There are six choices for the spectrometer response function, or scanning function. For convenience, these are listed as part of Table 28. It is always necessary to specify a full-width at half maximum (FWHM) for these functions. For four of them, it is also necessary to specify a cutoff distance beyond which the contribution of a given line is not evaluated. This is item 7. It is entered in units of the FWHM, and is necessary because the continuous scanning functions all extend infinitely far from the line centers and thus in principle have contributions from all lines at all points. There are no default values for item 7 that are specialized for the different scanning functions, so it is advisable to test the effect of the cutoff once the FWHM is determined. The cutoff is ignored for the triangular and rectangular response functions.

The eighth and ninth items on the menu are the names of the output and input data files, respectively. The last item allows the user to pick a single column of input data—that is, a single LOS—for processing, or else specify that all the stick spectra be used.

Table 28. CONV Menu Items
1. Choice of units (μm or cm^{-1})
2. Lower bound of spectra
3. Upper bound of spectra
4. Number of points in spectra (*)

5. Spectrometer response function
    Triangular
    Gaussian
    Sinc [sin(x)/x]
    Hamming
    Rectangular
    Kaiser-Bessel

6. FWHM of response function
7. Number of FWHMs (*)
8. Name of destination file
9. Name of source file
10. Input column to process
* see text

4. MSX ACTIVITIES

4.1 Introduction

The Midcourse Space Experiment (MSX) satellite, launched into orbit in early 1996, carries a package of multi-spectral optical instruments for studying the earthlimb, terrestrial, and celestial backgrounds, plus supporting diagnostic equipment. The wavelength coverage runs from the extreme ultraviolet to the far infrared. The instruments include a set of infrared radiometers and interferometers comprising the SPatial and InfraRed Imaging Telescope (SPIRIT III), a suite of Ultraviolet and Visible Imagers and Spectrographic Imagers (UVISI), and a Space Based Visible camera (SBV). The spectral range, the global coverage that will be achieved with the high-inclination orbit, and the mission's multi-year duration are each important for the acquisition of what will become a unique and voluminous database of atmospheric emissions.

ARCON participated in the planning and development activities of the Earthlimb Backgrounds Team, which is one of several teams coordinating the investigations that the MSX program was tasked to carry out. Our principal responsibilities involved the UVISI instruments, and are discussed below. They were undertaken as part of a larger coordinated planning process having the purpose, among other things, of specifying what data were required, what instrument configurations (experiment modes) would be used, how the automated data processing system should be set up, what algorithms it should use, and specifically what software was needed to organize, process, and display this massive amount of information.

Papers describing MSX in general *(Mill et al, 1994)* and the Earthlimb observations in particular *(O'Neil et al, 1994)* are listed among the Technical References.

4.2 Automated Data Processing

Data from the MSX optical instruments is processed in many steps, starting with raw telemetry and ending with reduced data products in the form of files, graphical displays and searchable databases. A most succinct summary of the overall procedure is this: information is first broken out according to instrument, then converted to physical units, and finally sorted, selected, and processed by specific algorithms to produce output files with summary data in predetermined forms and formats. This third step represents the end of the automated data analysis (ADA), a pipeline process that runs without operator intervention. The summary data are also made available for a fourth step, interactive data pro-

cessing, in which an analyst reviews the graphical data products and validates the experiments' results.

Software that is used to process data from the five UVISI spectrographic imagers (SPIMs) was designed and written by us, and later integrated into the larger ADA software product by other workers. In particular, we drew up specifications for the SPIM data products, produced pseudocode for an initial design, and wrote the C-language code that was merged into the ADA software. The stand-alone program was named SPIMDRVR, and it fits into the ADA at the third of the four steps listed above. That is, the program takes all the Level 2 SPIM data, which are data that have been broken out by instrument and converted to physical units, and processes them into the required forms and formats as Level 3 files. SPIMDRVR V3.2 is the latest version delivered to the Phillips Laboratory Data Analysis Center (PL/DAC).

The specifications for the data products, and the design of the code, evolved throughout the development period. As the SPIMs themselves were assembled and tested, new issues arose that had to be addressed. The original plan was laid out in the Earthlimb Automated Analysis Plan *(O'Neil et al, 1993)*. Progress on the SPIM software was reported by us at the Earthlimb System Design Review on 4 June 1993 and at the PL/DAC Critical Design Review on 4 March 1994, as well as at Earthlimb PI meetings that were held periodically.

The following discussion and figures summarize the principal features of the SPIM software, and the requirements that it was designed to meet. For reference, a description of the UVISI instrument can be found in reports by *Carbary (1992)* and the UVISI Instrument Team *(1992)*. For the immediate purpose at hand, we note that the spectrographs' two-dimensional pixel arrays acquire many spectra simultaneously. These spectra correspond to lines-of-sight (LOS) with slightly different horizontal orientations, thereby enabling the instrument to identify spatial structure with dimensions on the order of 20 km. The spectra are said to accumulate in different "spatial pixels". The number of spatial pixels may be 5, 10, 20, or 40, depending on how the instrument is configured.

4.2.1 Requirements

The direct requirement for the SPIM automated software is to produce Level 3 files in suitable form for use in the interactive processing.

For the Earthlimb experiments, the infrared data are the prime data of interest. One function of the visible and ultraviolet data is to provide diagnostic support for the SPIRIT III data analysis. For example, given that infrared data might suggest the presence of, say, an aurora, one important role for the visible-wavelength data would be to confirm the

suggestion by providing intensity levels for emissions at 3914 A or 5577 A or other auroral wavelengths. If the infrared data would appear to have anomalous features, the short-wave spectral data might be expected to provide clues as to the source of the anomaly.

The software for the SPIM automated processing was written with this accommodation in mind. That is, the spectra and image data arrays that SPIMDRVR retrieves or constructs from the Level 2 data were selected partly on the basis of providing this diagnostic support. Therefore, the spectra that are saved are taken from spatial pixels that coincide with, or "overlap", the views of the two SPIRIT III radiometer stacks. Sub-bands, which are wavelength ranges covering particular spectral features, were selected to provide automatic access to intensity levels for important visible and ultraviolet emissions that might serve diagnostic purposes. Radiance profiles are constructed from sub-band data acquired from the pixels overlapping the radiometer stacks, as well.

In addition to supporting the infrared measurements, the SPIM data may be used on their own to identify key features and scenes, and for the purposes of phenomenology assessment. In addition to easily-recognized emissions such as those from aurora, for example, it may be possible to detect noctilucent clouds or transient signals from upward-propagating lightning (sprites) using these data. The use of templates and indicators, discussed briefly in the section on data products, was expected to be one way to automate some of the phenomenology assessment, and the software was designed accordingly. However, the lack of suitable models for short-wave emissions made it impossible to implement the proposed algorithms as envisioned.

In summary, the basic purpose of the SPIM software was to produce Level 3 files, and this was done in such as way as to satisfy the requirement of providing diagnostic support for the infrared data analysis and also the requirement of producing scenes and data profiles that would be most useful for independent phenomenology assessment.

4.2.2 Design and Implementation

Figure 43 gives a schematic outline of the flow of the SPIM data and lists the file types (e.g., calibration files) required at each step. It starts with Level 1B data, which are already broken out by instrument. CONVERT is the module that converts the data to physical units and produces Level 2 files. Four Level 3 files that comprise the SPIM-DRVR output are shown as input to SUMGRAPHX, the interactive processing software.

MAMBA is the module that uses the spacecraft attitude data to determine the target points for the lines-of-sight (LOS) of individual detector elements, or pixels. SPIMDRVR has to calculate the LOS in Earth Centered Inertial (ECI) J2000 coordinates, the standard MSX reference frame, for times corresponding to the beginning of every frame. To do

94

SPIM Data Processing: Outline
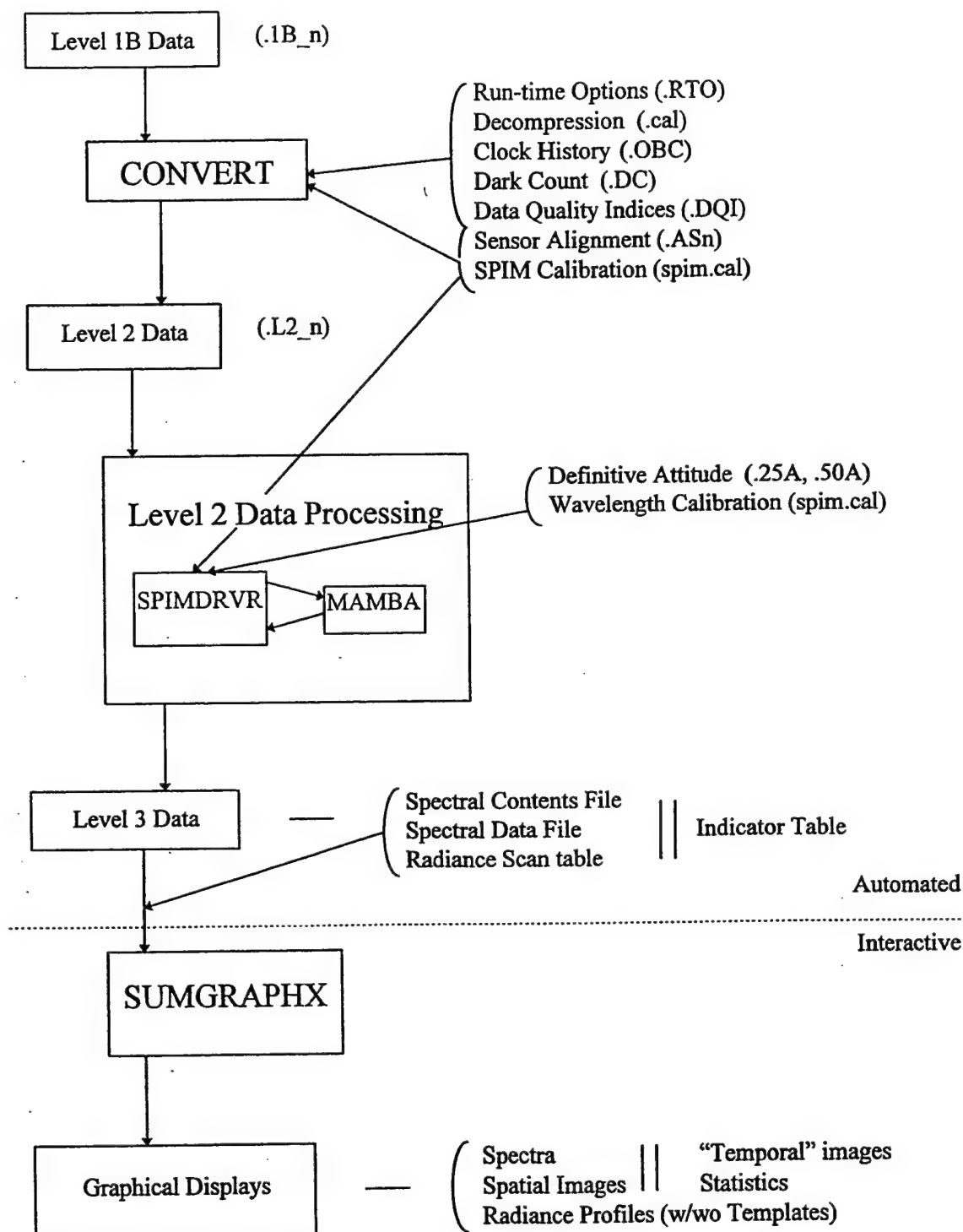
Figure 43. Schematic outline of the SPIM data processing flow, starting with Level 1B data. The principal data types, processing modules, auxiliary input files, and data products are indicated.

this, it performs a number of transformations. Each pixel's LOS is related to the sensor boresight (of that particular instrument) by a fixed *pixel offset* determined by the pixel's position in the array and the position of the scanning mirror *(Carbary, 1992)* and by a *distortion correction* that accounts for non-linearities in the positioning of the pixels within the array. The sensor boresight is related to the spacecraft body coordinates by an *alignment transformation*. The spacecraft body coordinates are related to the ECI J2000 frame by the *attitude transformation*.

The input files that provide the information needed to effect these transformations are listed on the right side in Figure 43. The first two transformations require expansion coefficients given in the SPIM calibration file. The alignment transformation takes the sensor boresight into the spacecraft frame using a rotation matrix whose elements are derived from data in the sensor alignment file. This would be the identity matrix if the instrument were lined up perfectly. The attitude transformation is calculated from an attitude matrix that is in turn calculated from so-called MSX quaternions given in the definitive attitude file.

The attitude transformation depends on the orientation of the spacecraft with respect to the ECI frame, so the definitive attitude file has entries every 50 milliseconds throughout the data collection event (DCE). The other transformations simply relate to the instrument and the spacecraft, and vary only with the mirror position. The files supplying the coefficients they use are updated periodically following in-flight calibrations.

After completing the LOS calculation for a given pixel, SPIMDRVR passes the information to MAMBA in the form of a unit vector. It also passes the spacecraft position and velocity from the definitive attitude file. MAMBA calculates the coordinates of the target point and other required information. For limb-viewing geometry the main quantities it returns are the latitude, longitude, and altitude of the tangent point, and the solar zenith angle at the tangent point. For nadir viewing, the nadir angle to the pierce point is returned in place of the tangent altitude.

SPIMDRVR also requires a wavelength calibration. The calibration coefficients are given in the same SPIM calibration file that has the coefficients for the offset and distortion corrections.

SPIMDRVR was run using Level 2 test files that were based on model calculations for certain atmospheric emitters. After much effort, we realized that the data in these files were not realistic in any sense, except for an occasional isolated spectrum. These files were useful for checking the input functions and some other operations, but it was not possible to use them to verify the functionality of most of the algorithms that we had programmed.

96

SPIM Sub-bands

Instrument or Feature	Sub-band	Code	Wavelength (nm)	Width (nm)	Width (pxl)	Notes	Comments
SPIM #1		FUV	110.0-170.0	60	272	(2)	1 pixel = 0.22 nm
1216, Lyman alpha	1	HI_Ly_alph	121.0-122.2	1.2	5.4	(1)	DMI-1; dominant SPIM_1 feature
1304, Atomic oxygen	2	OI_1304	129.8-131.0	1.2	5.4	(1)	DMI-2
1356, Atomic oxygen	3	OI_1356	135.0-136.2	1.2	5.4	(1)	DMI-3
N2 Lyman-Birge-Hopfield	4	N2_LBH_1	151.0-152.2	1.2	5.4	(1,3)	DMI-5; LBH (2,3)
N2 Lyman-Birge-Hopfield	5	N2_LBH_2	165.0-170.0	5.0	22.7	(1)	DMI-6; LBH (0,4); (1,5)
SPIM #2		MUV	165.0-258.0	93	272	(2)	1 pixel = 0.34 nm
N2 Lyman-Birge-Hopfield	6	N2_LBH_3	192.0-196.0	4.0	11.7	(1,4)	DMI-1; LBH (4,11); (5,12)
NO delta (0,1)	7	NO_d(0,1)	196.0-200.0	4.0	11.7		
NO gamma (0,1)	8	NO_g(0,1)	234.0-238.0	4.0	11.7		
No feature	9	Control_2	239.0-242.0	3.0	8.8	(1)	DMI-5
SPIM #3		NUV	251.0-387.0	136	272	(2)	1 pixel = 0.50 nm
Noctilucent Clouds	10	NLC	260.0-270.0	10.0	20.0	(5)	
N2 Vegard-Kaplan (0,6)	11	N2_VK(0,6)	275.0-285.0	10.0	20.0	(1,6)	DMI-1 is 270-296 nm
O2 Herzberg I (6,3)	12	O2_HI(6,3)	289.0-292.0	3.0	6.0		
N2 2nd positive (0,0)	13	N2_2P(0,0)	336.0-339.0	3.0	6.0	(7)	
No feature	14	Control_3	339.0-342.0	3.0	6.0	(1)	DMI-4
SPIM #4		VIS	381.0-589.0	208	272	(2)	1 pixel = 0.76 nm
3914, N2+ 1st neg (0,0)	15	N2+_3914	385.0-392.0	7.0	9.2	(1)	DMI-1
No feature	16	Control_4	392.5-395.5	3.0	3.9	(1)	DMI-2
4278, N2+ 1st neg (0,1)	17	N2+_4278	421.0-431.0	10.0	13.1		
5577, Green Line	18	OI_5577	550.0-560.0	10.0	13.1	(1)	DMI-5 is 555-560
SPIM #5		NIR	581.0-900.0	319	272	(2)	1 pixel = 1.17 nm
No feature	19	Control_5	617.5-622.5	5.0	4.3	(1)	DMI-1
6300, Red line	20	OI_6300	629.0-637.4	8.4	7.2	(1)	DMI-2 is 628-632
OH Meinel (8,3)	21	OH_Mn(8,3)	720.0-740.0	20.0	17.1	(8)	
O2 Atmospheric (0,0)	22	O2_At(0,0)	760.0-770.0	10.0	8.5	(1,9)	DMI-3
OH Meinel (6,2)	23	OH_Mn(6,2)	830.0-840.0	10.0	8.5	(1)	DMI-4
O2 Atmospheric (0,1)	24	O2_Atm(0,1)	860.0-870.0	10.0	8.5	(1)	DMI-6

Notes:

(1) DMI-x refers to Data Measurement Indices defined by the UVISI team at APL

(2) Spectral resolution is 2 to 3 times the nominal pixel width in nm, given above

(3) N2 LBH (2,3) overlaps (1,2)

(4) N2 LBH (3,10) is near 191 nm

(5) Also includes N2 VK lines above NLC altitudes in daytime and O2 Herzberg I lines (night)

(6) Also includes Mg II line at 279.3 nm

(7) N2 2P (1,1) and (2,2) fall just on the short-wavelength side of this sub-band

(8) Also includes O II line at 732 nm

(9) O2 Atmospheric (0,0) is actually just below 760; (1,1) is at 770.

Table 29. List of sub-bands used for processing SPIM data for Earthlimb experiments.

For reference purposes, Table 29 gives a list of the sub-bands that were chosen for analysis by SPIMDRVR.

4.2.3 Graphical Data Products

The SPIM data products that we originally specified for summary graphics display *(O'Neil et al, 1993)* include spectra, images, radiance profiles, and statistical summaries.

The need to be able to view spectra is obvious, and little needs to be said about them.

The images were conceived and realized as false-color representations of the sub-band radiances. The color gives the intensity of emissions within individual sub-bands, such as those covering the green line or the O_2 Atmospheric band. The data are displayed as two-dimensional spatial images, one dimension being the tangent height (for limb-viewing experiments) and the other being horizontal distance. The horizontal extent of the image is achieved automatically by using data from all the spatial pixels. The vertical field-of-view is made possible by the scanning mirrors, which displace the lines-of-sight upward or downward by changing their position after each accumulation (frame), or after every third or fourth accumulation if the "dwell" is three or four. Since the data are ac-quired at the rate of 2 or 4 Hz, corresponding to frame times of 500 and 250 ms, it takes between 5 and 40 seconds to cover the full vertical range of 20 mirror positions and ac-quire the data needed for a complete image. During this time, if the spacecraft is in a drift mode, the horizontal field-of-view moves considerably, so an accurate spatial representa-tion for a single scan produces a SPIM sub-band image in the shape of a parallelogram.

The radiance profiles also consist of sub-band radiances. Intensity is plotted against tangent height in order to evaluate the altitude-dependence of the emission features. As with the images, it takes some time to accumulate the profiles, which therefore sample a region with a non-negligible horizontal extent. The profiles, however, are constructed from data in pixels overlapping the radiometer stacks.

The statistical summaries are designed to give an overview of a complete DCE. For a single emission feature, as represented by the sub-band data, the displays give the mean, maximum, and minimum intensity levels as a function of tangent height, and also the standard deviations about the mean.

It was originally envisioned that all sub-band radiance profiles would be matched by so-called "templates", or altitude profiles giving a nominal in-band intensity for each emission feature for a number of different standard atmospheric conditions. That is, for each sub-band there would be templates for night and daytime conditions and for differ-ent latitudes and seasons that would simulate "normal" radiant intensities. For each scan, the vertical radiance profile data would be divided by the appropriate template, and sub-

stantial deviations from unity in this ratio would indicate something extraordinary. (For this reason, the ratios are called "indicators".) Part of the graphical statistical summary would then be plots of the indicators for the whole DCE, or direct plots of radiance data and templates side by side. These would provide a useful visual picture of the deviations from "normal".

SPIMDRVR was written with provisions for reading templates and performing all intended operations involving them. Unfortunately, it was not possible to obtain sufficiently good model calculations of visible and ultraviolet emissions to construct useful templates, so this function is presently not implemented. It may be possible to construct them from actual MSX data, once that becomes available. In the meantime, the SPIM software uses a "unit template", which is nothing but a unit vector, and performs trivial operations on the data to construct indicators that are identical to the radiance data themselves.

Limb-viewing experiments having meaningful tangent heights were assumed for the purposes of the preceding discussion. For downlook experiments the proper parameter for the graphical displays is the nadir angle of the LOS, not the tangent height.

4.2.4 Level 3 SPIM Data Products

The data products that SPIMDRVR produces are described in Figure 44, which is a summary viewgraph presented at one of the recent PI meetings.

The SPIM Spectral Data File contains spectra from every frame. There is no need for processing the Level 2 spectra themselves, and the Level 3 file is basically an excerpted version of the file that SPIMDRVR reads, written in the same format but with only a subset of the total number of spectra. Conservation of disk space was the reason for eliminating much of the data. As mentioned earlier, the selected spectra are those accumulated in the spatial pixels overlapping the radiometer stacks.

The SPIM Spectral Contents File serves as a "table of contents" for all the data accumulated during the DCE. It has an entry for every frame (listing UT, instrument settings, etc.) and, more importantly, entries for every spectrum accumulated during each frame. The individual spectrum entries are [1] the spatial pixel number; [2-5] the latitude in degrees, the longitude in degrees, the tangent height in kilometers, and the nadir angle in degrees at the target point on the LOS at the center of the pixel's field-of-view; [6] the solar zenith angle in degrees at this point; [7-8] the vertical and horizontal extents of the field-of-view at the target point in kilometers; [9] the address of the spectrum in the Level 3 file, in bytes, if it was saved. When either the nadir angle or tangent altitude is not meaningful, a default is written to that field.

Description of Level 3 Data Files (SPIMs)

Spectral Data File

Contains spectra from spatial pixels overlapping stacks ADE/BC
Data formatted exactly as in Level 2 files
Data retained for all dwell states

Spectral Contents File

For every frame, provides information from UVISI Std Header

Instrument settings
Experiment Time (UT)

For every spatial pixel, provides derived quantities

Geolocation data (tangent height, etc.) and SZA
Apparent pixel size
Location of science data in Spectral Data File

Radiance Scan Table

Provides arrays of sub-band radiances
One array per sub-band for each scan

All spatial pixels, all mirror positions

Uses last dwell state only

Indicator Table

Provides radiance/template ratio for each sub-band
Uses spatial pixels overlapping stacks ADE and BC
1-km grid
At present, unit templates used
Uses last dwell state only

Figure 44. Cursory description of the principal Level 3 files produced by SPIMDRVR.

The Radiance Scan Table is the file containing the sub-band radiances, which are obtained by integrating spectral radiance over the sub-bands. For each SPIM there are either four, five, or six such sub-bands. The file is organized by scan. [A scan includes data from all the spatial pixels during a full range of mirror motion, which is to say over many frames.] For each scan there is a header giving information common to all the sub-bands. This is followed by several two-dimensional arrays, one per sub-band, giving the sub-band radiances. One array index is the spatial pixel number, and the other is the number of the frame within the scan. When the dwell is greater than unity, the table holds data only from the last frames before the change in mirror position. Note that each array, corresponding to one sub-band and one scan, contains exactly the data used to construct a sub-band image.

SPIMDRVR writes a SPIM Indicator Table that basically contains sub-band radiance profiles, averaged over one-minute periods. These quantities are derived from the entries in the Radiance Scan Table, but they are written onto a tangent height grid having a 1-km spacing. (For downlook experiments, they are written onto a nadir-angle grid having a 0.02-degree spacing.) They are also divided by the unit templates, which is why they are called indicators, but as explained in the previous section this has no practical effect. The indicators are calculated using the data from the two spatial pixels that overlap the radiometer stacks, so there are two tables for each one minute period for each sub-band.

The original purpose of the one-minute averaging was to examine variations within a DCE without looking at the total data set. With dwells of three or four frames, however, there can be no more than two scans per interval for experiments with a frame rate of 2 Hz , so the average is over a small set and this function is severely diluted. SPIMDRVR therefore writes a secondary SPIM Indicator Table that contains averages of these same quantities over the DCE, as well as minimum and maximum intensities for each tangent height (nadir angle), and standard deviations. These are the data that are used to produce the DCE statistical summaries for summary graphics.

4.3 UVISI Instrument Configurations

Experiment Plans that were submitted to Mission Planning and later to Mission Operations describe the purpose and means of execution of each of the nineteen Earthlimb experiments. One of our tasks was to make recommendations about using the UVISI imagers and spectrographic imagers in the Earthlimb experiments. These included general recommendations, and also specific ones regarding the details of configuring the instruments. In the end, we tabulated the selected instrument configurations in various formats, and forwarded them for inclusion in the final version of the experiment plans and for use in writing command packets for spacecraft operations.

The instrument settings in question include frame rates, choice of the automatic gain table, automatic gain count thresholds, whether or not to compress the data for recording and downlink, and similar sorts of things. For the imagers, the choice of filters is very important. For the SPIMs, additional issues involve the choice of slits, mirror parameters, and partitioning the pixel array in the spectral and spatial dimensions.

For both imagers and SPIMs, the DCE data recording rate has a lot to do with what choices are available for the instrument settings. For the low data rate (5 Mbps) DCEs, a lot of tradeoffs have to be made. It is not possible, for example, to have maximum spatial and spectral resolution for the SPIMs in a 5 Mbps experiment because the data set would be too large.

In setting up the desired UVISI instrument configurations, one general guideline was to use as few sets of instrument parameters as possible. With similar settings, it may be easier to validate and compare data taken under differing geophysical conditions. Therefore one default configuration for daytime conditions was chosen for each experiment, and also one default nighttime configuration. These were the same or similar for many of the experiments. Then we specified a number of other configurations that were variations on the defaults, so that experiments could be fine-tuned in certain ways. The primary way in which the setups vary is in the choice of filters for the imagers.

Another guideline was to use automatic gain for all instruments. Yet another, regarding the SPIMs alone, was to optimize the spectral resolution at the expense of the spatial resolution where necessary, but this was followed only loosely in the end.

After a lengthy process, consensus was reached on a set of operation modes for each experiment. It was also agreed that the best way to evaluate the various modes is with on-orbit data, however, so there may eventually be a reassessment of all this.

For all experiments, the daytime configurations were set up to protect the detectors wherever necessary. Neutral density filters are used for the visible wavelength instruments for all modes (SPIMs) or nearly all modes (imagers) for daytime conditions. SPIM 2 uses a bandpass filter centered at 220 nm for all modes, and SPIM 3, the near-UV instrument, uses one centered at 260 nm for daytime modes to eliminate Rayleigh scattered light from the longer wavelengths. The maximum gate was reduced for many daytime experiments as well, especially for the imagers. The imagers are cycled for 5 Mbps experiments to save space, and data compression is always used (except for the SPIMs during the 25 Mbps experiments) for the same reason.

The tradeoff between spectral and spatial resolution in the SPIM data is driven by the record rate (and the requirements for the telemetry stream), with the constraints being

much more severe for the 5 Mbps experiments. Spatial resolution is determined by how the 40 individual detector elements across the slit are ganged together. Possible configurations allow them to be combined in groups of 8, 4, or 2 adjacent elements, or not to be combined at all. The possible number of individual "pixels" that can be read out is therefore either 5, 10, 20, or 40. However, optical considerations limit the spatial resolution of the instrument to about twice the angular field-of-view of a single element, so there is no benefit in using more than 20 spatial pixels. Spectral resolution is determined by the number of spectral pixels, which can be 272, 136, or 68.

For most 5 Mbps experiments, the SPIMs were set at 272 spectral pixels and 5 spatial pixels to maximize the spectral resolution. However, for the two downlooking experiments, and for three other experiments in which structured radiance may be expected (e.g., EL-14, terminator experiment) the configuration was 68 by 20, to maximize the spatial resolution. For the high-rate experiments, the configuration was always 272 by 20, which is as good as can be achieved.

The experiment modes that were adopted in the end were tabulated in various formats. Some of these were arranged with separate tables for each experiment, and thus run many pages in length. The most compact form is given in the appendix of this report, where the default imager settings for all experiments are listed in one table, the default SPIM settings in another, and the imager filter combination options for night and day conditions are given in two others.

4.4 Appendix

The following tables give, in compact form, the UVISI instrument settings comprising the Earthlimb experiment modes. The same information has also been documented in more extensive tables, not given here, that are specialized to the individual experiments.

Table 30 gives the default instrument settings for the four UVISI imagers for all the Earthlimb experiments, including two (EL-16, EL-17) that have been dropped from consideration since the list was compiled. Separate default modes have been adopted for daytime and nighttime conditions, and for low and high data rate DCEs.

Table 31 gives the default settings for the five SPIMs.

Tables 32 and 33 give the combinations of imager filter settings that were adopted for use in each of the experiments, for nighttime and daytime conditions respectively.

Table 30   Default settings for the four UVISI imagers for Earthlimb experiments

Experiment Title	D Rate (Mbps)	D/N	Rate (Hz)	Imager Cyclic	Bits (/px)	IP	Gain Table	Gate (ms)	IUW	IUN	IVW	IVN	Bins (x)	Bins (y)
AIRGLOW STRUCTURE EXPERIMENTS														
EL-02 Constant Tang. Ht. Scan	5	N	2	Yes	8	OFF	2	468	F3-1304	F4-Open	F4-Open	F4-Open	256	244
	5	D	2	Yes	8	OFF	2	468	F3-1304	F2-Atten	F2-Atten	F2-Atten	256	244
EL-14 Terminator Region	5	D/N	2	Yes	8	OFF	0	468	F6-LBH	F5 (200-230)	F2-Atten	F2-Atten	256	244
	25	D/N	2	No	8	OFF	0	468	F6-LBH	F5 (200-230)	F2-Atten	F2-Atten	256	244
EL-15 Ground Site Track	5	N	2	Yes	8	OFF	0	468	F3-1304	F4-Open	F4-Open	F4-Open	256	244
	5	D	2	Yes	8	OFF	0	50	F3-1304	F2-Atten	F2-Atten	F2-Atten	256	244
	25	N	2	No	8	OFF	0	468	F3-1304	F4-Open	F4-Open	F4-Open	256	244
	25	D	2	No	8	OFF	0	50	F3-1304	F2-Atten	F2-Atten	F2-Atten	256	244
BTH MWIR STRUCTURE EXPERIMENTS														
EL-18 BTH MWIR Structure	5	N	2	Yes*	8*	OFF	0*	468*	-	F5 (200-230)	-	F4-Open	256*	244*
	5	D	2	Yes*	8*	OFF	0*	10*	-	F2-Atten	-	F2-Atten	256*	244*
	25	N	2	No	8	OFF	0	468	F3-1304	F4-Open	F4-Open	F4-Open	256	244
	25	D	2	No	8	OFF	0	10	F3-1304	F5 (200-230)	F3-5577	F5 (305-315)	256	244
EL-09 BTH/ATH MWIR Structure	5	N	2	Yes*	8*	OFF	0*	468*	-	F5 (200-230)	-	F4-Open	256*	244*
	5	D	2	Yes*	8*	OFF	0*	10*	-	F2-Atten	-	F2-Atten	256*	244*
	25	N	2	No	8	OFF	0	468	F3-1304	F4-Open	F4-Open	F4-Open	256	244
	25	D	2	No	8	OFF	0	10	F3-1304	F5 (200-230)	F3-5577	F5 (305-315)	256	244
AURORAL/JOULE HEATING EXPERIMENTS														
EL-05 Sector Scan	25	N	2	No	8	OFF	0	468	F3-1304	F4-Open	F5-4278	F3-3914	256	244
	25	D	2	No	8	OFF	0	100	F3-1304	F2-Atten	F2-Atten	F2-Atten	256	244
EL-03 Bright Spot Track	25	N	2	No	8	ON	0	468	F6-LBH	F4-Open	F4-Open	F4-Open	256	244
EL-06 Constant Tang. Ht. Scan	5	N	2	Yes	8	OFF	0	468	F3-1304	F4-Open	F3-5577	F3-3914	256	244
EL-07 Ground Site Track	5	D	2	Yes	8	OFF	0	100	F6-LBH	F5 (200-230)	F2-Atten	F2-Atten	256	244
	25	N	2	No	8	OFF	0	468	F3-1304	F4-Open	F5-4278	F3-3914	256	244
EL-08 Coordinated Satellite	25	D	2	No	8	OFF	0	100	F6-LBH	F5 (200-230)	F2-Atten	F3-3914	256	244
	25	N	2	No	8	OFF	0	468	F3-1304	F4-Open	F5-4278	F3-3914	256	244
EL-13 Joule Heated Atmosphere	5	N	2	Yes	8	OFF	0	100	F3-1304	F2-Atten	F2-Atten	F2-Atten	256	244
	5	D	2	Yes	8	OFF	0	468	F3-1304	F4-Open	F3-5577	F3-3914	256	244
HIGH LATITUDE EVENTS														
EL-04 Conical Scan Survey	25	N	2	No	8	OFF	0	50	F3-1304	F4-Open	F4-Open	F4-Open	256	244
EL-11 Stratospheric Warming	5	N	2	Yes	8	OFF	2	468	F3-1304	F4-Open	F4-Open	F4-Open	256	244
	5	D	2	Yes	8	OFF	2	468	F3-1304	F2-Atten	F2-Atten	F2-Atten	256	244
EL-12 PMC	5	D	2	Yes	8	OFF	0	100	F5-Ly a	F6-POL	F2-Atten	F2-Atten	256	244
EL-16 PMC Fixed Point	5	D	2	Yes	8	OFF	0	100	F5-Ly a	F6-POL	F2-Atten	F2-Atten	256	244
EL-17 PMC Ground Site	5	D	2	Yes	8	OFF	0	100	F5-Ly a	F6-POL	F2-Atten	F2-Atten	256	244

Table 30　Default settings for the four UVISI imagers for Earthlimb experiments (continued)

Experiment Title	D Rate (Mbps)	D/N	Rate (Hz)	Imager Cyclic	Bits (/px)	IP	Gain Table	Gate (ms)	IUW	Default Filter IUN	IVW	IVN	Bins (x)	Bins (y)
ALTITUDE PROFILES														
EL-01 Staircase Scan	5	N	2	Yes	8	OFF	2	468	F3-1304	F4-Open	F4-Open	F4-Open	256	244
	5	D	2	Yes	8	OFF	2	468	F3-1304	F2-Atten	F2-Atten	F2-Atten	256	244
EL-10 Vertical Profile Scan	5	N	2	Yes	8	OFF	0	468	F3-1304	F4-Open	F4-Open	F4-Open	256	244
	5	D	2	Yes	8	OFF	0	100	F3-1304	F2-Atten	F2-Atten	F2-Atten	256	244
EL-19 Stratospheric Gas Survey	5	N	2	Yes	8	OFF	0	468	F3-1304	F4-Open	F4-Open	F4-Open	256	244
	5	D	2	Yes	8	OFF	0	100	F3-1304	F2-Atten	F2-Atten	F2-Atten	256	244

Notes:

Even though many parameters can be set differently for each imager, for example the gain table or the number of pixels, the standard way of operating is to use the same settings for each (except for the filters, as noted)

D Rate:　Rate at which data are recorded: either 5 or 25 Mbps
D/N:　These tables give default day (D) and night (N) configurations. Variations involve different imager filter combinations
Rate:　Rate (Hz) at which imager frames are accumulated
Imager cyclic: Indicates whether imagers accumulate data simultaneously (No) or cyclically (Yes)
Bits/px:　The number of bits per pixel. With data compression, this is 8; without compression, it's 16
IP:　Image processor
Gain Table: The number of the gain table selected for the default configuration
Gate:　The (selected) maximum accumulation time for any frame. For 2 Hz (4 Hz) this cannot be greater than 468 (218) ms.
Default Filter:　These are the default filter combinations for day and night configurations
　　Other filter combinations are given in the accompanying tables, entitled Imager Filter Settings
　　More details about the imager filters is given in the accompanying UVISI Performance Characteristics Table
Bins:　The number of pixels in the x and y directions

For EL-09 and EL-18 operating in the low data-rate mode (5 Mbps) only two imagers are used.　Settings marked with (*) apply only to IUN and IVN.

Table 31   Default settings for the five UVISI spectrographic imagers for Earthlimb experiments

Experiment Title	D Rate (Mbps)	D/N	Rate (Hz)	Bits (/px)	Gain Table	Gate (ms)	SPIM 1	SPIM 2	Slit SPIM 3	SPIM 4	SPIM 5	Bins (x)	Bins (y)	Dwell (fr)	MIRROR Motion (deg)	Step (deg)
AIRGLOW STRUCTURE EXPERIMENTS																
EL-02 Constant Tang. Ht. Scan	5	N	2	8	2	468	S2-NO	S2-NO	S1-NO	S2-NO	S2-NO	272	5	3	0 +/- 0.5	0.05
	5	D	2	8	2	468	S2-NO	S2-NO	S2-NOf	S4-NA	S4-NA	272	5	3	0 +/- 0.5	0.05
EL-14 Terminator Region	5	D/N	2	8	0	468	S2-NO	S2-NO	S2-NOf	S4-NA	S4-NA	68	20	1	0 +/- 0.5	0.05
	25	D/N	4	16	0	218	S2-NO	S2-NO	S2-NOf	S4-NA	S4-NA	272	20	1	0 +/- 0.5	0.05
EL-15 Ground Site Track	5	N	2	8	0	468	S2-NO	S2-NO	S1-NO	S2-NO	S2-NO	68	20	3	0 +/- 0.5	0.05
	5	D	2	8	0	468	S2-NO	S2-NO	S2-NOf	S4-NA	S4-NA	68	20	3	0 +/- 0.5	0.05
	25	N	4	16	0	218	S2-NO	S2-NO	S1-NO	S2-NO	S2-NO	272	20	3	0 +/- 0.5	0.05
	25	D	4	16	0	218	S2-NO	S2-NO	S2-NOf	S4-NA	S4-NA	272	20	3	0 +/- 0.5	0.05
BTH MWIR STRUCTURE EXPERIMENTS																
EL-18 BTH MWIR Structure	5	N	2	8	0	468	S2-NO	S2-NO	S1-NO	S2-NO	S2-NO	68	20	1	0 +/- 0.5	0.05
	5	D	2	8	0	40	S2-NO	S2-NO	S2-NOf	S4-NA	S4-NA	68	20	1	0 +/- 0.5	0.05
	25	N	4	16	0	218	S2-NO	S2-NO	S1-NO	S2-NO	S2-NO	272	20	1	0 +/- 0.5	0.05
	25	D	4	16	0	40	S2-NO	S2-NO	S2-NOf	S4-NA	S4-NA	272	20	1	0 +/- 0.5	0.05
EL-09 BTH/ATH MWIR Structure	5	N	2	8	0	468	S2-NO	S2-NO	S1-NO	S2-NO	S2-NO	68	20	1	0 +/- 0.5	0.05
	5	D	2	8	0	40	S2-NO	S2-NO	S2-NOf	S4-NA	S4-NA	68	20	1	0 +/- 0.5	0.05
	25	N	4	16	0	218	S2-NO	S2-NO	S1-NO	S2-NO	S2-NO	272	20	1	0 +/- 0.5	0.05
	25	D	4	16	0	40	S2-NO	S2-NO	S2-NOf	S4-NA	S4-NA	272	20	1	0 +/- 0.5	0.05
AURORAL/JOULE HEATING EXPERIMENTS																
EL-05 Sector Scan	25	N	4	16	0	218	S2-NO	S2-NO	S1-NO	S2-NO	S2-NO	272	20	4	0 +/- 0.5	0.05
	25	D	4	16	0	218	S2-NO	S2-NO	S2-NOf	S4-NA	S4-NA	272	20	4	0 +/- 0.5	0.05
EL-03 Bright Spot Track	25	N	4	16	0	218	S2-NO	S2-NO	S1-NO	S2-NO	S2-NO	272	20	4	0 +/- 0.5	0.05
EL-06 Constant Tang. Ht. Scan	5	N	2	8	0	468	S2-NO	S2-NO	S1-NO	S2-NO	S2-NO	272	5	3	0 +/- 0.5	0.05
	5	D	2	8	0	468	S2-NO	S2-NO	S2-NOf	S4-NA	S4-NA	272	5	3	0 +/- 0.5	0.05
EL-07 Ground Site Track	25	N	4	16	0	218	S2-NO	S2-NO	S1-NO	S2-NO	S2-NO	272	20	3	0 +/- 0.5	0.05
	25	D	4	16	0	218	S2-NO	S2-NO	S2-NOf	S4-NA	S4-NA	272	20	3	0 +/- 0.5	0.05
EL-08 Coordinated Satellite	25	N	4	16	0	218	S2-NO	S2-NO	S1-NO	S2-NO	S2-NO	272	20	3	0 +/- 0.5	0.05
	25	D	4	16	0	218	S2-NO	S2-NO	S2-NOf	S4-NA	S4-NA	272	20	3	0 +/- 0.5	0.05
EL-13 Joule Heated Atmosphere	5	N	2	8	0	468	S2-NO	S2-NO	S1-NO	S2-NO	S2-NO	68	20	3	0 +/- 0.5	0.05
	5	D	2	8	0	468	S2-NO	S2-NO	S2-NOf	S4-NA	S4-NA	68	20	3	0 +/- 0.5	0.05
HIGH LATITUDE EVENTS																
EL-04 Conical Scan Survey	25	N	4	16	0	218	S2-NO	S2-NO	S1-NO	S2-NO	S2-NO	272	20	3	0 +/- 0.5	0.05
EL-11 Stratospheric Warming	5	N	2	8	2	468	S2-NO	S2-NO	S1-NO	S2-NO	S2-NO	272	5	3	0 +/- 0.5	0.05
	5	D	2	8	2	468	S2-NO	S2-NO	S2-NOf	S4-NA	S4-NA	272	5	3	0 +/- 0.5	0.05
EL-12 PMC	5	D	2	8	0	468	S2-NO	S2-NO	S2-NOf	S4-NA	S4-NA	272	5	3	0 +/- 0.5	0.05
EL-16 PMC Fixed Point	5	D	2	8	0	468	S2-NO	S2-NO	S2-NOf	S4-NA	S4-NA	272	5	3	0 +/- 0.5	0.05
EL-17 PMC Ground Site	5	D	2	8	0	468	S2-NO	S2-NO	S2-NOf	S4-NA	S4-NA	272	5	3	0 +/- 0.5	0.05

Table 31   Default settings for the five UVISI spectrographic imagers for Earthlimb experiments (continued)

19 Jan 1995   ARCON

| Experiment | Title | D Rate (Mbps) | D/N | Rate (Hz) | Bits (/px) | Gain Table | Gate (ms) | Slit | | | | | Bins (x) | Bins (y) | Dwell (fr) | MIRROR Motion (deg) | Step (deg) |
								SPIM 1	SPIM 2	SPIM 3	SPIM 4	SPIM 5					
ALTITUDE PROFILES																	
EL-01	Staircase Scan	5	N	2	8	2	468	S2-NO	S2-NO	S1-NO	S2-NO	S2-NO	272	5	3	0 +/- 0.5	0.05
		5	D	2	8	2	468	S2-NO	S2-NO	S2-NOf	S4-NA	S4-NA	272	5	3	0 +/- 0.5	0.05
EL-10	Vertical Profile Scan	5	N	2	8	0	468	S2-NO	S2-NO	S1-NO	S4-NO	S2-NO	272	5	3	0 +/- 0.5	0.05
		5	D	2	8	0	468	S2-NO	S2-NO	S2-NOf	S4-NA	S4-NA	272	5	3	0 +/- 0.5	0.05
EL-19	Stratospheric Gas Survey	5	N	2	8	0	468	S2-NO	S2-NO	S1-NO	S2-NO	S2-NO	68	20	3	0 +/- 0.5	0.05
		5	D	2	8	0	468	S2-NO	S2-NO	S2-NOf	S4-NA	S4-NA	68	20	3	0 +/- 0.5	0.05

Notes:

Even though many parameters can be set differently for each SPIM, for example the number of spectral or spatial pixels, the standard
way of operating is to use the same settings for each (except for the slits, as noted)

D Rate: Rate at which data are recorded: either 5 or 25 Mbps
D/N: These tables give default day (D) and night (N) configurations. At present there are no variations involving SPIM settings.
Rate: Rate (Hz) at which SPIM frames are accumulated
Bits/px: The number of bits per pixel. With data compression, this is 8; without compression, it's 16
Gain Table: The number of the gain table selected for the default configuration
Gate: The (selected) maximum accumulation time for any frame. For 2 Hz (4 Hz) this cannot be greater than 468 (218) ms.
Slit: These are the default slit/filter combinations for day and night configurations
            "NO" means the narrow (0.05 deg) open slit
            "NA" means the narrow (0.05 deg) slit with the neutral-density (attenuating) filter
            "NOf" means the narrow (0.05 deg) slit with a bandpass filter (centered at 260 nm for SPIM 3)
            For SPIM 2 there is actually no narrow open slit; slit 2 has a bandpass filter centered at 220 nm, but the APL tables refer to it as "NO"
            More detail about the meaning of the slit/filter codes is given in the accompanying UVISI Performance Characteristics Table
Bins (x):   The number of pixels in the spectral "direction"
Bins (y):   The number of pixels in the spatial "direction" (along the slit)
Dwell: The number of frames accumulated before the mirror steps to its next position
Motion: "0 +/- 0.5" means the full mirror excursion is 0.5 degrees on either side of the central position.
Step: The amount the mirror moves whenever it changes its position

107

Table 32   Alternative UVISI imager filter settings for nighttime conditions

IUW	IUN	IVW	IVN	ELE-1 5 Mbps	ELE-2 5 Mbps	ELE-3 25 Mbps	ELE-4 25 Mbps	ELE-5 25 Mbps	ELE-6 5 Mbps	ELE-7 25 Mbps	ELE-8 25 Mbps	ELE-9 25 Mbps	ELE-9 5 Mbps	ELE-10 5 Mbps
F3-1304	F3 (230-260)	F3-5577	F3-3914											
F3-1304	F3 (230-260)	F4-Open	F6-5577	X	X	X	X	X	X	X	X	X		X
F3-1304	F3 (230-260)	F5-4278	F6-5577						X					
F3-1304	F4-Open	F3-5577	F3-3914	X	X	X	X	X	DEF	X	X	X		DEF
F3-1304	F4-Open	F4-Open	F4-Open	DEF	DEF		DEF	DEF				DEF		X
F3-1304	F4-Open	F4-Open	F6-5577	X	X		X					X		X
F3-1304	F4-Open	F3-5577	F6-5577	X	X	X	X	X				X		
F3-1304	F4-Open	F5-4278	F3-3914							DEF	DEF			
F5-Ly a	F4-Open	F4-Open	F6-5577	X	X	X	X	X		DEF		X		X
F6-LBH	F3 (230-260)	F5-4278	F3-3914						X					
F6-LBH	F4-Open	F4-Open	F3-3914	X	X	X	X	X	X	X	X	X		X
F6-LBH	F4-Open	F4-Open	F4-Open			DEF								
F3 (230-260)			F6-5577										X	
F4-Open			F3-3914										X	
F4-Open			F6-5577										X	
F5 (200-230)			F4-Open										DEF	

IUW	IUN	IVW	IVN	ELE-11 5 Mbps	ELE-13 5 Mbps	ELE-15 5 Mbps	ELE-15 25 Mbps	ELE-18 25 Mbps	ELE-18 5 Mbps	ELE-19 5 Mbps
F3-1304	F3 (230-260)	F3-5577	F3-3914	X	X					
F3-1304	F3 (230-260)	F4-Open	F6-5577	X		X	X	X		X
F3-1304	F3 (230-260)	F5-4278	F6-5577							
F3-1304	F4-Open	F3-5577	F3-3914		DEF	X	X	X		X
F3-1304	F4-Open	F4-Open	F4-Open	DEF		DEF	DEF	DEF		DEF
F3-1304	F4-Open	F4-Open	F6-5577	X	X	X	X	X		X
F3-1304	F4-Open	F3-5577	F6-5577	X			X	X		X
F3-1304	F4-Open	F5-4278	F3-3914							
F5-Ly a	F4-Open	F4-Open	F6-5577	X	X	X	X	X		X
F6-LBH	F3 (230-260)	F5-4278	F3-3914							
F6-LBH	F4-Open	F4-Open	F3-3914	X	X	X	X	X		X
F6-LBH	F4-Open	F4-Open	F4-Open							
F3 (230-260)			F6-5577						X	
F4-Open			F3-3914						X	
F4-Open			F6-5577						X	
F5 (200-230)			F4-Open						DEF	

Note:

DEF indicates default setting

8 Dec 1994   ARCON

Table 33   Alternative UVISI imager filter settings for daytime conditions

IUW	IUN	IVW	IVN	ELE-1 5 Mbps	ELE-2 5 Mbps	ELE-5 25 Mbps	ELE-6 5 Mbps	ELE-7 25 Mbps	ELE-8 25 Mbps	ELE-9 25 Mbps	ELE-9 5 Mbps	ELE-10 5 Mbps	ELE-11 5 Mbps	ELE-12 5 Mbps
F3-1304	F2-Atten	F2-Atten	F2-Atten	DEF	DEF	DEF			DEF			DEF	DEF	
F3-1304	F3 (230-260)	F2-Atten	F5 (305-315)							X				
F3-1304	F5 (200-230)	F2-Atten	F5 (305-315)							DEF				
F5-Ly a	F3 (230-260)	F2-Atten	F2-Atten	X	X					X			X	X
F5-Ly a	F4-Open	F2-Atten	F2-Atten											X
F5-Ly a	F5 (200-230)	F2-Atten	F2-Atten	X	X	X			X			X	X	X
F5-Ly a	F6-POL	F2-Atten	F2-Atten											DEF
F6-LBH	F3 (230-260)	F2-Atten	F2-Atten				DEF							
F6-LBH	F5 (200-230)	F2-Atten	F2-Atten	X	X	X			X	X		X	X	
F6-LBH	F5 (200-230)	F2-Atten	F3-3914					DEF						
F6-LBH	F5 (200-230)	F2-Atten	F6-5577											
	F2-Atten		F2-Atten								DEF			
	F3 (230-260)		F2-Atten								X			
	F5 (200-230)		F2-Atten								X			

IUW	IUN	IVW	IVN	ELE-13 5 Mbps	ELE-14 5 Mbps	ELE-14 25 Mbps	ELE-15 5 Mbps	ELE-15 25 Mbps	ELE-16 5 Mbps	ELE-17 5 Mbps	ELE-18 25 Mbps	ELE-18 5 Mbps	ELE-19 5 Mbps
F3-1304	F2-Atten	F2-Atten	F2-Atten	DEF	X	X	DEF	DEF					DEF
F3-1304	F3 (230-260)	F2-Atten	F5 (305-315)										
F3-1304	F5 (200-230)	F2-Atten	F5 (305-315)										
F5-Ly a	F3 (230-260)	F2-Atten	F2-Atten		X	X			X	X	X		
F5-Ly a	F4-Open	F2-Atten	F2-Atten						X	X	DEF		
F5-Ly a	F5 (200-230)	F2-Atten	F2-Atten	X	X	X	X	X	X	X			
F5-Ly a	F6-POL	F2-Atten	F2-Atten						DEF	DEF			X
F6-LBH	F3 (230-260)	F2-Atten	F2-Atten		X	X	X	X					X
F6-LBH	F5 (200-230)	F2-Atten	F2-Atten	X	DEF	DEF	X	X	X		X		X
F6-LBH	F5 (200-230)	F2-Atten	F3-3914		X		X	X					
F6-LBH	F5 (200-230)	F2-Atten	F6-5577		X								
	F2-Atten		F2-Atten									DEF	
	F3 (230-260)		F2-Atten									X	
	F5 (200-230)		F2-Atten									X	

5. REFERENCES

5.1 Technical References

The following papers and presentations are referenced in the technical sections of this report.

Armstrong, P.S., S.J. Lipson, J.A. Dodd, J.R. Lowell, W.A.M. Blumberg, and R.M. Nadile, "Highly Rotationally Excited NO(v,J) in the Thermosphere from CIRRIS 1A Limb Radiance Measurements", *Geophys. Res. Lett.*, **21**, 2425-2428, 1994.

Carbary, J., "UVISI Instrument: A Tutorial", Johns Hopkins Univ., Applied Physics Laboratory, S1G-R92_04.1, 1992.

Dickinson, R.E., "Infrared Radiative Cooling in the Mesosphere and Lower Thermosphere", *J. Atmos. Terr. Phys.* **46**, 995-1008, 1984.

Dodd, J.A., S.J. Lipson, J.R. Lowell, P.S. Armstrong, W.A.M. Blumberg, R.M. Nadile, S.M. Adler-Golden, W.J. Marinelli, K.W. Holtzclaw, and B.D. Green, "Analysis of Hydroxyl Earthlimb Airglow Emissions: Kinetic Model for State-to-State Dynamics of OH(v,N)", *J. Geophys. Res.*, **99**, 3559-3585, 1994.

Espy, P.J., C.R. Harris, A.J. Steed, J.C. Ulwick, R.H. Haycock, and R. Straka, "Rocketborne Interferometer Measurement of Infrared Auroral Spectra", *Planet. Space Sci.*, **36**, 543-551, 1988.

Goody, R.M., and Y.L. Yung, Atmospheric Radiation, Theoretical Basis, 2nd edition, Oxford University Press, Oxford, 1989.

Grossmann, K.U., D. Homann, and J. Schulz, "Lower Thermospheric Infrared Emissions from Minor Species during High-Latitude Twilight—A. Experimental Results", *J. Atmos. Terr. Phys.*, **56**, 1885-1897, 1994.

Kumer, J.B., A.T. Stair, Jr., N. Wheeler, K.D. Baker, and D.J. Baker, "Evidence for an $OH^* \overset{vv}{\rightarrow} N_2^* \overset{vv}{\rightarrow} CO_2(v_3) \rightarrow CO_2 + h\nu \, (4.3 \, \mu m)$ Mechanism for 4.3-μm Airglow", *J. Geophys. Res.* **83**, 4743-4747, 1978.

Lipson, S.J., P.S. Armstrong, J.A. Dodd, J.R. Lowell, W.A.M. Blumberg, and R.M. Nadile, "Subthermal Nitric Oxide Spin-Orbit Distributions in the Thermosphere", *Geophys. Res. Lett.*, **21**, 2421-2424, 1994.

Lopez-Puertas, M., M.A. Lopez-Valverde, and F.W. Taylor, "Vibrational Temperatures and Radiative Cooling of the CO_2 15 μm Bands in the Middle Atmosphere", *Q. J. R. Meteorol. Soc.*, **118**, 499-532, 1992a.

Lopez-Puertas, M., M.A. Lopez-Valverde, C.P. Rinsland, and M.R. Gunson, "Analysis of the Upper Atmosphere $CO_2(\nu_2)$ Vibrational Temperatures Retrieved from the ATMOS/ Spacelab 3 Observations", *J. Geophys. Res.,* **97**, 20469-20478, 1992b.

Lopez-Puertas, M., P.P. Wintersteiner, R.H. Picard, J.R. Winick, and R.D. Sharma, "Comparison of Line-by-Line and Curtis Matrix Calculations for the Vibrational Temperatures and Radiative Cooling of the CO_2 15 μm Bands in the Middle and Upper Atmosphere", *J. Quant. Spectrosc. Radiat. Transfer,* **52**, 409-423, 1994.

Makhlouf, U.B., R.H. Picard, and J.R. Winick, "Photochemical-Dynamical Modeling of the Measured Response of Airglow to Gravity Waves 1. Basic Model for OH Airglow", *J.Geophys. Res.,* **100**, 11289-11311, 1995.

McClatchey, R.A., W.S. Benedict, S.A. clough, D.E. Burch, R.F. Calfee, K. Fox, L.S. Rothman, and J.S. Garing, "AFCRL Atmospheric Absorption Line Parameters Compilation", AFCRL-TR-73-0096, 1973, A*D*762904.

Mill, J.D., R.R. O'Neil, S.Price, G.J. Romick, O.M. Uy, and E.M. Gaposchkin, "Midcourse Space Experiment: Introduction to the Spacecraft, Instruments, and Scientific Objectives", *J. Spacecraft & Rockets,* **31**, 900-907, 1994.

Nebel, H., P.P. Wintersteiner, R.H. Picard, J.R. Winick, and R.D. Sharma, "CO_2 Non-Local Thermodynamic Equilibrium Radiative Excitation and Infrared Dayglow at 4.3 μm: Application to Spectral Infrared Rocket Experiment Data", *J. Geophys. Res.,* **99**, 10409-10419, 1994.

Offermann, D., "The DYANA Campaign: A Survey", *J. Atm. Terr. Phys.,* **56**,1639-1657, 1994.

O'Neil, R.R., H.A.B. Gardiner, J. Gibson, C. Humphrey, R. Hegblom, M.E. Fraser, M. Kendra, P. Wintersteiner, and C. Rice, "Midcourse Space Experiment (MSX): Plans and Capability for the Measurement of Infrared Earthlimb and Terrestrial Backgrounds", *Proc. SPIE,* **2223** (25): 264-273, 1994.

O'Neil, R., H. Gardiner, M. Fraser, R. Armstrong, W. Grieder, C. Humphrey, A. Zachor, M. Kendra, W. Gallery, P. Wintersteiner, J. Gibson, R. Hegblom, and R. Beland, "MSX: Earthlimb Automated Analysis Plan, Version 1.0", PSI1131/TR-1233, April 1993.

Ratkowski, A.J., R.H. Picard, J.R. Winick, K.U. Grossmann, D. Homann, J.C. Ulwick, and A.J. Paboojian, "Lower Thermospheric Infrared Emissions from Minor Species during High-Latitude Twilight—B. Analysis of 15 μm Emission and Comparison with Non-LTE Models", *J. Atm. Terr. Phys.,* **56**, 1899-1914, 1994.

Rodgers, C.D., F.W. Taylor, A.H. Muggeridge, M. Lopez-Puertas, and M.A. Lopez-Valverde, "Local Thermodynamic Equilibrium of Carbon Dioxide in the Upper Atmosphere", *Geophys. Res. Lett.,* **19**, 589-592, 1992.

Rothman, L.S., R.R. Gamache, R.H. Tipping, C.P. Rinsland, M.A.H. Smith, D. Chris Benner, V. Malathy Devi, J.-M. Flaud, C. Camy-Peyret, A. Perrin, A. Goldman, S.T. Massie, L.R. Brown, and R.A. Toth, "The HITRAN molecular database: editions of 1991 and 1992", *J. Quant. Spectrosc. Radiat. Transfer 48*, 469-507, 1992.

Sharma, R.D., and P.P. Wintersteiner, "CO_2 Component of Daytime Earth Limb Emission at 2.7 Micrometers", *J. Geophys. Res.,* **90**, 9789-9803, 1985.

Sharma, R.D., and P.P. Wintersteiner, "Role of Carbon Dioxide in Cooling Planetary Thermospheres", *Geophys. Res. Lett.,* **17**, 2201-2204, 1990.

Streit, G.E., and H.S. Johnson, "Reactions of Quenching of Vibrationally Excited Hydroxyl Radicals", J. Chem. Phys., 64, 95, 1976.

Thekaekara, M.P., "Solar Energy Outside the Earth's Atmosphere", *Solar Energy,* **14**, 109-127, 1971.

UVISI Instrument Team, "User's Guide for the UVISI Instrument, v 1.0", Johns Hopkins Univ., Applied Physics Laboratory, S1G-R92-01, 1992.

von Zahn, U., "The Project MAP/WINE: An Overview", *J. Atmos. Terr. Phys.*, **49**, 607-620, 1987.

Winick, J.R., R.H. Picard, P.P. Wintersteiner, R.A. Joseph, A.J. Paboojian, M. Lopez-Puertas, and U. Makhlouf, "Re-examination of $O(^1D)$ as a Source of $N_2(v)$ and its Effect on CO_2 4.3 µm Non-LTE Emission and the Energy Budget of the Middle Atmosphere", presented at the Fall Meeting of the American Geophysical Union, San Francisco, CA, 6-10 December 1993.

Winick, J.R., R.H. Picard, P.P. Wintersteiner, A.J. Pabojian, and R.A. Joseph, "On Determining the Carbon Budget (CO_2 and CO) of the Lower Thermosphere from Non-Equilibrium Infrared Radiance", presented at the Sixth Topical Meeting on Optical Remote Sensing of the Atmosphere, Optical Soceity of America, Salt Lake City, UT, 8-12 March 1993.

Winick, J.R., R.H. Picard, R.A. Joseph, R.D. Sharma, and P.P. Wintersteiner, "An Infrared Spectral Radiance Code for the Auroral Thermosphere", AFGL-TR-87-0334, 1987, ADA202432.

Wintersteiner, P.P., and R.D. Sharma, "Update of an Efficient Computer Code (NLTE) to Calculate Emission and Transmission of Radiation Through Non-Equilibrium Atmospheres", AFGL-TR-85-0240, 1985, ADA172556.

Wintersteiner, P.P., R.H. Picard, R.D. Sharma, J.R. Winick, and R.A. Joseph, "Line-by-line Radiative Excitation Model for the Non-Equilibrium Atmosphere: Application to CO_2 15 μm Emission", *J. Geophys. Res.*, **97**, 18083-18117, 1992.

5.2 Refereed Publications

The following refereed publications describe in detail some of the research carried out by ARCON personnel.

Wintersteiner, P.P., R.H. Picard, R.D. Sharma, J.R. Winick, and R.A. Joseph, "Line-by-line Radiative Excitation Model for the Non-Equilibrium Atmosphere: Application to CO_2 15 μm Emission", *J. Geophys. Res.*, **97**, 18083-18117, 1992.

Sharma, R.D., and P.P. Wintersteiner, "Role of Carbon Dioxide in Cooling Planetary Thermospheres", *Geophys. Res. Lett.*, **17**, 2201-2204, 1990.

Nebel, H., P.P. Wintersteiner, R.H. Picard, J.R. Winick, and R.D. Sharma, "CO_2 Non-Local Thermodynamic Equilibrium Radiative Excitation and Infrared Dayglow at 4.3 μm: Application to Spectral Infrared Rocket Experiment Data", *J. Geophys. Res.*, **99**, 10409-10419, 1994.

Lopez-Puertas, M., P.P. Wintersteiner, R.H. Picard, J.R. Winick, and R.D. Sharma, "Comparison of Line-by-Line and Curtis Matrix Calculations for the Vibrational Temperatures and Radiative Cooling of the CO_2 15 μm Bands in the Middle and Upper Atmosphere", *J. Quant. Spectrosc. Radiat. Transfer*, **52**, 409-423, 1994.

Ratkowski, A.J., R.H. Picard, J.R. Winick, K.U. Grossmann, D. Homann, J.C. Ulwick, and A.J. Paboojian, "Lower Thermospheric Infrared Emissions from Minor Species during High-Latitude Twilight—B. Analysis of 15 μm Emission and Comparison with Non-LTE Models", *J. Atm. Terr. Phys.*, **56**, 1899-1914, 1994.

5.3 Presentations

The following presentations were based in whole or in part on work performed by ARCON personnel. They are listed in reverse chronological order.

113

Picard, R.H., J.R. Winick, W.A.M. Blumberg, P.P. Wintersteiner, and R.A. Armstrong, "Transient 4.3 μm Rovibrational Emission from Carbon Dioxide in Sprites and Auroras", presented at the IUGG XXI General Assembly, Boulder, CO, 2-14 July 1995.

Winick, J.R., J. Wang, J.-L. Moncet, H. Snell, and P.P. Wintersteiner, "Non-LTE Effects on Nadir Viewing Temperature Sounding in the CO_2 4.3 μm and 15 μm Bands", presented at the IUGG XXI General Assembly, Boulder, CO, 2-14 July 1995.

Wintersteiner, P.P., R.H. Picard, and J.R. Winick, "Phillips Lab Atmospheric Radiance Code (ARC): Extensions and Recent Applications", in Proceedings of the 18th Annual Conference on Atmospheric Transmission Models, 6-8 June 1995 (G.P. Anderson, R.H. Picard, and J.H. Chetwynd, eds), PL-TR-96-2080, 1996, ADA307971.

Winick, J.R., J.-L. Moncet, H.E. Snell, D.B. Hogan, P.P. Wintersteiner, and J. Wang, "Non-LTE Effects on Nadir Viewing Temperature Sounding in the Stratosphere Using the CO_2 4.3 μm Band", in Proceedings of the 18th Annual Conference on Atmospheric Transmission Models, Hanscom AFB, MA, 6-8 June 1995 (G.P. Anderson, R.H. Picard, and J.H. Chetwynd, eds), PL-TR-96-2080, 1996, ADA307971.

Wintersteiner, P.P., R.H. Picard, and J.R. Winick, "Improved Modeling of NO Radiative Processes", presented at the NO/NO^+ Review, Hanscom AFB, MA, 7 February 1995.

Winick, J. R., R.H. Picard, P.P. Wintersteiner, R.A. Joseph, A.J. Paboojian, M. Lopez-Puertas, and U.B. Makhlouf, "Spectral Measurements and Modeling of Nonequilibrium 4.3 μm Emissions from Space Shuttle and Rocketborne Platforms", presented at the SPIE International Symposium on Optics, Imaging, and Instrumentation", San Diego, CA, 25-29 July 1994.

Picard, R.H., J.R. Winick, P.P. Wintersteiner, and U.B. Makhlouf, "Role of Non-LTE Radiative Transfer in the Energy Budget of the Middle Atmosphere", presented at the 30th Scientific Assembly, COSPAR, Hamburg, Germany, 11-21 July 1994.

Wintersteiner, P.P., M. Lopez-Puertas, J.R. Winick, and R.H. Picard, "Comparison of Line-by-Line and Modified Curtis Matrix Narrow-Band Approaches to Radiative Transfer in the CO_2 15 μm Bands", presented at the 17th Annual Conference on Atmospheric-Transmission Models, Hanscom, AFB, MA, 7-8 June 1994.

Winick, J.R., R.H. Picard, P.P. Wintersteiner, and J.A. Dodd, "Structure in Radiative Excitation as a Source of High Altitude Radiance Structure: CO(v=1) Radiance", presented at the 17th Annual Conference on Atmospheric Transmission Models, Hanscom AFB, MA, 7-8 June 1994.

O'Neil, R.R., H.A.B. Gardiner, J. Gibson, C. Humphrey, R. Hegblom, M.E. Fraser, M. Kendra, P. Wintersteiner, and C. Rice, "Midcourse Space Experiment (MSX): Plans and Capability for the Measurement of Infrared Earthlimb and Terrestrial Backgrounds",

Proc. SPIE, **2223** (25): 264-273, presented at the session on Characterization of Sources and Backgrounds, International Symposium on Optical Engineering in Aerospace Remote Sensing, Orlando, FL, 4-8 April 1994.

Wintersteiner, P.P., and R.A. Joseph, "Progress on the Automated Analysis of UVISI SPIM Data", presented at the PL DAC Critical Design Review, Hanscom AFB, MA, 4 March 1994.

Winick, J.R., R.H. Picard, P.P. Wintersteiner, R.A. Joseph, A.J. Paboojian, M. Lopez-Puertas, and U. Makhlouf, "Re-examination of $O(^1D)$ as a Source of $N_2(v)$ and its Effect on CO_2 4.3 μm Non-LTE Emission and the Energy Budget of the Middle Atmosphere", presented at the Fall Meeting of the American Geophysical Union, San Francisco, CA, 6-10 December 1993.

Wintersteiner, P.P., R.H. Picard, J.R. Winick, R.A. Joseph, and A.J. Paboojian, "Evaluation of 4.3 Micron CIRRIS Data", presented at the CIRRIS 1A Program Review, 8-9 September 1993.

Joseph, R.A., A.J. Paboojian, R.H. Picard, J.R. Winick, and P.P. Wintersteiner, "Analysis of CIRRIS 1A 4.3 μm Spectral Data Using a Unique Fitting Method", presented at the CIRRIS 1A Program Review, 8-9 September 1993.

Lopez-Puertas, M., P.P. Wintersteiner, R.H. Picard, J.R. Winick, and R.D. Sharma, "Comparison of Line-by-Line and Curtis Matrix Calculations for the Vibrational Temperatures and Radiative Cooling of the 15 μm Bands in the Middle and Upper Atmosphere", presented at the Third Atmospheric Spectroscopy Applications Colloquium, Reims, France, 8-10 September 1993.

Picard, R.H., J.R. Winick, P.P. Wintersteiner, R.A. Joseph, and A.J. Paboojian, "Spectral Measurements and Modeling of High-Latitude Nonequilibrium Midwave Infrared Emissions from Space Shuttle and Rocketborne Platforms", presented at the EUROPTO International Symposium on High-Latitude Optics, Tromso, Norway, 28 June-2 July, 1993.

Picard, R.H., J.R. Winick, A.J. Ratkowski, U. Makhlouf, J.C. Ulwick, A.J. Paboojian, K.U. Grossmann, and D. Homann, "Critical Tests of Non-LTE Radiative Models against High-Latitude Rocket Data", presented at the 16th Annual Conference on Atmospheric Transmission Models, Hanscom AFB, MA, 8-9 June 1993.

Wintersteiner, P.P., and R.A. Joseph, "Automated Analysis of UVISI SPIM Data", presented at the MSX Earthlimb System Design Review, Hanscom AFB, MA, 4 June 1993.

Ratkowski, A.J., R.H. Picard, J.R. Winick, U.B. Makhlouf, J.C. Ulwick, K.U. Grossmann, D. Homann, J. Schulz, and A.J. Paboojian, "Rocketborne Measurements and Modeling of Summer High-Latitude Nitric Oxide", presented at the Eleventh ESA Sympo-

sium on European Rocket and Balloon Programmes and Related Research, Montreux, Switzerland, 24-28 May 1993.

Winick, J.R., R.H. Picard, P.P. Wintersteiner, A.J. Paboojian, and R.A. Joseph, "On determining the carbon budget (CO_2 and CO) of the lower thermosphere from non-equilibrium infrared radiance", presented at the Sixth Topical Meeting on Optical Remote Sensing of the Atmosphere, Optical Soceity of America, Salt Lake City, UT, 8-12 March 1993.

Nebel, H., P.P Wintersteiner, R.H. Picard, R.D. Sharma, and J.R. Winick, "CO_2 non-LTE excitation and emission at 4.3 µm from a line-by-line radiative transfer model", presented at the Sixth Topical Meeting on Optical Remote Sensing of the Atmosphere, Optical Society of America, Salt Lake City, UT, 8-12 March 1993.

Winick, J.R., R.H. Picard, U. Makhlouf, E.T.P. Lee, W.M. Blumberg, D.R. Smith, R.M. Nadile, A. Paboojian, P.P. Wintersteiner, and R.A. Joseph, "Analysis of the 4.3 µm limb emission observed from STS-39", presented at the Fall Meeting of the American Geophysical Union, San Francisco, CA, 7-11 December 1992.

Winick, J.R., R.H. Picard, A. Paboojian, P.P. Wintersteiner, and R.A. Joseph, "Analysis of STS-39 CO 4.7 µm limb emission", presented at the Chapman Conference on the Upper Mesosphere and Lower Thermosphere, Asilomar, CA, 16-20 November 1992.

Picard, R.H., E.T.P. Lee, J.R. Winick, U. Makhlouf, D. Smith, R.D. Sharma, J.R. Wise, R.M. Nadile, A.J. Paboojian, R.A. Joseph, and P.P. Wintersteiner, "Global behavior of the 4.3 µm CO_2 earthlimb emission from STS-39 CIRRIS-1A data", presented at the Chapman Conference on the Upper Mesosphere and Lower Thermosphere, Asilomar, CA, 16-20 November 1992.

Winick, J.R., R.H. Picard, D. Dean, R.M. Nadile, A.J. Paboojian, and P.P. Wintersteiner, "Analysis of STS-39 CO 4.7 µm Limb emission", presented at the Spring Meeting of the American Geophysical Union, Montreal, Canada, 12-16 May 1992.

Picard, R.H., E.T.P. Lee, J.R. Winick, D.R. Smith, J.O. Wise, R.M. Nadile, A.J. Paboojian, and P.P. Wintersteiner, "STS-39 Measurement of 4.3 µm Earthlimb Emission from CO_2 and NO^+", presented at the Spring Meeting of the American Geophysical Union, Montreal, Canada, 12-16 May 1992.

Wintersteiner, P.P., M. Lopez-Puertas, R.H. Picard, J.R. Winick, and R.D. Sharma, "Comparison of Line-by-Line and Band-Model Calculations for Radiances and Atmospheric Cooling Rates in CO_2 15 µm Bands", presented at the Fall Meeting of the American Geophysical Union, San Francisco, CA, 9-13 December 1991.

Wintersteiner, P.P., U. Makhlouf, R.H. Picard, and J.R. Winick, "Atmospheric Cooling from Longwave Infrared Emission in CO_2 Bands; Effects of Gravity-Wave Modulations",

presented at the Fall Meeting of the American Geophysical Union, San Francisco, CA, 9-13 December 1991.

Lee, E.T.P., R.H. Picard, J.R. Winick, R.D. Sharma, J.O. Wise, M.A. Ahmadjian, R.M. Nadile, B. Bartschi, and A.J. Paboojian, "Non-LTE 4.3 μm Limb Emission Measured from STS-39", presented at the Fall Meeting of the American Geophysical Union, San Francisco, CA, 9-13 December 1991.

Wintersteiner, P.P., R.H. Picard, R.D. Sharma, and J.R. Winick, "CO_2 Cooling Rates for the Mesosphere and Thermosphere Determined from a Line-by-Line Radiative Transfer Model", presented at the IUGG XX General Assembly, Vienna, Austria, 11-24 August 1991.

Wintersteiner, P.P., R.H. Picard, R.D. Sharma, H. Nebel, A.J. Paboojian, J.R.Winick, and R.A. Joseph, "RAD: A Line-by-Line Radiative Excitation Model with Application to CO_2", presented at the 13th Annual Conference on Atmospheric Transmission Models, Hanscom AFB, MA, 5-6 June 1990.

Wintersteiner, P.P., A.J. Paboojian, J.R. Winick, R.H. Picard, R.D. Sharma, and G.P. Anderson, "Non-LTE CO_2 Vibrational Temperature Profiles for FASCOD3", presented at the 13th Annual Conference on Atmospheric Transmission Models, Hanscom AFB, MA, 5-6 June 1990.